REPRESENTATION OF PROPRIOCEPTIVE INFORMATION FOR

GENERATION OF ARM DYNAMICS

by

Eun Jung Hwang

A dissertation submitted to Johns Hopkins University in conformity with the

requirements for the degree of Doctor of Philosophy

Baltimore, Maryland

December, 2004

Abstract

The goal of this thesis was to investigate how the brain represents proprioceptive information about limb state, i.e., position, velocity and acceleration to generate reaching movements. To achieve this goal, human behaviors during point-to-point reaching in multiple novel dynamic environments were examined and neural coding schemes in the brain were inferred from the observed behaviors, e.g. the pattern of generalization. The patterns of generalization across limb position in multiple dynamic conditions suggested that the internal model encodes limb position and velocity using a gain-field scheme. That is, neural elements in the brain seem to encode limb velocity and position multiplicatively. This multiplicative combining scheme seems to extend to encoding of limb velocity and acceleration as the pattern of generalization across acceleration space rejects a linearly separable encoding of acceleration and velocity. The nonlinear combining of all sensory information in the brain might originate from the properties of the proprioceptive sensors in our body, muscle spindles. Muscle spindles respond to all three sensory information in highly nonlinear way due to the nonlinear relationship between tension and muscle spindle length. Surprisingly, some tuning functions that were independently derived from the mathematical model of muscle spindle closely resemble the tuning functions derived from the gain-field scheme and thus, can explain the patterns of generalization across various state spaces.

So far, at least in a force field paradigm, motor learning has been considered as an implicit procedure and the effect of explicit knowledge has been ignored. However, a proper assessment of relevant explicit knowledge indicates that there is a small but significant effect of explicit knowledge on motor performance. Interestingly, the formation of explicit knowledge is primarily driven by visual information while the formation of implicit internal model is primarily driven by proprioceptive information.

Advisor: Dr. Reza Shadmehr

Table of Contents

Table of Figures

Chapter 1

Introduction

Understanding how the brain controls movements is a fundamental challenge in neuroscience research and prosthetic applications. The movement that the brain controls can be as simple as blinking an eye or as complex as playing an instrument. Among this variety of movements, arm reaching has been widely adopted as an experimental protocol to study fundamentals of movement control in both animals and human (Bhushan and Shadmehr, 1999;Taylor et al., 2002;Todorov, 2000). Even for this seemingly simple point-to-point reaching, studies find that the brain needs to deal with a series of complex computations including a coordinate transformation from visual space to joint space and a computation of muscle forces to produce the desired joint displacement (Wolpert, 1997). A specific computational challenge arises from the fact that the computation of muscle forces involves solving a complex nonlinear dynamics imposed by a multi-joint arm (Atkeson, 1989;Bastian et al., 1996). For example, even for a simple elbow flexion, the brain needs to send motor commands to both elbow and shoulder joints to prevent a passive shoulder motion caused by the interaction torque existing in the multi-joint dynamics. The complexity becomes even greater when the reaching condition varies such as reaching while turning, or reaching while holding an object. Despite this overwhelming complexity, people make so many reaching movements in so many different conditions without any conscious difficulty. Then how does the brain perform the neural computations required to control reaching movements?

An important insight was gained into this problem through perturbation studies. People tend to reach in a straight line from one point to another with a typical bell shaped velocity profile (Flash

and Hogan, 1985). This tendency continues even when their reaching movements are perturbed by an external force field or by a modified arm inertial property (Shadmehr and Mussa-Ivaldi, 1994b;Krakauer et al., 1999;Lackner and Dizio, 1994). When perturbations are first introduced, movements deviate from the typical straight line and the velocity profiles differ from the bell shape. However, with practice, people recover the typical kinematic features in their reaching movements. Interestingly, when the learned perturbation is unexpectedly removed, subjects make errors that are almost equal and opposite to their initial errors in perturbation. The recovered kinematic features and aftereffects in a velocity dependent force field suggest that the brain is able to build an internal model that relates the limb velocity to forces in the external world. The existence of such internal models is further supported by the finding that adaptation to a velocity dependent force field is transferred from point-to-point reaching movements to circular movements despite the drastic difference in these two movements' trajectories (Conditt et al., 1997). That is, kinematic features of circular movements after training to point-to-point reach in a velocity dependent force field are similar to what it would be if subjects expected the forces that followed the same velocity dependent rule at each point along the circle.

Another key finding about the internal model is the ability to generalize the learned mapping to unvisited states. Subjects who trained in a velocity dependent force field for one direction of reaching expected a similar velocity dependent force field in other directions of reaching although generalization decayed with the angular distance between the trained direction and test direction (Gandolfo et al., 1996;Thoroughman and Shadmehr, 2000). Similarly, subjects generalize learning a velocity dependent force field from one arm configuration to another, from a right arm to a left arm, and from fast movements to slow movements (Shadmehr and Moussavi, 2000;Malfait et al., 2002;Goodbody and Wolpert, 1998;Criscimagna-Hemminger et al., 2003).

These patterns of generalization allowed us to determine how the brain might or might not represent the internal model. First, generalization to unvisited states rejects a lookup-table-like representation such as a simple memory of a muscle activation and sensory feedback pattern. Second, decay of generalization as unvisited states become distant from the visited states rejects an abstract representation of analytical rule of dynamics such as inertia and viscosity. Thus far, the most plausible representation is through a neural network model that performs a function approximation using basis elements (Poggio and Girosi, 1990;Thoroughman and Shadmehr, 2000). Basis elements are tuned functions in the input sensory space thus a given sensory input elicits a unique activation pattern of basis elements. The output of the network, motor commands in the case of internal model, is a weighted sum of all the basis elements' activation. Since assigning different weights result in a different output for the same sensory input, this network can approximate any input-output relationship by finding a proper set of weights. In this neural network representation, generalization is an inherent property because the output is a continuous function in the domain of input sensory state while the extent of generalization depends on the specific shape of the tuning functions of basis elements. The basic logic that the pattern of generalization is determined by the shape of basis functions provides scientists a powerful tool to probe the neural representation of the internal model in the brain. That is, the tuning functions of basis elements can be inferred by examining patterns of generalization across the sensory input space of interest.

A conventional way to measure generalization is through a block designed experiment that consists of training in one region of space and testing outside the trained space. The training session is usually long enough to ensure that subjects acquire the appropriate internal model for the trained states and the testing session is brief to eliminate the possibility that the observed effect results from learning within the test session. Recently, a novel way to measure generalization between single trials instead of between blocks was introduced (Thoroughman and

Shadmehr, 2000). The idea is that the brain adjusts the internal model after every trial based on the movement error feedback signal during that trial and this change of the internal model affects the performance of the following movement. Then, quantitative characterization of this effect of movement error on the following movement is a way to measure generalization. Using a state space model as a tool to measure the error effect on the subsequent movement, the trial-to-trial generalization pattern across reaching movement direction was measured during velocity dependent force field adaptation (Donchin et al., 2003).

As aforementioned, the pattern of generalization provides a unique window to examine the representational structure of the internal model. The shape of tuning functions that encode hand velocity in the internal model was inferred using this approach. When the tuning function of the basis elements is Gaussian with a certain width and the internal model performed function approximation to fit a velocity dependent force field, the simulated trial-to-trial generalization pattern matches closely to the generalization pattern observed from the human subjects (Donchin et al., 2003;Thoroughman and Shadmehr, 2000). The mathematical properties of the inferred basis function resemble the tuning curves of some Purkinje cells in cerebellum although the direct demonstration that these cells are indeed involved in the representation of the internal model remains to be shown (Coltz et al., 1999).

Often, reaching movement occurs while holding an object. Any object that we hold in our hand, e.g., a tennis racquet, shifts the center of mass in our arm and imposes forces on the arm that depends on limb position, velocity, and acceleration while reaching (Slotine, 1991). The fact that with practice, we adapt to move skillfully with novel objects that impose unfamiliar dynamics suggests that the internal model has an ability to map limb position, velocity, and acceleration to force. Learning of velocity dependent forces has been clearly demonstrated in multiple experimental conditions and a biologically compatible neural representation of velocity in the

internal model has been proposed. However, representation of limb position and acceleration has not been well investigated yet.

In neurophysiology, many studies find cells that show sensitivity to limb position and acceleration in peripheral and central nervous system. Limb position, velocity and acceleration dependent cells' activity might originate from the muscle spindle receptor activities. The muscle spindle response is best studied in a muscle stretch paradigm (Edin B.B. and Vallbo A.B.., 1990). The typical response to stretch is an initial burst, slow increase during stretch interval, depression at the end of stretch and slow decrease after the end of stretch. The steady state response to stretch is proportional to the stretched muscle length, indicating monotonic position sensitivity. The dynamic response, i.e. increasing rate during stretch is proportional to the stretching velocity. A model that multiplicatively combines muscle length and the third power of velocity fits well the steady state and dynamic responses except the lack of initial burst (Houk et al., 1981). Spindle-like responses to ramp displacements of hindlimb joint were found in area 3a, M1, and S1 (Wise and Tanji, 1981), i.e. initial burst, velocity-, and position-dependent modulation were shown in cell responses. The limb position dependent modulation was further studied in spinocerebellar tract (Bosco et al., 1996), S1(Tillery et al., 1996), 5a and M1 (Georgopoulos et al., 1984;Prud'homme and Kalaska, 1994;Sergio and Kalaska, 1997). The cell activities of these areas are globally and often linearly modulated with limb position, agreeing with the monotonic position coding of muscle spindle receptors. Acceleration dependent responses were found in 5a and M1 although these responses were less frequently found than direction dependent responses (Ashe and Georgopoulos, 1994;Flament and Hore, 1988). These findings in neurophysiology provide a guideline for computational modeling when reconstructing representations of limb states in the internal model based on behavioral data.

In this thesis, an attempt is made to understand how the brain represents limb states, i.e., limb position, velocity and acceleration, to generate movements. A series of psychophysical experiments were conducted to measure adaptation and generalization using a force field paradigm. Computational models were proposed to explain the observed adaptation ability and generalization. In chapter 2, psychophysical experiments in which subjects trained to reach in a position-velocity dependent force field were conducted. The learning ability and generalization as a function of spatial distance between movements were measured. In chapter 3, a computational model that describes how the brain represents limb position and velocity was proposed. This model, a so called "gain-field model", reproduced not only the position-velocity dependent force field experimental result but also several previous experimental results. Two counter-intuitive predictions resulting from the monotonic position encoding in the gain-field model were experimentally confirmed. In chapter 4, a psychophysical experiment using an acceleration dependent curl field was conducted to measure the learning ability and generalization in other untrained directions. Using the force channel technique, adaptation and generalization were directly quantified. In chapter 5, a physiologically inspired computational model was proposed to describe how the brain represents limb states including position, velocity, and acceleration. The model encodes limb states similar to the way that muscle spindles respond to limb motion. The model's ability to reproduce experimental results from several adaptation and generalization studies and its limitation was discussed. In chapter 6, the relative contribution of vision and proprioception to limb state information used in the internal model was studied as was the formation of explicit knowledge during force field learning.

Chapter 2

Human motor adaptation to position dependent force fields and generalization.

When people reach to various directions in a small workspace, velocity- or acceleration-dependent forces that they experience are generalized broadly to other arm positions as far as 80 cm away (Shadmehr and Moussavi, 2000). These results argue that the neural elements with which the brain represents the dynamics of reaching movements may not be very sensitive to limb position, in contrast to findings that they are quite sensitive to velocity and acceleration. Lack of sensitivity would explain extensive generalization. However, it is known that humans can adapt reaching movements to position-dependent spring-like forces (Flash and Gurevich, 1997). The ability to adapt to position-dependent fields suggests that the internal model can have steep position sensitivity (Tong et al., 2002). This apparent contradiction raised doubts about our understanding of representation and generalization of limb position. Therefore, it seems necessary to closely examine patterns of generalization as a function of limb position and ask whether these results can be explained by a single representation.

In this chapter, as a first step to investigate the representation of position information in internal model, we test whether or not people can learn a position dependent force field. This will help us determine whether or not representation of limb position exist in internal model. Then, we characterize generalization in the limb position space while subject adapt to a position dependent force field. This generalization pattern will be used in the following chapter to infer the shape of position-velocity dependent basis functions.

2.1 Experimental setup and data analysis

Twenty-four healthy individuals (8 women and 16 men) participated in this study. The average age was 27.3 y (range: 21-38 y). The study protocol was approved by the Johns Hopkins University School of Medicine Institutional Review Board and all subjects signed a consent form.

2.1.1 Task

Figure 2.1 describes an experiment in which subjects performed reaching movements in force fields that depended on both velocity and position of the limb. Subjects made movements in the horizontal plane while holding the handle of a robot. The task was to reach a target (displacement of approximately 10 cm) within 500 ± 50 ms. Handle and target positions were continuously projected onto a screen placed directly above the subject's hand (Shadmehr and Moussavi, 2000). Feedback on performance was provided immediately after target acquisition, but feedback related only to the subject's success in arriving at the target within the prescribed time window and not to the shape of the hand trajectories. After completion of each movement, the robot moved the hand to a new start position and another target was presented. The start positions were pseudorandomly chosen from three possible locations: left, center, and right. Twenty-four subjects were divided into four groups, and the start positions for the four groups were separated by 0.5 cm, 3 cm, 7 cm, or 12 cm, respectively (Figure 2.1). Different colors were used for the left, center, and right start positions and targets so that we could be certain that subjects could distinguish the locations even when the separation distances were small. The targets were placed so that movements from all three starting locations required the same joint angle displacement. Thus, the movements were parallel in joint space and not in Cartesian space (Figure 2.1). Therefore, the movements explored the same joint velocity space but at different joint positions.
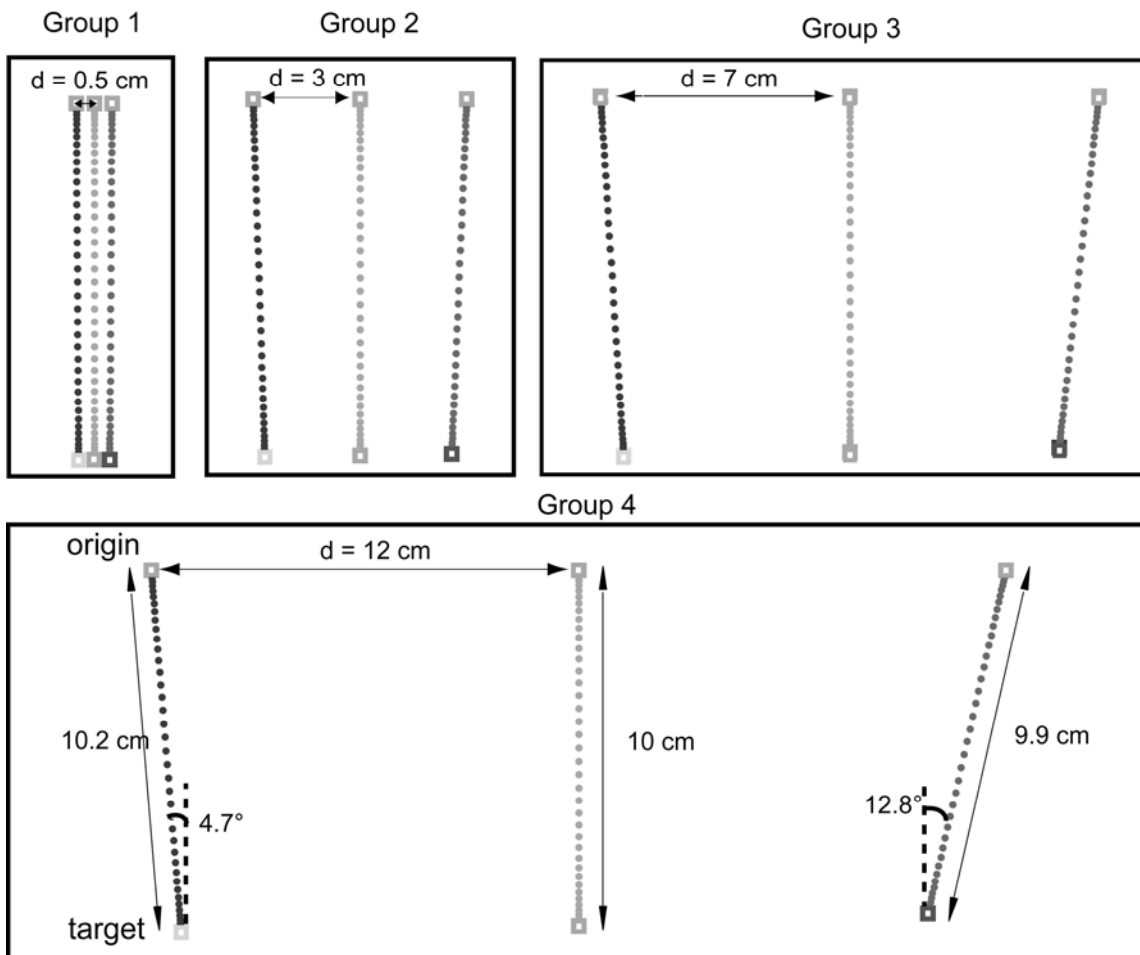
Figure 2.1 Experimental designs to test position-velocity dependent force fields.
The origin of the center movements is aligned with the subject's body midline, and the origins of the left and right movements are symmetrically positioned with a given separation distance *(d)* for each group. The target positions shown here are an example for a subject with typical arm lengths (20, 33, 34 cm shoulder, upper arm, and lower arm lengths, respectively). In order to help subjects distinguish among locations, different colors were provided for targets at different locations (yellow, green, and blue for the left, center, and right, respectively).

2.1.2 Force fields

The robot could apply arbitrary patterns of force to the hand. We programmed it so that the movements were perturbed by a viscous curl-field. In a viscous curl-field, the force is proportional to speed and perpendicular to velocity. However, our viscous curl-fields also depended on position. During movements from the left starting position, the robot perturbed the hand with a clockwise curl-field ($B = [0\ 13;\ -13\ 0]$ N·s/m, pushing the arm leftward during the movement). For movements starting on the right, a counterclockwise curl-field ($B = [0\ -13;\ 13\ 0]$ N·s/m) was present (pushing the arm rightward). For the center movements, the field was always null (no forces were applied). Thus, to succeed in the task, the subjects needed to produce three different force patterns although the movements required the same joint angular velocities. The idea was to find out how far apart the movements needed to be in position space for the task to become learnable. To familiarize the volunteers with the task and produce baseline performance, subjects first did three sets of 84 movements in which no forces were applied. Following the baseline sets, subjects did five force-field sets.

2.1.3 Performance Measures

As a measure of error, we report the displacement perpendicular to target direction at 250 ms into the movement (PE). However, we also tried other measures, such as perpendicular displacement at the maximum tangential velocity, maximum perpendicular displacement, and averaged perpendicular displacement during early phase of movement. Results that we present here are consistent among all these measures of error.

During adaptation, trajectories in field trials become straighter, while the trajectories of catch trials become approximately a mirror image of those in earlier field movements (Shadmehr and

10

Mussa-Ivaldi, 1994a). Therefore, the PE of field trials decreases and the PE of catch trials increases. Based on this observation, we quantified a learning index:

$$Learning \ Index = \frac{p.e._{catch \ trial}}{p.e._{catch \ trial} - p.e._{field \ trial}} \qquad (2.1)$$

2.1.4 Generalization Measure

We quantified the effect of error experienced in one movement on another movement as a function of their spatial distance. In the experiment outlined in Figure 2.1, there were never any forces during the center movement. The error experienced in a neighboring movement would cause a change in the subsequent movement at center. This change results in increased variance of errors at center. Therefore, a measure of generalization of error is the ratio of variance of error in trials where forces were present to the left and right of the center movement, to variance of error in baseline trials when no forces were present:

$$Generalization \ Index = \frac{standard \ deviation \ of \ p.e._{adaptation}}{standard \ deviation \ of \ p.e._{baseline}} \qquad (2.2)$$

2.2 Adaptation to Position Dependent Fields

Figure 2.2a and 2.2b displays the average hand paths of movements during the first and last sets of training for typical subjects from each group. The figures show movements both in field trials and in catch trials (occasional trials interspersed with the field trials in which the robot did not apply any forces). In the early phase of training, field trials were strongly curved toward the direction of force, although slight adaptation appeared in the largest separation distance group (d = 12 cm; Figure 2.2a). Late in training (Figure 2.2b), subjects with the largest separation in
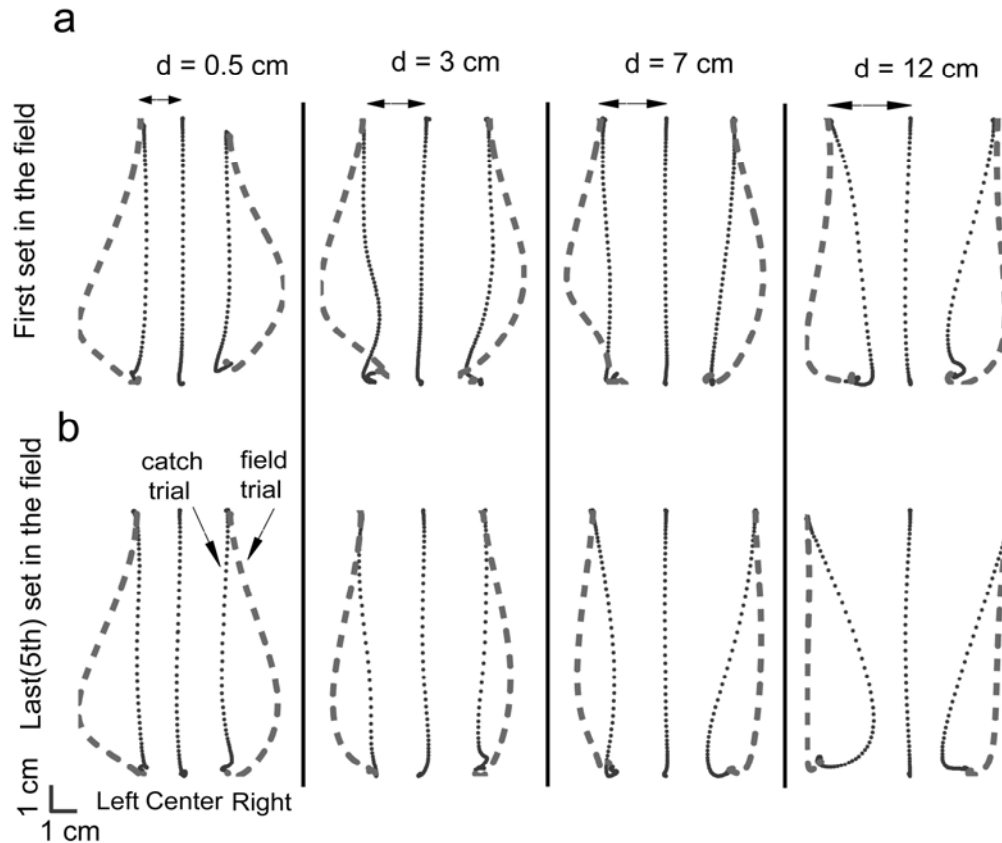
Figure 2.2 Adaptation to a position-velocity dependent force field. **(a)** The average trajectories in three positions—left, center, and right (one subject per column)—for the first third of the movements from the first field set (trials 1-28). Dashed lines are movements during which force field is on and dotted lines are catch trials. Separation distances between neighboring movements *(d)* are not scaled in this figure. **(b)** The average trajectories for the first third of the fifth field set (trials 337-364). The task is much easier to learn when the three movements are spatially separated from each other.

starting position showed manifest adaptation. Hand paths in the field trials became straighter, and trajectories of catch trials showed large aftereffects (Figure 2.2b). In contrast, subjects with the smallest separation in starting position showed little improvement in performance. Therefore, it appeared that movements that were spatially close to each other could not be easily associated with different force patterns. As the movements became farther apart, different forces could be more readily associated with them.
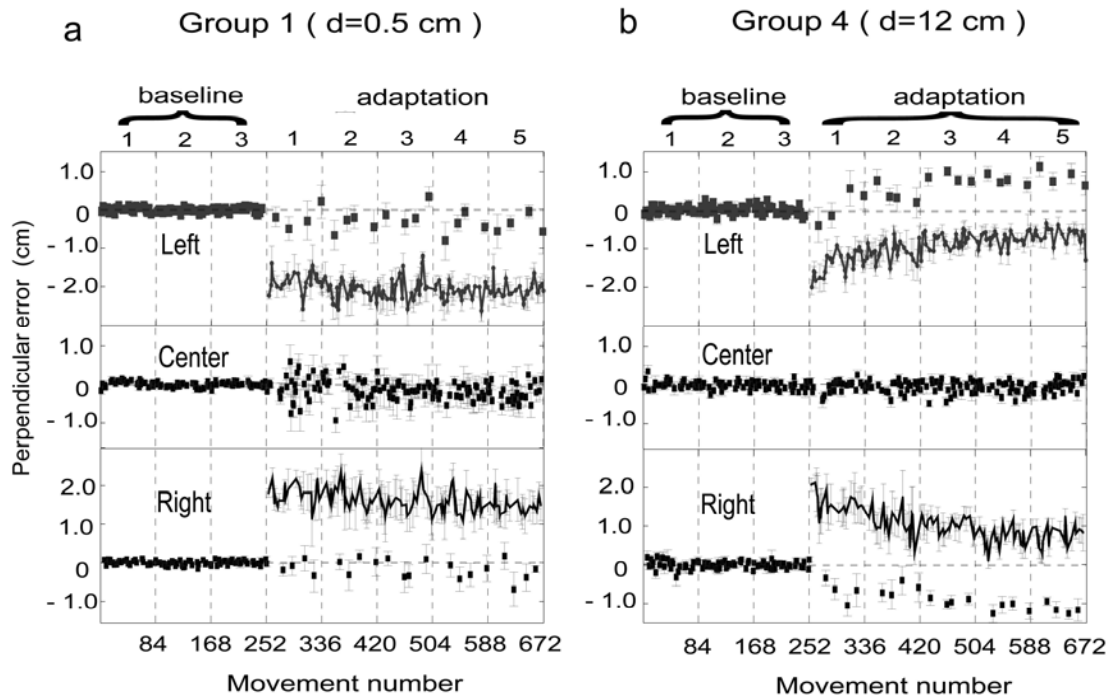
Figure 2.3 Movement errors. **(a)** PE averaged across six subjects of Group 1 ($d = 0.5$ cm). Squares indicate catch trials. Error bars show SEM. The average SEM at the center is 1.3 mm in the baseline sets and 6.6 mm in the adaptation sets for Group 1. The average SEM is 2.1 mm in the baseline sets and 2.4 mm in the adaptation sets for Group 4. **(b)** Errors were averaged across six subjects of Group 4 ($d = 12$ cm).

As a measure of error, we used displacement perpendicular to target direction at 250 ms into the movement (perpendicular error, PE). Figure 2.3 shows the error on each trial averaged across subjects and plotted in a time series for Group 1 ($d = 0.5$ cm; Figure 2.3a) and Group 4 ($d = 12$ cm; Figure 2.3b). A gradual decrease in error magnitude and an increase in aftereffects in catch trials were apparent in Group 4, but not in Group 1. A learning index combining performance on field and catch trials (equation 2.1) allows a comparison of performance across groups (Figure 2.4a). An ANOVA on the learning index showed a significant effect both for separation distance and set number ($F = 41.78$, d.f. $= 3$, $p < 1.0 \times 10^{-8}$ for distance factor; $F = 3.02$, d.f. $= 4$, $p < 0.02$ for set number factor), suggesting that subjects performed better in the groups where targets were
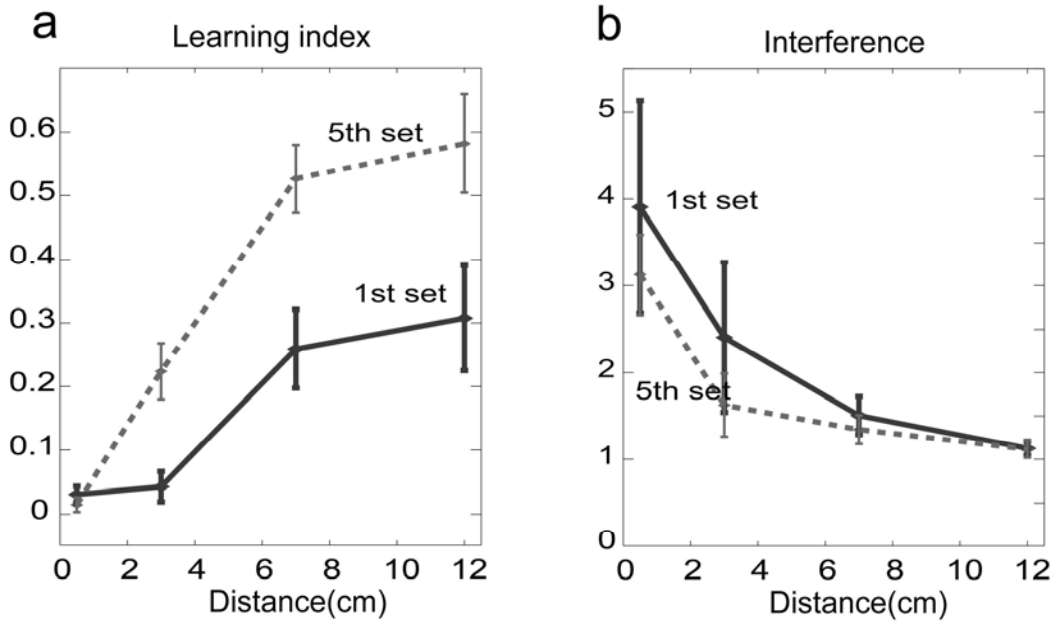
Figure 2.4 Learning performance and generalization as a function of the separation distance **(a)** Average learning index (Equation 1) across groups. Learning index is plotted against the separation distance between movements. Thin lines show the first adaptation set and thick lines show the last adaptation set. $n = 6$ for each distance. Error bars show SEM. **(b)** Generalization index (Equation 2) against spatial distance between movements.

spatially separated. Similar trend is visible in other measures of errors such as averaged perpendicular errors, maximum perpendicular errors and perpendicular errors at the maximum tangential velocity (figure 2.5).
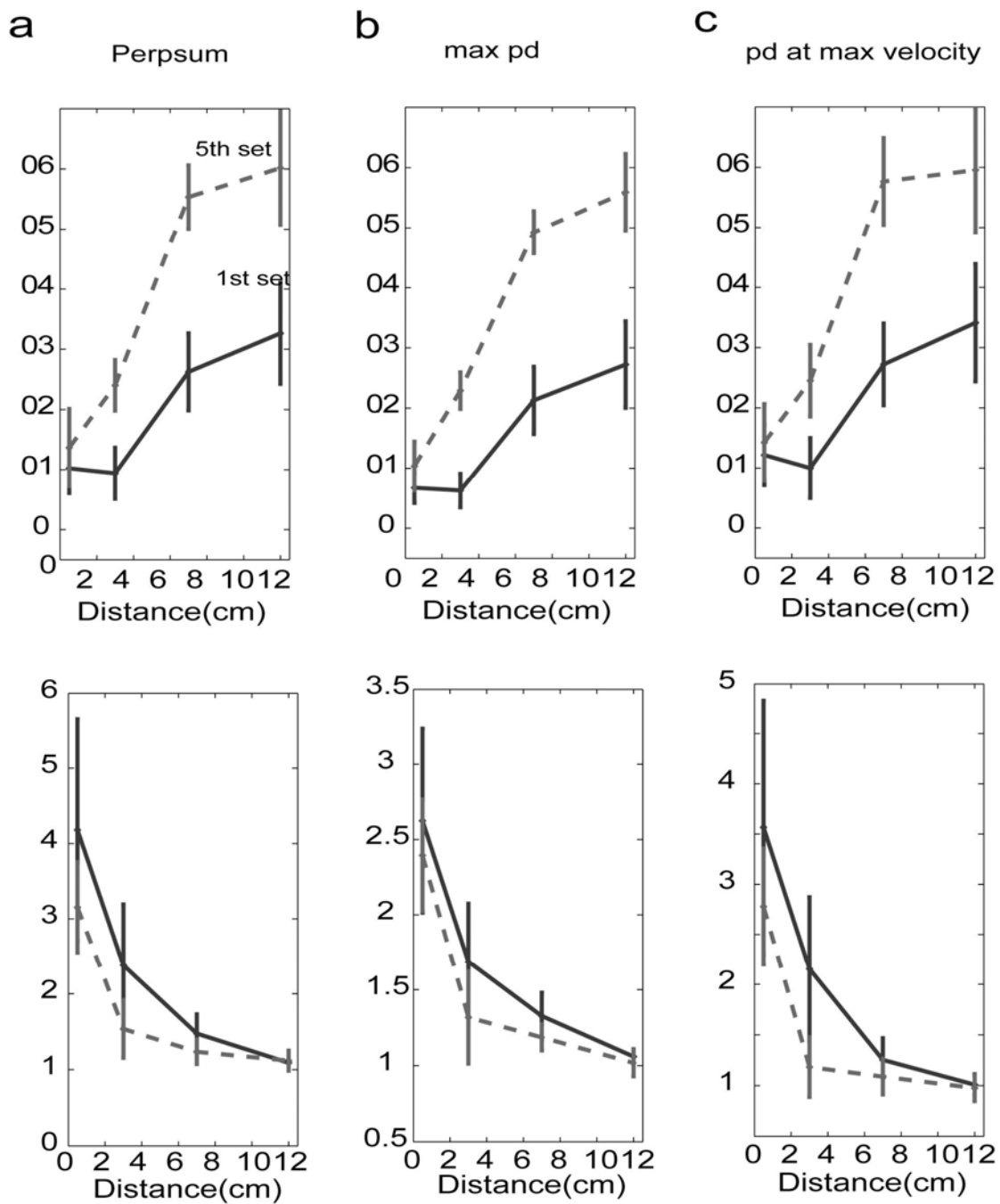
Figure 2.5 Learning performance and generalization for three other measures of errors. **(a)** Averaged perpendicular error during the initial 250 ms into movements. Learning index is plotted in the top panel and generalization index is plotted in the bottom panel. **(b)** Maximum perpendicular error. **(c)** Perpendicular error at the maximum tangential velocity.

2.3 Generalization across arm position

We were struck by another difference between Figure 2.3a and 2.3b. There were never any forces for the center movement. However, the variance in these movements (middle traces) changed when going from the baseline sets to the field sets. For instance, the center movements in Group 1 have a much larger variability in field sets than in baseline sets. Our interpretation of this is that the forces subjects experienced on the left and the right influenced the center movement through generalization. For example, after a movement in the right spatial location, rightward forces experienced in that location should generalize to the center movement, causing a leftward after-effect. This point is illustrated for three consecutive movements in Figure 2.6a. The sequence of movements is center-right-center. The error in the first center movement (#301, 49th movement in the set) is small. This movement is followed by a movement at the right, where a large error is experienced (#302). This is followed by another movement at the center (#303), where a large change in the opposite direction is observed. It appears that when two movements at the center have an intervening movement at either the left or right, that intervening movement affects the upcoming movement at the center. In the group with the larger separation distance, no such effect is apparent (Figure 2.6b).

To quantify whether there was a consistent pattern to this interference between movements, we plotted the change of error from one center movement to the next as a function of the number of field trials between them (Figure 2.6c). For example, when the target sequence is center-left-right-left-center, the value on the ordinate is -1 (one right movement minus two left movements) and the abscissa value is the difference in error between the first and last movements in the sequence. If the force experienced at the left or right influences the expected force at the center, the movements in the center will show increased compensation for rightward force when there are

16
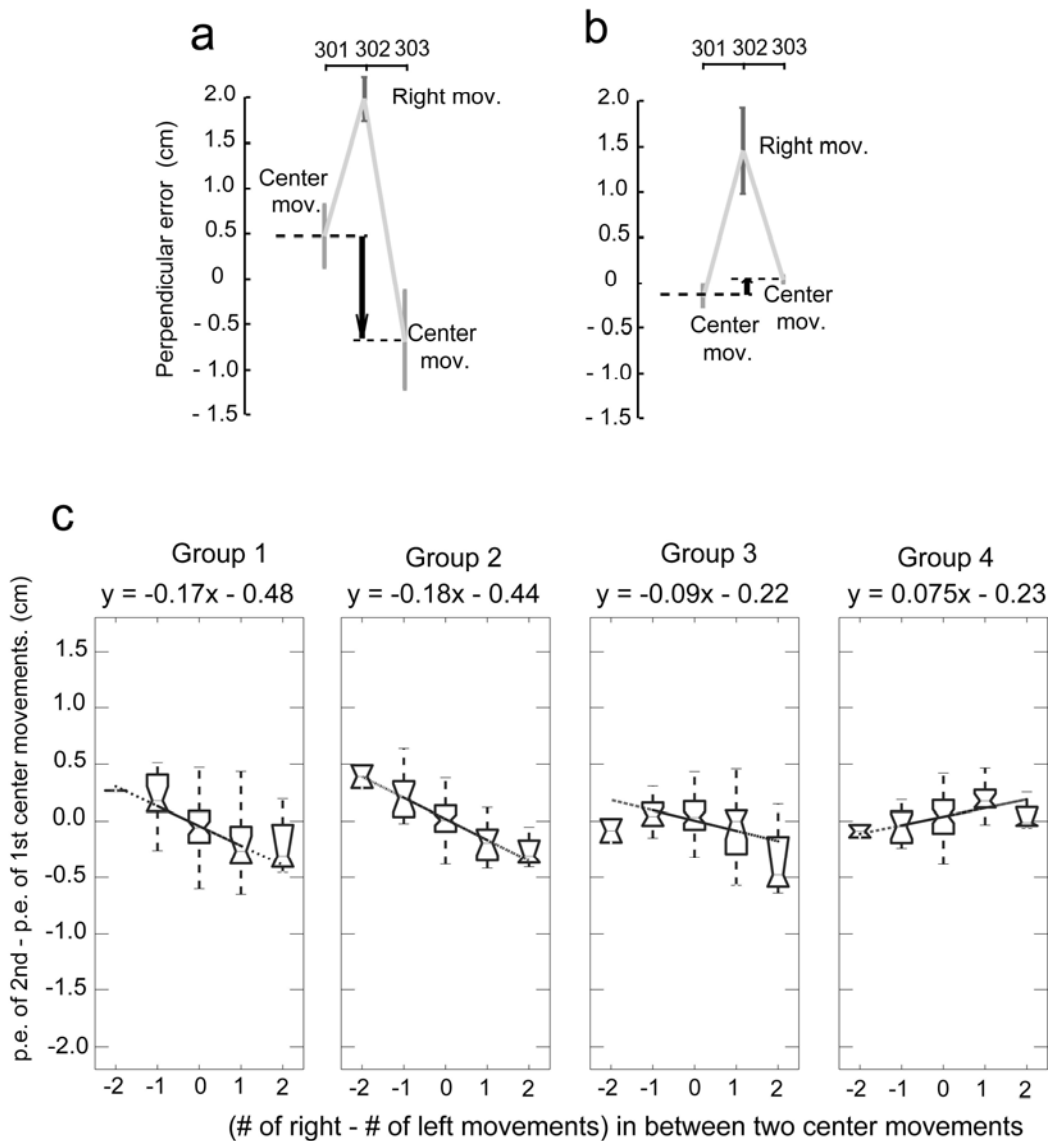
Figure 2.6 Measures of interference. **(a)** Expanded view of movement errors in movements 301 to 303 in Fig. 2(a). The arrow indicates change of expected force at center after *movement 302* (right movement) in Fig. 2(a). **(b)** Movement errors in movements 301 to 303 in Fig. 2(b). **(c)** Abscissa is the difference between the number of fielded movements on the right and the number of fielded movements on the left between two center movements. Ordinate is change of *p.e.* from the first movement in the center to the second movement in the center. The box has lines at the lower quartile, median, and upper quartile values. The whiskers are lines extending from each end of the box to show the range of the data. The gray line superimposed on each plot is a linear regression, and the equation of the line is shown. A steeper slope indicates a greater influence of the intervening movements.

17

more movements at right and increased compensation for leftward force when there are more movements at left. The magnitude of the change in error measures the influence of side movements on the center movement. We found that this influence, as quantified by the slope of the lines in Figure 2.6c, is larger in the group with the smaller distance. That is, as the neighboring movements became closer, the effect on the center movement became stronger. In this analysis, we treated sequence C-L-R-C, C-C, and C-R-L-C as if they would affect the second center movement by the same amount ignoring the temporal effect. To eliminate this complex temporal-effect, we also did the same analysis using only sequences C-L-L-C, C-L-C, C-C, C-R-C, and C-R-R-C. However, we do not find any significant difference (equations form linear regression: y = - 0.17x - 0.43, y = - 0.18x - 0.45, y = - 0.086x - 0.21, and y = 0.064x - 0.16 for each group).

We quantified this generalization (or interference) to center movements using a generalization index (equation 2.2). In Figure 2.4d, the generalization index is shown for all groups. An ANOVA on separation distance by set number shows that generalization varies significantly with separation distance but not with set number ($F = 15.56$, d.f. = 3, $p < 2.2 \times 10^{-8}$ for the distance factor; $F = 0.83$, d.f. = 4, $p > 0.5$ for set number factor). As neighboring movements became spatially farther apart, generalization among them appeared to decrease. Similar trend is visible in generalization indices calculated from other measures of errors (figure 2.5).

2.4 Discussion

As a first step to investigate the representation of position information in internal model, we performed behavioral experiments to demonstrate that human subjects were able to learn a position dependent force field and then to characterize the generalization in the limb position

18

space. When different forces are to be associated with two movements that are in the same direction but at different spatial locations, generalization decreases with increased distance between them. On the other hand, earlier results had found that when movements to various directions are learned at a single location, learning generalizes to other arm locations very far away (Ghez et al., 2000;Shadmehr and Moussavi, 2000;Malfait et al., 2002). These two results appear to be contradicting. However, in the next chapter, we will show that a single representation of position and velocity information can actually explain both our current result and previous results.

Another issue is that our findings may be the result of limits of visual acuity; i.e., a decreased ability to distinguish the starting positions might cause a spurious finding of position-dependent coding. One way we addressed this concern was to use color-coding to make sure subjects could distinguish the left, center, and right targets. However, it is possible that the system is not capable of using color cues while it is capable of using spatial cues. Note that this interpretation implies that, at large separations, position serves as an explicit cue triggering separate internal models. That interpretation is not consistent with the earlier results in which generalization across large distances seemed to imply that position is represented continuously. If position is a discrete cue for building different internal models, then it is not clear how one could learn a force field that depends continuously on position, as in spring-like fields. Thus, although it is quite possible that some effects are due to the explicit cues as will be discussed in chapter 6, this cannot entirely explain our findings without a continuous encoding of position.

Chapter 3

A Gain-field Encoding of limb position and velocity

Internal models can be modeled as networks of basis elements that perform function approximation (Poggio, 1990; Thoroughman and Shadmehr 2000). Then, the encoding properties of basis elements implementing this computation dictate how errors should generalize from one limb position and velocity to another. For example, generalization of velocity dependent force field learning occurs in intrinsic coordinates, suggesting that basis elements encode joint velocity instead of hand velocity. Another example is that generalization of velocity dependent force field learning decays with the angular distance between movements, indicating that basis elements are directionally tuned. In this chapter, based on the pattern of generalization we obtained in the last chapter, we propose a gain-field as a coding scheme for the internal model to encode limb position and velocity. In our gain-field model, basis functions combine limb position and velocity information multiplicatively. The validity of our gain-field model is further tested by comparing simulation results to other previously published experimental results. We also present new experimental results that agree with counter-intuitive predictions made by our gain-field model.

3.1 Computational modeling of internal model as function approximation

The internal model may be computed as a population coding via a set of basis elements, each encoding some aspect of the limb's state (Donchin and Shadmehr, 2002). Neurophysiological studies show that in tasks similar to the current paradigm, the preferred direction of cells tend to change during adaptation (Gribble and Scott, 2002;Li et al., 2001). In our model, we assumed a

"preferred" torque vector is associated with each basis. With training, the preferred torque vectors change, resulting in a more accurate representation of the force field. The internal model is:

$$\hat{\tau}_{env} = \sum_i w_i \cdot g_i(\underline{z}) \qquad (3.1)$$

where $\hat{\tau}_{env}$ is the expected environmental torque, $\underline{z}$ is a desired state of the limb (consisting of limb position and velocity), g_i is a basis element, and w_i is a torque vector composed of shoulder torque and elbow torque, corresponding to each basis element. In training, adaptation is realized by a trial-to-trial update of torque vectors following gradient descent in order to decrease the difference between the actual torque experienced during the movement and the expectation of torque currently predicted by the internal model.

We hypothesized that the bases have a receptive field in terms of the arm's velocity (in joint space) and that the discharge at this receptive field is modulated monotonically as a function of the arm's position; i.e., the elements represent the arm's position and velocity as a gain-field:

$$g(\underline{q}, \underline{\dot{q}}) = g_{position,i}(\underline{q}) \cdot g_{velocity,i}(\underline{\dot{q}})$$
$$g_{position,i}(\underline{q}) = k^T \cdot \underline{q} + b \qquad (3.2)$$
$$g_{velocity,i}(\underline{\dot{q}}) = \exp\left(-\left\|\underline{\dot{q}} - \underline{\dot{q}}_i\right\|^2 \big/ 2\sigma^2\right)$$

Typical output of this basis for various limb positions and movement directions is plotted in Figure 3.1. The position-dependent term is a linear function that encodes joint angles, $\underline{q} = (\theta_{shoulder}, \theta_{elbow})$, while the velocity-dependent term encodes joint velocities. The choice of intrinsic rather than extrinsic coordinates is important because the extrinsic representation of limb velocity cannot account for behavioral data on patterns of generalization (Shadmehr and Moussavi, 2000;Malfait et al., 2002). The gradient vector k reflects sensitivities for the shoulder and elbow displacement, and b is a constant. The direction of gradient vectors is uniformly distributed in joint angle space with 45° increments. A basis function with 0° direction of gradient is sensitive
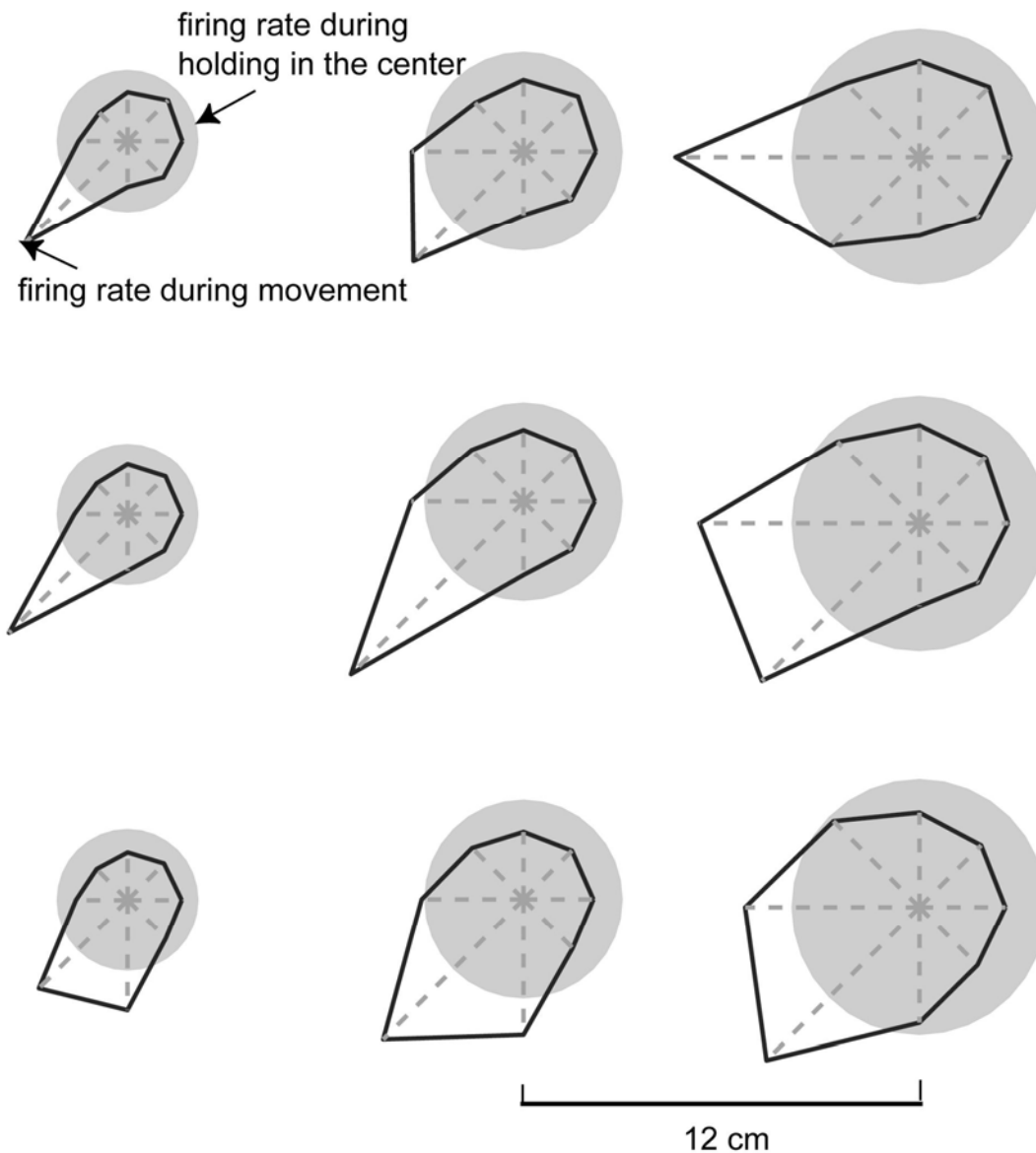
Figure 3.1 A polar plot of activation pattern for a typical basis function in a gain-field model. The polar plot at the center represents . activation for an eight-direction center-out reaching task (targets at 10 cm). Starting point of each movement is the center of the polar plot. The shaded circle represents the activation during a center-hold period and the polygon represents average activation during the movement period. The eight polar plots on the periphery represent activation for eight different starting positions. Each starting position corresponds to the location of the center of each polar plot. The preferred positional gradient of this particular basis function has a rightward direction. The preferred velocity is an elbow flexion at 62°/s.

only to the shoulder angle changes, whereas a basis with a gradient in 90° direction is sensitive

only to elbow angle changes. The velocity-dependent term is a Gaussian function encoding joint

angular velocity ($\dot{\underline{q}}_d$, a 2×1 vector composed of shoulder and elbow joint velocity) centered on

the preferred velocity ($\dot{\underline{q}}_i$).

To fit experimental data, we varied only two parameters of the model: the slope (*k*, magnitude of

a gradient vector) and the constant *(b)* in Equation 3.2. All the other parameters were fixed in the

following manner: (1) the directions of gradient vectors were uniformly distributed from 0° to

315° with a 45° increment; (2) the preferred velocities are uniformly tiled in joint velocity space

with a 20.6°/s spacing and width; (3) the total number of basis elements was equal to the number

of the preferred positional gradients multiplied by the number of preferred velocities because we

used every possible combination of gradient and preferred velocity; (4) random noise was

injected into the torque in the simulated system so that movements in the null field had the same

standard deviation of PE as did the subjects' movements. In exploring the parameter space of *k*

and *b*, we found that 1 rad^{-1} and 1.3 for the slope and constant, respectively, gave a good fit of

generalization as a function of separation distance.

3.2 Simulation of human arm reaching in 2D space

To simulate human arm reaching, we used the following model of the arm's dynamics that

described the physics of our experimental setup (Shadmehr and Mussa-Ivaldi, 1994a). For every

time step (10 ms), we calculate the joint acceleration ($\ddot{\underline{q}}$) using

$$\ddot{\underline{q}} = H(\underline{q})^{-1}\{H(\underline{q}_d)\ddot{\underline{q}}_d + C(\underline{q}_d,\dot{\underline{q}}_d)\dot{\underline{q}}_d - K_p(\underline{q} - \underline{q}_d) - K_v(\dot{\underline{q}} - \dot{\underline{q}}_d) - \hat{\tau}_{env} + \tau_{env} - C(\underline{q},\dot{\underline{q}})\dot{\underline{q}}\} \qquad (3.3)$$

where

$\underline{q}$: a 2×1 vector composed of shoulder and elbow joint displacement.

$\underline{\dot{q}}$: a 2×1 vector composed of shoulder and elbow joint velocity.

H: inertia matrix that varies as a function of joint displacement.

$$H(\underline{q}) = \begin{bmatrix} a_3 + a_1 \cdot l_1^2 + a_4 + 2 \cdot a_2 \cdot l_1 \cdot \cos(q_{elbow}) & a_2 \cdot l_1 \cdot \cos(q_{elbow}) + a_4 \\ a_2 \cdot l_1 \cdot \cos(q_{elbow}) + a_4 & a_4 \end{bmatrix} \qquad (3.4)$$

C: coriolis matrix that varies as function of joint displacement and velocity.

$$C(\underline{q},\underline{\dot{q}}) = \begin{bmatrix} -a_2 \cdot l_1 \cdot \sin(q_{elbow}) \cdot \dot{q}_{elbow} & -a_2 \cdot l_1 \cdot \sin(q_{elbow}) \cdot (\dot{q}_{shoulder} + \dot{q}_{elbow}) \\ a_2 \cdot l_1 \cdot \sin(q_{elbow}) \cdot \dot{q}_{shoulder} & 0 \end{bmatrix} \qquad (3.5)$$

K_p, K_v : spinal and muscle feedback coefficient.

τ_{env} : the actual torque experienced during the movement, followed the rule

$$\tau_{env} = J^T \cdot F_{env} = J^T \cdot B \cdot \underline{\dot{x}}$$

J : jacobian matrix that varies as a function of arm position

$$J = \begin{bmatrix} -l_1 \cdot \sin(q_{shoulder}) - l_2 \cdot \sin(q_{shoulder} + q_{elbow}) & l_2 \cdot \sin(q_{shoulder} + q_{elbow}) \\ l_1 \cdot \cos(q_{shoulder}) + l_2 \cdot \cos(q_{shoulder} + q_{elbow}) & l_2 \cdot \cos(q_{shoulder} + q_{elbow}) \end{bmatrix} \qquad (3.6)$$

$\hat{\tau}_{env}$: estimated torque and calculated using $\hat{\tau}_{env} = \sum_i w_i \cdot g_i(\underline{z})$.

Then, we calculate the joint velocity and position for the next time step by integrating this acceleration. The parameters for this simulation were K_p = [15 6; 6 16] kg^2·m^2/s^2, K_v = 0 .15· K_p, l_1= 0.33 m, l_2= 0.34 m, a_1 = 1.5187 kg, a_2 = 0.3442 kg·m, a_3 = 0.0667 kg·m^2, and a_4 = 0.0968 kg·m^2.

3.3 Experimental setup

Nine healthy individuals (5 women and 4 men) participated in this study. The average age was 27.1 y (range: 21-31 y). The study protocol was approved by the Johns Hopkins University School of Medicine Institutional Review Board and all subjects signed a consent form.

Subjects performed reaching movements in a similar condition as described in the chapter 2. Five subjects participated in the nonlinear position dependent force field experiment and four subjects participated in the hyper-generalization experiment. The nonlinear position dependent force field condition is exactly the same as the previous position dependent force field condition with the 14 cm separation distance except that the order of forces changed into leftward, rightward and null for the left, center and right respectively (Figure 3.7b). The hyper-generalization experiment consists of two phases, training and test phases. During the training phase, subjects made movements at the center and right positions that were separated by 7 cm. Movements in the center were perturbed by the counter-clockwise force field and movements at the right were not perturbed. During the test phase, subjects made movements three times at the left and two times in the center without any force field applied to measure the aftereffects while most of movements were made in the center and right positions with the same force fields as in the training phase (Figure 3.8a).

3.4 Accounting for the Experimental Data with a Model

In internal model that performs function approximations, the force field was represented as a population code via a weighted sum of basis elements. Each element was sensitive to both the position and velocity of the arm. The crucial question was how each element should code limb position and velocity to best account for all the available data on generalization. Previous work

25

had shown that velocity encoding was consistent with Gaussian-like functions (Thoroughman and

Shadmehr, 2000). To account for both our data on adaptation to position-dependent viscous

forces (Figure 2.3) and previous data on generalization across large displacements (Shadmehr and

Moussavi, 2000), we considered both Gaussian and linear encoding of position space. We first

assumed a Gaussian coding of limb position space and assessed the optimal width of basis

elements to fit the data. We were surprised to find that the optimal full width at half-maximum of

each element was approximately 80 cm (standard deviation of Gaussian function, $\sigma = 34$ cm).

This very broad tuning of position space by Gaussian basis elements formed an essentially linear

position-dependent receptive field over a workspace three times the width of the training space.

Because this model produced essentially monotonic encoding of position throughout our training

space and beyond, we decided to study in detail a model with simple linear position encoding.

Indeed, studies of the motor cortex (Georgopoulos et al., 1984;Sergio and Kalaska, 1997),

somatosensory cortex (Prud'homme and Kalaska, 1994;Tillery et al., 1996), and spinocerebellar

tract (Bosco et al., 1996) have found that cells in these areas code limb static-position globally

and often linearly.

One way to represent limb position and velocity is with basis elements that encode each variable

and then add them. However, additive encoding cannot adapt to fields that are nonlinear functions

of position and velocity, e.g., $f(x, \dot{x}) = (x / d) \bullet B\dot{x}$. This is the force field that describes the task

we considered in the previous section. A theoretical study suggests that to adapt to such nonlinear

fields, the basis functions of the combined space must be formed multiplicatively rather than

additively (Pouget and Sejnowski, 1997). We chose to use a multiplicative combination of

position and velocity. Thus, we hypothesized that position and velocity encoding are combined

via a gain-field mechanism; i.e., the bases have velocity-dependent receptive fields and the

discharges in these receptive fields are linearly modulated by arm position (Figure 3.1).
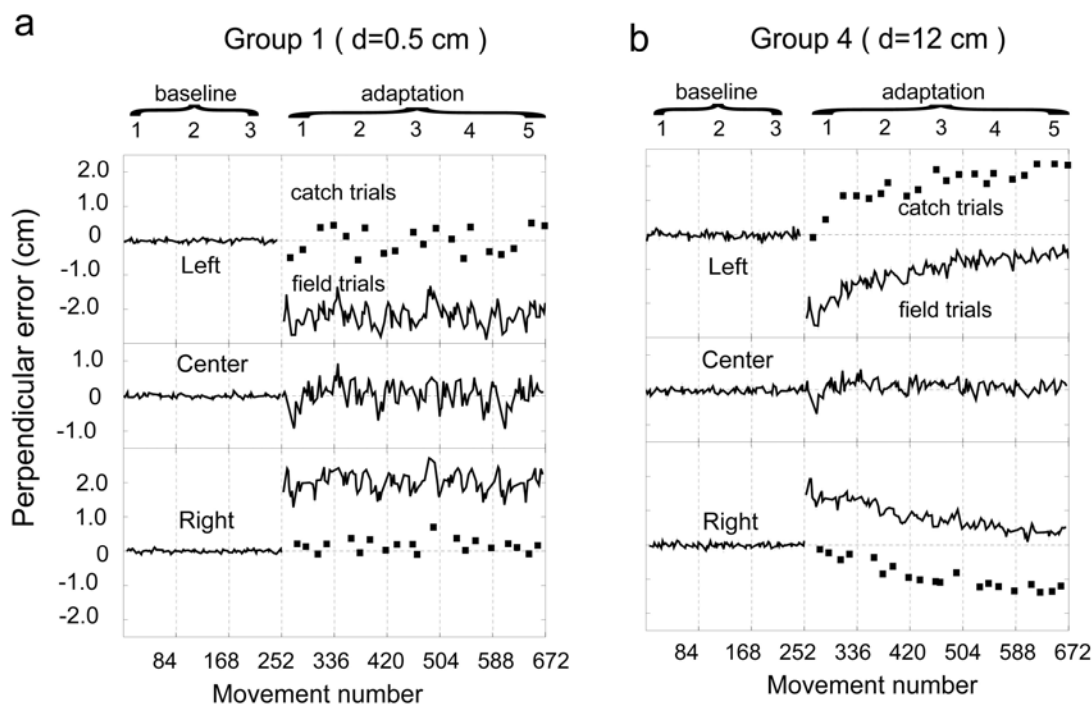
Figure 3.2 Simulation of adaptation to a position-velocity dependent force field. **(a)** The bases were used in an adaptive controller to learn the task in Figure 2.1. Format is the same as Figure 2.3a; correlation coefficient of the simulated to subject data is 0.97. **(b)** Simulated movement errors in an experiment where spatial distance was the same as in Group 4 in Figure 2.3b; correlation coefficient is 0.86.

We found that when a network learned to represent the force field via a gain-field encoding of limb position and velocity, it produced movements that matched the generalization pattern both in the current experiment and in earlier reports. Figure 3.2a and 3.2b shows the time series of errors from the simulated controller in the same format as in Figure 2.3. The learning and generalization indexes are plotted in Figure 3.3a and 3.3b, and when compared to the values calculated from subject data, they show good agreement (correlation coefficient = 0.96 for the learning index and 0.99 for generalization).
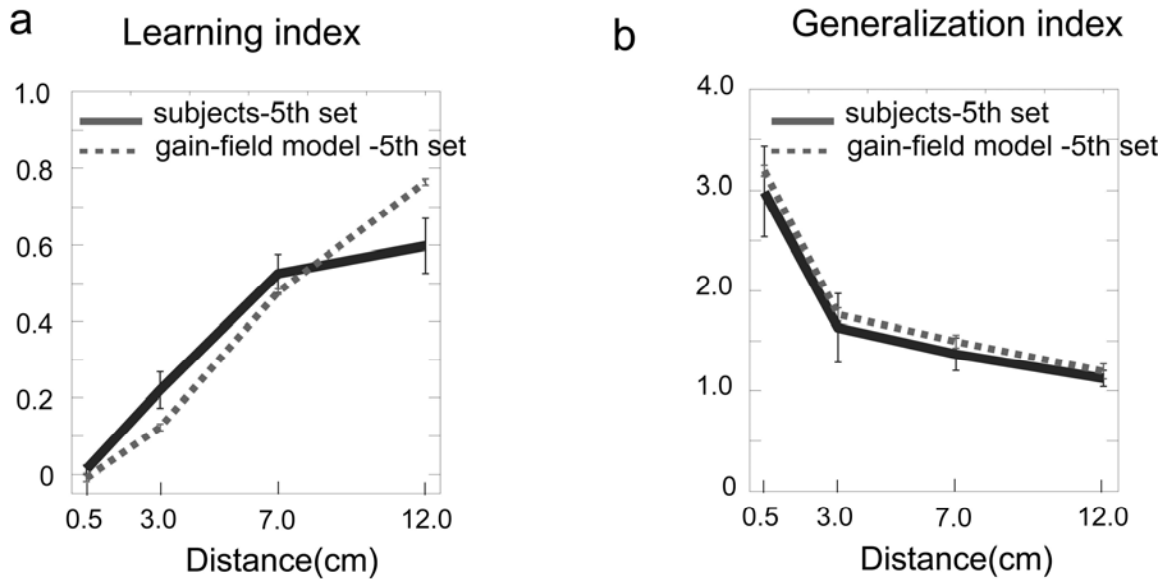
Figure 3.3 Simulated learning performance and generalization index. **(a)** Learning index of the last target set against spatial distance. Dotted lines are from the simulation and thick solid lines are from subjects; correlation coefficient is 0.96. Note that thick solid lines are the same lines as in Figure 2.4a. **(b)** Generalization index in the last target set against spatial distance. Dotted lines are from the simulation and solid lines are from subjects; correlation coefficient is 0.99.

3.5 Why Does Gain-Field Coding Account for the Patterns of Generalization?

We used the data in Figure 2.4b (which shows generalization as a function of spatial location) to estimate the position sensitivity of the basis elements. To explain how this works, we illustrated the process using a model that has only two basis elements and where the basis elements only encode position. We can limit ourselves to two basis elements because the position dependence of our task was restricted to a single dimension. Similarly, because our task only required movements in one direction, we can explain the behavior of the model without including velocity sensitivity. However, while the reduced model is useful in describing the basic principles, we fit the full model to the data. This was for two reasons. First, the actual adaptation requires velocity
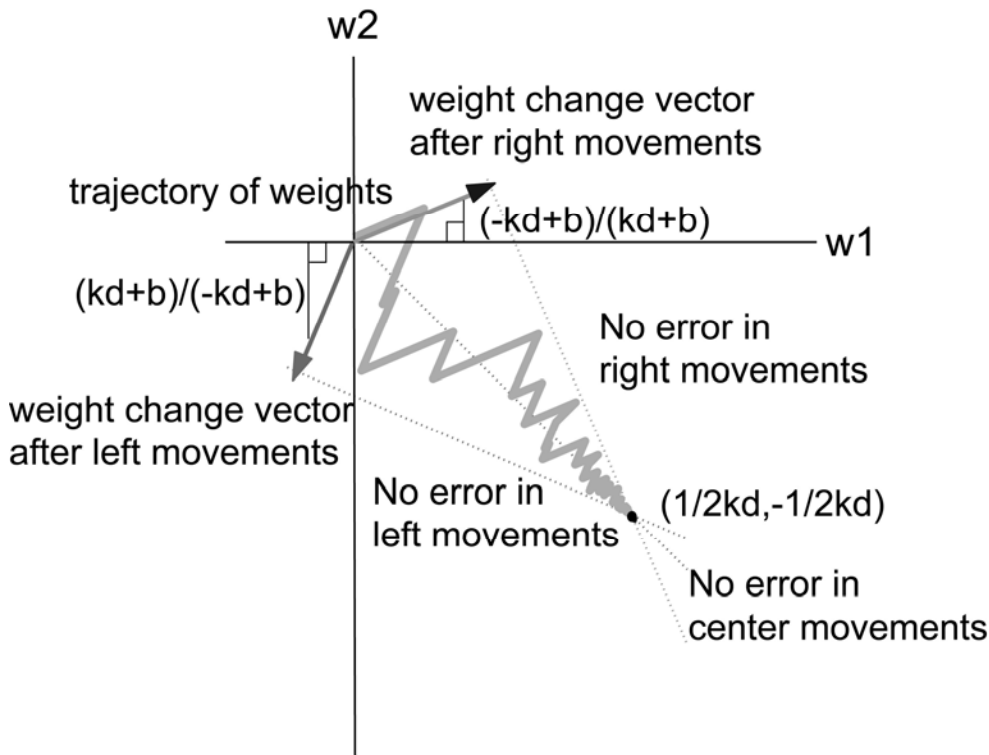
Figure 3.4 Mechanism of adaptation in a gain-field model. A state diagram of weights in a simple system with two basis functions. The trajectory from the origin to ($\frac{1}{2}kd$, $-\frac{1}{2}kd$) shows how weights converge to the final values trial-by-trial. Three dotted lines represent weights for no errors on the left, center, and right movements, respectively. Two vectors represent the direction of weight change after left and right movements each.

coding. Second, the full model is an extension of models used previously (Thoroughman and Shadmehr, 2000;Donchin and Shadmehr, 2002) and we wanted to be sure that the new model could account for all available datasets.

We chose to use hand position *(x)* for a simpler description of the model in this section. However, in the full model, the coordinate system of limb position is in terms of joint angles. In the simple model, the two bases are $g_1(x) = kx + b$ and $g_2(x) = -kx + b$, where x is hand position, k is the sensitivity of the element's output to changes in hand position, and b is the constant. The net expected force is a weighted sum of these two functions, $\hat{f}(x) = w_1 \bullet g_1(x) + w_2 \bullet g_2(x)$, , where

w_1 and w_2 are weights for g_1 and g_2, respectively. After each trial, weights were updated so that

the expected force function ultimately approximated the externally applied force. The applied

forces in the previous section were a linear function of hand position, e.g., $f(x) = x/d$, where d is

the separation distance. When $w_1 = \frac{1}{2}dk$ and $w_2 = -\frac{1}{2}dk$, this field is perfectly approximated by

the bases. Thus, with training, weights were updated to converge to these values. The weight

trajectory from the initial value to the final value is drawn on the state-space diagram in Figure

3.3. Three dotted lines represent weights where the expected force is correct for right, middle, and

left movements, respectively, and the intersecting point of these three lines is the correct weight

for all three positions, i.e., the final value. The amount of weight change after each trial depended

on the force error experienced on that trial and the activation of each basis element on that trial.

Thus, after movements on the right $(x = d)$, w_1 changed more than w_2 because g_1 was bigger than

g_2 for movements on the right, and after movements on the left $(x = -d)$, the opposite was true.

The diagram shows the weight change after right and left movements, respectively, where the

slope of each vector $(\Delta w_2 / \Delta w_1)$ is equal to the ratio $g_2(x)/g_1(x)$; e.g., the slope of the vector is

$(-kd + b)/(kd + b)$ after right movements and $(kd + b)/(-kd + b)$ after left movements. Fast

learning occurred if these vectors were closely aligned to the middle dotted line (slope $= -1$)

because weights can follow a shorter path from the initial to final values. Thus, we can see from

the simple model that a larger k, a larger d, or a smaller b will produce faster learning.

The trial-by-trial variation in the center movements is also clarified by examining this state-space

diagram; i.e., any deviation from the middle dotted line means a nonzero force expectation for the

center movements and larger deviations correspond to larger errors in the center movements.

Thus, update vectors with a slope near -1 lead to both faster learning and smaller variance in the

middle movements. Therefore, the slope k and the constant b are important parameters in our

model that determine the learning rate and the generalization to the center movements. For a

given k and b, the separation distance d will modulate the learning rate and generalization.

We adjusted k and b for the bases to fit the simulation's performance to the generalization observed in subjects (see Figure 2.4b). Figure 3.3 and 3.4 shows good agreement between our simulation and subject data. However, the question is, can this same model with the same parameter values explain other behavioral data?

3.6 Testing the Model on Previously Published Results

The gain-field model could also account for a number of other previously published results. The experiments we focus on here are adapting to a field that depended only on limb velocity and not position (Shadmehr and Moussavi, 2000) and adapting to a field that depended only on limb position and not velocity (Flash and Gurevich, 1997). We found that exactly the same basis elements that fit the generalization pattern in Figure 2.4b also accounted for behavior in these paradigms.

Shadmehr and Moussavi (2000), present an experiment where subjects trained in a position-independent field in one workspace (hand to the far left) and were then tested in a different workspace (hand to the far right). Essentially, the question was, if field $f = 1$ was presented at position $x = d$, what kind of force would be expected at another location? We can predict what will happen by analyzing the reduced model. All the weights that satisfy $w_1(kd + b) + w_2(-kd + b) = 1$ can approximate this force field correctly. However, the slope of the weight change vector, i.e., $(-kd + b)/(kd + b)$, will determine the final weights uniquely as $w_1 = (kd + b)/(2k^2d^2 + 2b^2)$ and $w_2 = (-kd + b)/(2k^2d^2 + 2b^2)$. Thus, the force function approximated by these weights is $\hat{f}(x)$ $= (k^2d \cdot x)/(k^2d^2 + b^2) + b^2/(k^2d^2 + b^2)$. Therefore, the expected force is again a linear function with slope $(k^2d)/(k^2d^2 + b^2)$. This slope decreases as the gain k decreases and the constant b increases.

Importantly, when the trained position d is close to the zero of the coordinate axis, the slope is also close to zero, making the generalization function flat (i.e., global generalization).

In the Shadmehr and Moussavi experiment (2000), subjects trained in a clockwise viscous curl-field ($F = B \bullet \dot{x}$, $B = [0 - 13; 13\ 0]\ N \bullet$ m/s) in the "left workspace" (shoulder in a flexed posture) and were then tested in the same field with the hand in a workspace 80 cm to the right (shoulder in an extended posture). The idea was to see whether there is any generalization of learning from the left workspace to the right workspace. Since the viscous curl-field perturbed the subject's hand in the perpendicular direction of hand velocity, as a movement error, they measured the maximum perpendicular displacement from the straight line connecting start and target position. For a direct comparison, we used the same measure, maximum PE, shown in Figure 3.5a. During the left workspace training, the movement errors decreased (Figure 3.5a). After the training on the left workspace, Shadmehr and Moussavi (2000) tested these subjects in the right workspace. Their errors on the right are significantly smaller than the errors of control subjects, who did not train on the left, indicating a transfer of adaptation from the left workspace to right (Figure 3.5a). When confronted with the same protocol, the bases that had fit out data in Figure 3.5a produced a pattern of generalization across large distances that was quite similar to that of the subjects' generalization (Figure 3.5b; correlation coefficient = 0.89).
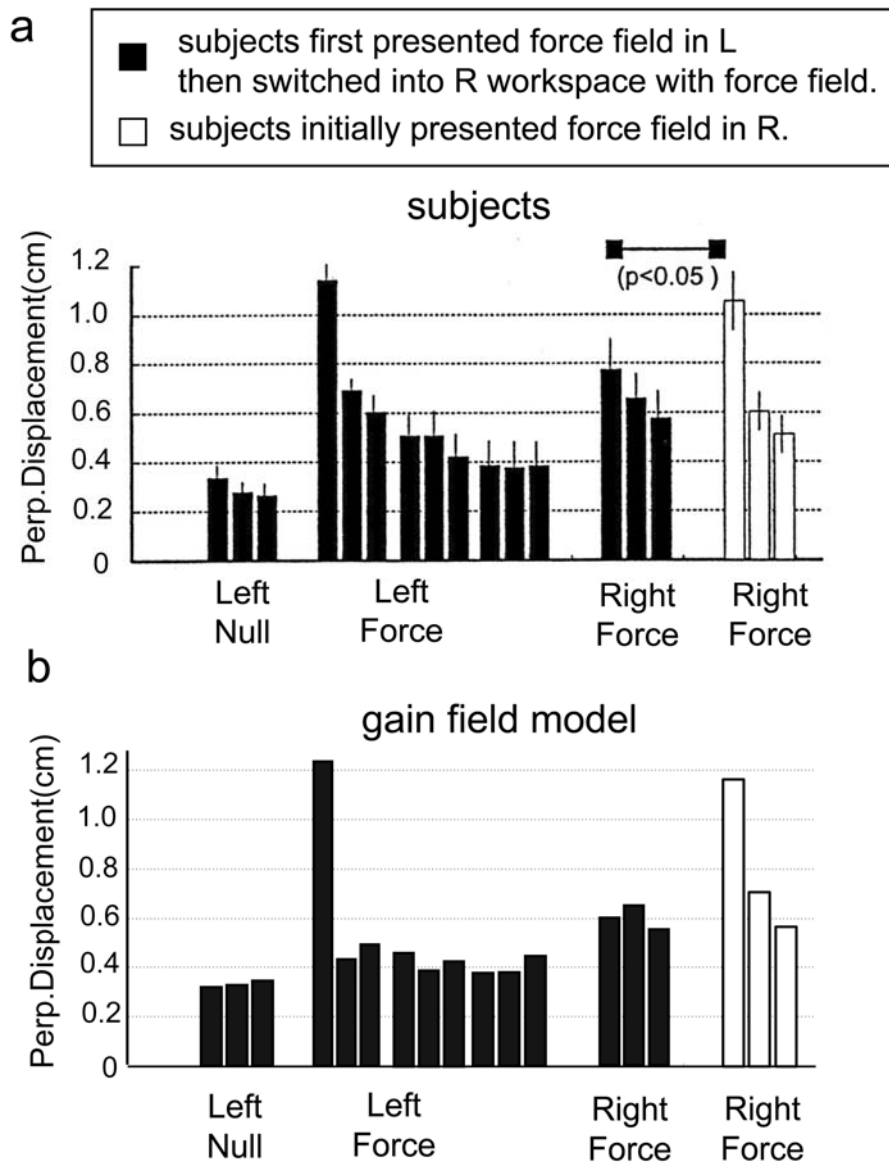
Figure 3.5 Gain-field representation reproduces previously reported patterns of spatial generalization. **(a)** Figure 4A from Shadmehr and Moussavi (2000). The right workspace is separated from the left workspace by 80 cm. Each histogram bar is average maximum PE of 64 movements. Smaller errors of trained group than those of control group at right workspace indicate the transfer of learning from left to right workspace. **(b)** Simulation results in the same format as (a) correlation coefficient to subject data is 0.89.

a

Y displacement (m)

0.5
0.45
0.4
0.35
0.3

-0.1 -0.05 0   0.05 0.1
X displacement (m)

5 N
5 N

b

field trials
baseline

Force field trials in early training

c

field trials
baseline

Force field trials in late training

d

catch trials
baseline

5 cm
5 cm

Catch trials in late training
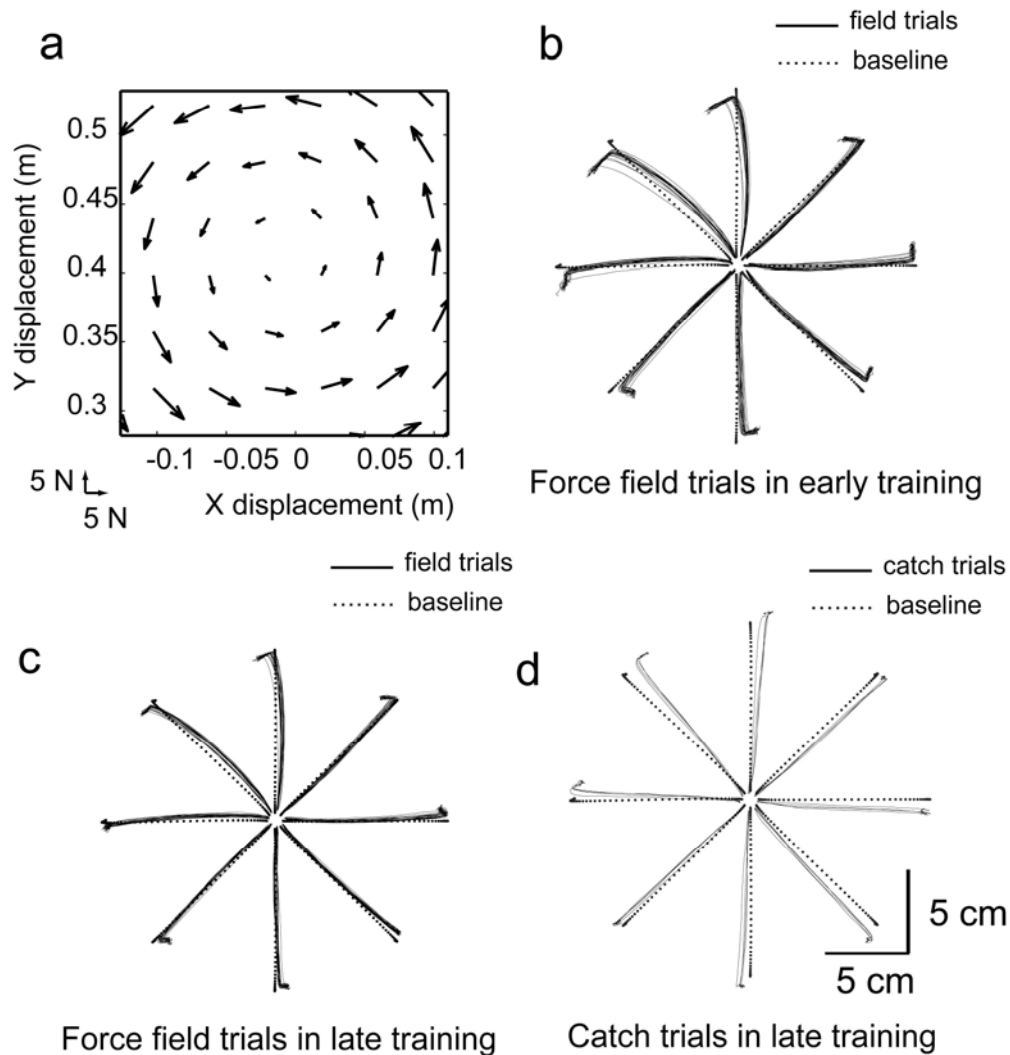
Figure 3.6. Gain-field representation reproduces previously reported learning of spring-like force field. **(a)** A spring-like force field, $\vec{F} = K \cdot \vec{x}$ ($K = [0 \ -55; 55 \ 0]$ *N/m*), was used for simulation. **(b)** Hand path trajectories in field trials from the first set in the spring-like force field. Each set consists of 192 center-out movements. Targets are given at eight positions on 10 cm circumference in pseudorandom order. **(c)** Hand path trajectories in field trials from the fifth set of training. **(d)** Hand path trajectories of catch trials from the fifth set.

It is also known that subjects can adapt to position-dependent spring-like force fields (Flash and Gurevich, 1997;Tong et al., 2002), where force increases linearly with hand displacement. Flash and Gurevich (1997) showed that immediately after the introduction of the force field, the movement trajectories deviated from straight hand paths with large endpoint errors. However, with training, movements became straighter and errors decreased. This was not simply a result of increased stiffness because, when the force field was removed unexpectedly, the trajectories and endpoint errors were on the opposite side of those in the early force field, indicating a proper internal model. Figure 3.6 shows a position-dependent field in this category, and Figure 3.6a-d shows movements made by the simulation as it adapts to this field. This pattern of adaptation is similar to reported values in human data (Flash and Gurevich, 1997).

3.7 Testing the Model's Predictions

Our hypothesis regarding adaptation with a basis that encodes position and velocity as a linear gain-field has two interesting consequences: (1) a change to the pattern of forces can substantially increase the difficulty of a task; and (2) there should be hypergeneralization; i.e., forces expected in an untrained part of the workspace may be larger than the ones experienced at a trained location.

Figure 3.7a shows the pattern of forces that was previously shown to be easily adaptable. Figure 3.7b shows a similar task, where the leftward and rightward forces are separated by the same distance, but instead of making null movements between the left and right positions, null movements are made off to the right of the field trials. The field in Figure 3.7a is learnable by gain-field basis elements. However, if the internal model is indeed computed with such elements, then for the field in Figure 3.7b we can make two predictions: (1) this pattern of forces should not

35
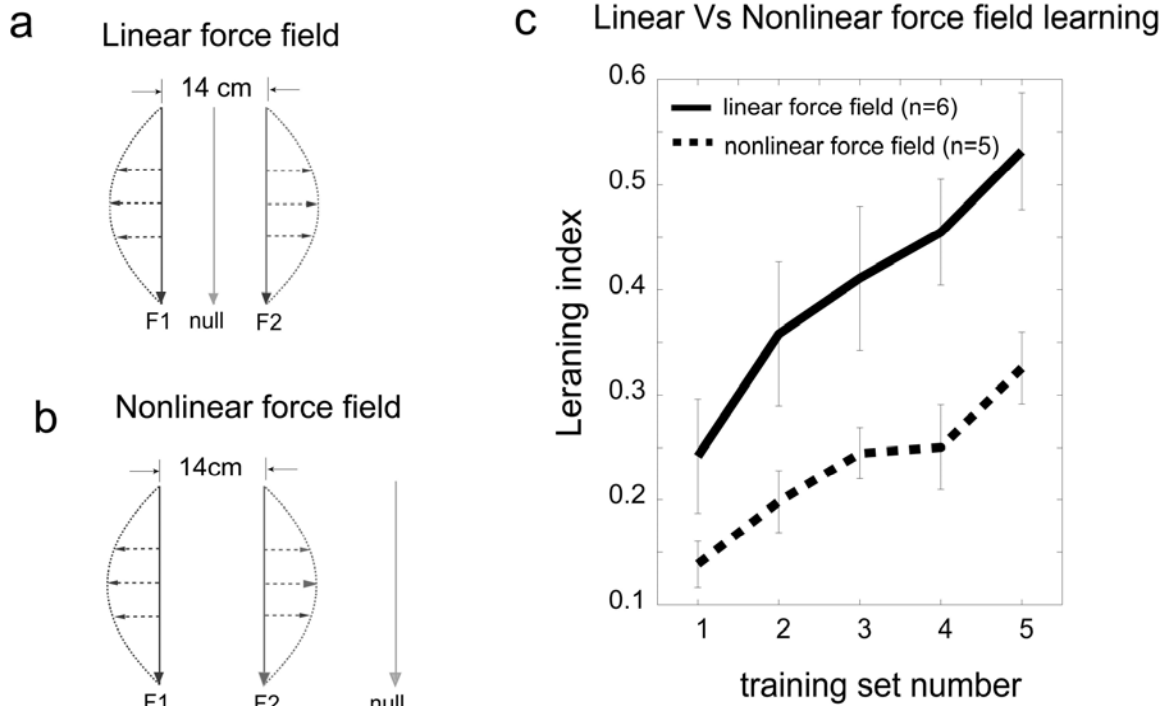
Figure 3.7 Nonlinear pattern of forces is more difficult to learn than linear pattern of forces. **(a)** A field where forces are linearly dependent on both limb position and velocity. **(b)** A field where forces are linearly dependent on limb velocity but nonlinearly dependent on limb position. Gain-field encoding predicts that the field in (B) will be harder to learn than one in (A). **(c)** Learning index of subjects ($n = 6$) for the paradigm in (A) and subjects ($n = 5$) for the paradigm in (B).

be learnable because no linear function can adequately describe this nonlinear pattern of force; and (2) null movements at the "right" should show aftereffects of the center movement despite the fact that no forces are ever present.

We tested these predictions in two separate groups of subjects. Six subjects trained in the force pattern of Figure 3.7a; their performance is shown in Figure 3.7c (part of the same data shown in Figure 2.4a and 2.4b). Five subjects trained in the force pattern of Figure 3.7b; their performance is also shown in Figure 3.7c. As the model predicted, the performance of subjects in the forces of Figure 3.7b was significantly worse than in forces of Figure 3.7a (paired t-test on average

36

learning index across sets: $t = 2.51$, d.f. $= 9$, $p < 0.05$). Recall that movements at the "right" were always in the null field. However, as the model predicted, there was significant generalization here since these movements were significantly biased to the left (t-test: $t = -8.13$, d.f. $= 4$, $p < 0.001$).

An interesting property of systems that learn with gain-fields is that in some conditions, local adaptation should result in an increasing extrapolation, i.e., hypergeneralization. Consider a situation in which, during the training sets, subjects make movements in the center as well as at 5 cm to the right (Figure 3.8a). A counterclockwise curl-field is applied to the center movements, while no forces are applied to movements at right. Because the coding of limb position is linear in the gain-fields, the approximated force function is a linear function that grows from right to left; i.e., the adaptive system should expect larger forces when movements are to the left of center. We tested this in four subjects. During the test set, catch trials were introduced for center movements and occasionally a movement was performed at left (Figure 3.8a). These movements at the left were always in a null field. The catch trials of left movements were significantly larger than those of center movements, which is consistent with the prediction of hypergeneralization (Figure 3.8b; paired t-test: $t = 4.35$, d.f. $= 6$, $p < 0.005$).

One concern is the weak learning during the training sets. However, the average learning index for the center movements in the last set is 0.46, and this is significantly different from zero (t-test: $t = 3.32$, d.f. $= 3$, $p < 0.05$). Considering that the separation distance between null and force field movements is only 5 cm, this learning index is consistent with the learning index curve in Figure 2.4a and consistent with the learning possible with the proposed bases. More importantly, despite this small learning in the training space, we found significantly bigger aftereffects in the test

space, i.e., hypergeneralization. Our simulations suggest that this hypergeneralization could not be due to varying limb inertia and/or stiffness as a function of limb position.
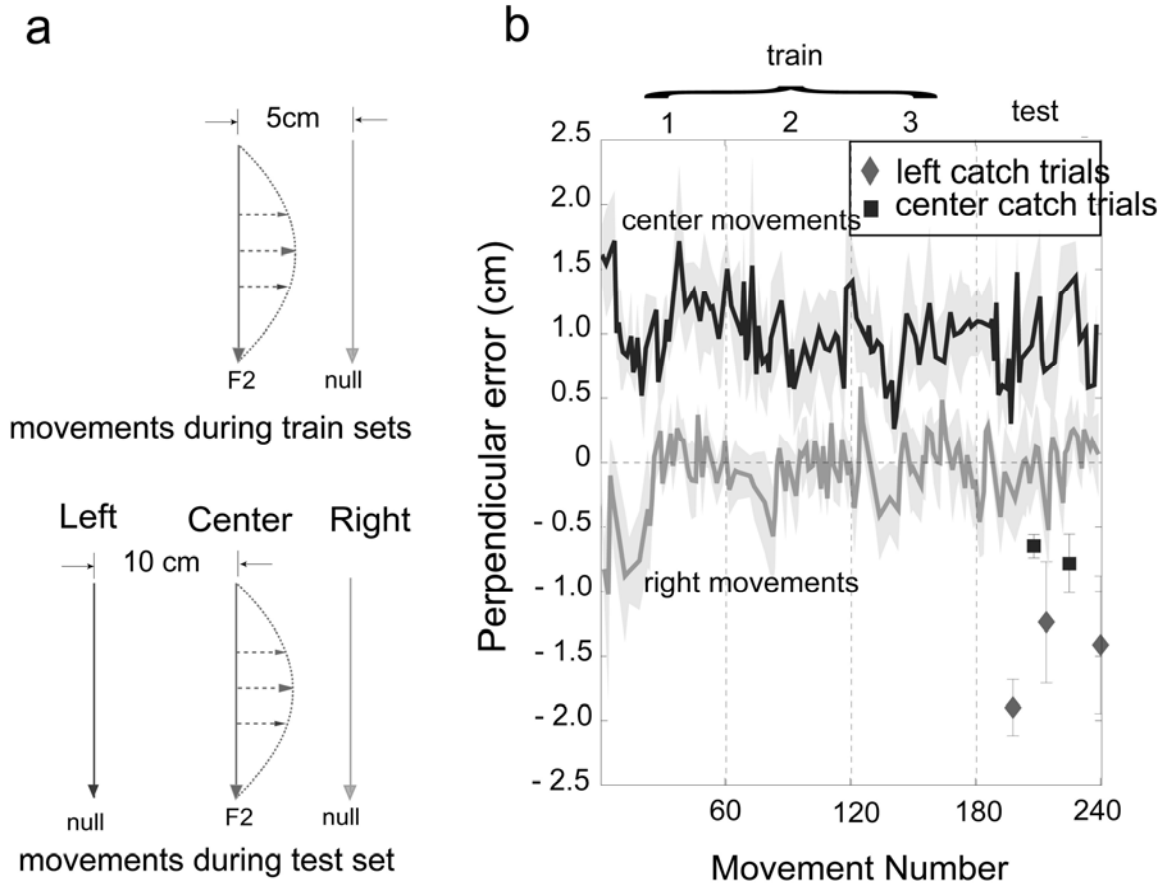
Figure 3.8 Gain-field encoding predicts hypergeneralization. **(a)** The figure shows movements and its associated force field during training and test sets. **(b)** Performance of subjects ($n = 4$) for the paradigm in (a). Dark lines are errors in center movements and gray lines are errors in right movements. The shaded areas represent the SEM. Filled diamonds show the catch trials for the left movements during test set; filled squares show the catch trials for center movements.

3.8 Discussion

We hypothesized that adaptation to arm dynamics was due to an internal model that computed a map from sensory variables (limb position and velocity) to motor commands (force or torque). These elements were sensitive to both the position and velocity of the arm. The main question

was how these variables were encoded. We first performed behavioral experiments to characterize the limits of adaptation to position-dependent forces. This allowed us to quantify the sensitivity of position coding. We found that generalization to neighboring movements decayed gradually with separation distance, implying a very broad position encoding. We found that a Gaussian representation would require a full width at half-maximum of approximately 80 cm to explain our results. Since a Gaussian this broad would be indistinguishable from a monotonic function, we used a linear function instead. A linear basis is a simple monotonic encoding of position space. We combined position and velocity by making position a linear gain-field on the directional sensitivity.

Using a gain-field basis to simulate the learning of arm movements, we found that the parameters that fit our pattern of decaying generalization could also account for a number of previously published results on generalization in position space. These results were the generalization of learning over a large workspace and the ability to learn stiffness fields. Additionally, we tested two behavioral predictions of our model to further test the hypothesis of gain-field coding. Theory predicted that a simple rearrangement of position-dependent forces would change a task from easily learnable to very difficult. It also predicted that in a two-point adaptation paradigm, expected forces would be extrapolated so that larger forces would be expected outside the trained workspace. The behavioral results agreed with these theoretical predictions. Thus, our model used a multiplicative interaction between coding of limb position and velocity to explain behavioral data during learning dynamics of reaching movements and successfully predicted data from a variety of experimental paradigms.

3.8.1 Learning by Population Coding via Gain-Fields vs. Modular Decomposition

Ghahramani and Wolpert (1997) studied similar starting-position-dependent visuomotor mappings in which two opposite visual perturbations were applied to the two starting positions of movements. Subjects learned the two starting-point-dependent visuomotor mappings and generalized this learning to intermediate starting positions using interpolation. Their interpretation of this result was that the brain employs two visuomotor experts, each of which is responsible for one of the two visuomotor mappings, and interpolates to intermediate starting locations using a weighted average of the two experts. If the brain employs this modular decomposition strategy in learning dynamics as well, two of our findings will be hard to explain: (1) learning ability changes with the separation distance between starting positions, although only three experts are required regardless of the separation distance; (2) learning ability decreases when the force field pattern is nonlinear, although the same number of experts (three) is required for both linear and nonlinear patterns.

However, if the internal models for dynamics are represented as a population code with gain-fields, these two factors are easily explained by the proximity of the population code for the close distance and the monotonic change of population code with the starting positions. Gribble and Scott (2002) examined cell responses for three different dynamics conditions: the elbow-joint-dependent viscous curl-field, the shoulder-joint-dependent viscous curl-field, and both joint-dependent viscous curl-fields. In all three conditions, monkeys were trained to the level that the kinematic properties of movements were close to the baseline. Gribble and Scott (2002) found that many cells that responded to one joint-dependent field also responded continuously to the other joint-dependent field, supporting a single controller hypothesis with population coding

rather than separate experts. Therefore, the available data on learning of internal models of dynamics seem to be inconsistent with modular decomposition.

3.8.2 Gain-Field Coding of Position and Velocity

Multiplicative interaction of two independent variables in cell encoding is called gain-field coding. Although we described our gain-field as a velocity-dependent signal that is modulated by limb position, it can also be described as a position-dependent signal that gets modulated by limb velocity. Gain-fields originally described the tuning properties of cells that are responsive to both visual stimuli and eye position in area 7a of the parietal cortex. The receptive field of these cells remains retinotopic while the gain of the retinotopic curve is modulated linearly by eye position (Andersen et al., 1985). This multiplicative response is computationally advantageous because a population of such cells provides a complete basis set for the combined space (Poggio and Girosi, 1990;Pouget and Sejnowski, 1997); i.e., any arbitrary function, linear or nonlinear, in the combined space can be approximated as the weighted sum of these basis elements. Considering that many computational problems in the motor system use both direction of reaching movement and hand position information, it seems attractive to have a complete set of basis functions encoding these two variables. The behavior that we recorded from our subjects is in agreement with the patterns of interference that such bases would produce.

There are other ways to form a basis set. A prominent example is an additive basis set. In an additive set, a function of position is added to a function of movement direction. Some neurophysiological experiments have used this kind of model, rather than a multiplicative model, to relate neural discharge in the motor cortex and cerebellum to limb position and velocity (Fu et al., 1997a;Fu et al., 1997b). However, if limb position and velocity are coded additively, a population of such basis elements cannot approximate the force fields that our subjects learned,

41

e.g., as shown in Figure 2.1b. With an additive basis set, one cannot approximate functions that include a nonlinear interaction between two independent variables, such as multiplication, even if each basis set before combining is complete for each independent subspace (Pouget and Sejnowski, 1997). Simulation results using additive basis elements corroborate this argument, as these simulations showed much less learning than our subjects.

3.8.3 Neurophysiological Findings Related to Our Model

Although our computational model was derived from psychophysical experiments, a number of neurophysiological findings seem to be consistent with properties of our basis elements. First, neurophysiological recordings support our monotonic position encoding in joint angle coordinates. Human muscle spindle afferents, both individually and as a population, represent static joint position monotonically (Cordo et al., 2002). This monotonic position encoding, possibly originating from the property of such peripheral afferents, is consistently found in the central nervous system as well. Georgopoulos et al. (1984) found that the steady-state discharge rate of cells in the motor cortex and area 5 varied with the static position of the hand in two-dimensional space, and the neuronal response surface was described by a plane, indicating that individual cells in these areas encode position of the hand monotonically (and continuously) in space (Prud'homme and Kalaska, 1994;Sergio and Kalaska, 1997). This monotonic response to hand or foot position was also observed in S1 of primates and spinocerebellar neurons of cats (Bosco et al., 1996;Tillery et al., 1996). However, in those studies, it is unclear which variable between hand position and joint angle is an independent input to these cell responses since these two variables are almost linearly related in a small workspace. Scott et al. elucidated this point, showing that neural activity in parietal and motor cortical cells changed when the hand was maintained at the same location but with two different arm orientations (Scott and Kalaska, 1997;,

Scott et al., 1997); i.e., at least parts of the motor cortex seem to encode limb position in joint angle coordinates rather than hand-based Cartesian coordinates.

Another distinct property of our basis elements is that their activity is modulated by both position and velocity. Caminiti et al. (1990) found that as movements with similar trajectories were made within different parts of space, some motor cortical cells' preferred directions changed spatial orientation, indicating that they encoded direction of movement in a way that was dependent on the position of the arm in space. Similar interaction between movement direction and arm posture, wherein cells were directionally tuned but the overall activity levels varied with arm postures, was found in S1 (Prud'homme and Kalaska, 1994). Sergio and Kalaska (1997) studied this interaction more systematically during the static isometric force generation. They found that the overall level of tonic activity of M1 cells varied monotonically with the hand position, and the preferred direction tended to rotate with the hand position in an arc-like pattern. All of this is reflected in the gain-field representation of the bases shown in Figure 3.1.

Lastly, the output of our basis elements is associated with a preferred joint torque vector. With adaptation, these torques rotate. Prud'homme and Kalaska (1994) found that the discharge of M1 cells changed when the monkey compensated for inertial loads. Li et al. (2001) also found similar load-dependent activity changes during adaptation, and for the entire neuronal population, the shift in preferred direction of M1 cells matched the shift observed for muscles. Similar studies by Gribble and Scott (2002) support the idea that the output of elements representing internal models is related to joint torques.

3.8.4 Monotonic Position Encoding

Although we used a linear encoding of limb position because of its mathematical simplicity, data based on three positions are not sufficient to distinguish a linear from a nonlinear basis function. Therefore, at this point, our basis functions are best viewed as having a monotonic property. Monotonic gain-field coding of position and velocity makes an intriguing prediction regarding behavior. When two different forces are experienced at two different arm positions (as in Figure 3.8a), the generalization function is a linear function that connects the two forces at the two positions. Thus, the forces could grow outside the trained workspace. We observed this strange feature of linear gain-fields in the experiment shown in Figure 3.8a. In that experiment, we found that the aftereffects in the movements at a new workspace (left side) were larger than the aftereffects in the trained space (center). This suggests that larger forces were expected at left, an example of hypergeneralization. This raises the concern that with gain-fields, generalization in two-point adaptation might keep growing. However, considering that the reach workspace is bounded and the gain change by the position is very gradual, significantly larger generalization occurs only when trained force fields are specifically position dependent (Figure 3.8a).

Chapter 4

Adaptation and generalization in acceleration dependent force fields

Any passive inertial object that we freely hold in our hand imposes a field of forces on the arm that depends on limb position, velocity, and acceleration. Thus, it is a natural conjecture that the internal model encodes limb position, velocity and acceleration information. In the previous two chapters, we examined adaptation of human subjects to a position-velocity dependent force field and proposed a gain-field model in which each basis element in internal model encodes both limb position and velocity information multiplicatively. However, comparably little is known about the generalization patterns associated with limb acceleration. This is mainly because it is technically difficult to control robots to produce inertial fields. In this chapter, we overcome this technical difficulty by mounting an accelerometer to the robot handle. A pure acceleration dependent force field was implemented to examine how subjects adapt to an acceleration dependent force field and generalize to other directions of movement.

4.1 Hypothesis

In the last chapter, we demonstrated that internal model can be implemented as a function approximation that performs $(\theta, \dot{\theta}) \to \hat{f}$. Here, we expand our model to $(\theta, \dot{\theta}, \ddot{\theta}) \to \hat{f}$ and attempt to infer the sensitivity of the basis elements to limb acceleration. There are two possible scenarios: 1) the basis elements that are sensitive to limb acceleration are not sensitive to limb velocity and the basis elements that are sensitive to limb velocity are not sensitive to limb

acceleration (Figure 4.1b): $\hat{f} = \sum p_{1,i} g_{1,i}(\theta, \dot{\theta}) + p_{2,i} g_{2,i}(\theta, \ddot{\theta})$, and 2) the basis elements that

are sensitive to limb acceleration are also sensitive to limb velocity (Figure 4.1c).

These two scenarios make different predictions about generalization across acceleration space.

Suppose we present a force field that depends solely on acceleration (Figure 4.1a). This is a curl

field in acceleration space (drawn for 1D movements). If one reaches toward a single target, that

movement's trajectory may explore a portion of the space described by the dotted black ellipse.

The task is to learn to predict the forces that are present during this trajectory. An important point

is that for this trajectory, the forces at any given velocity have zero mean. Because of this, in

scenario 1 the velocity sensitive basis elements cannot make a significant contribution to $\hat{f}$.

Rather, learning will be dominated by the acceleration dependent basis elements. Because these

basis elements are also active for movements of similar acceleration but at different velocities,

scenario 1 predicts that adaptation will generalize from the movement that visited quadrants I and

IV (the black dotted ellipse) to movements that visit quadrants II and III (the grey dotted ellipse).

In scenario 2, generalization will be incomplete or absent.

For example, a reach movement toward a given direction visits roughly the same portion of the

position and acceleration space as a reach toward 180° away (in a center-out-and-back

arrangement). Therefore, under scenario 1, adaptation should generalize. Under scenario 2,

adaptation should show incomplete generalization.
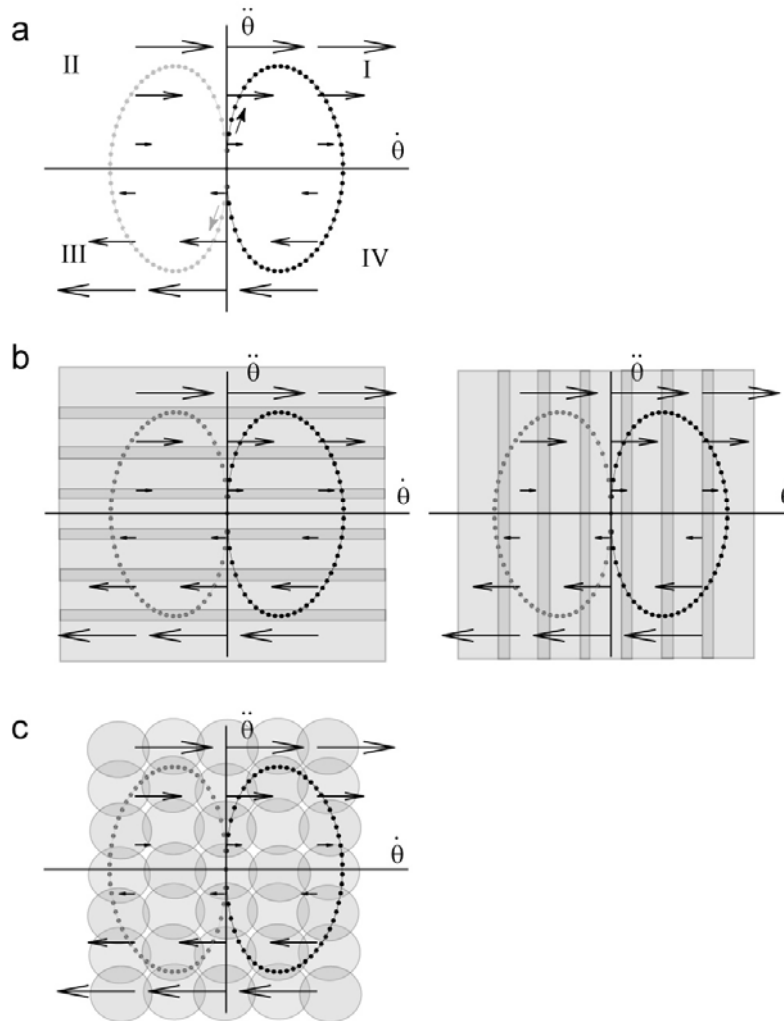
Figure 4.1. Description of the hypothesis for acceleration and velocity encoding. **(a)** The black dots represent the trajectory of a reaching movement toward a single target in the combined space of velocity and acceleration. The grey dots represent a trajectory of a movement to a target in the opposite direction. Arrows represent magnitudes of forces. Note that the field is acceleration dependent so that for points along the trajectory that have the same velocity, forces are zero mean. **(b)** Hypothesis 1: The basis elements that are sensitive to one state variable are not sensitive to another state variable. Each strip elongated along an axis represents a receptive field of a basis element. The darker regions represent overlap of the basis. **(c)** Hypothesis 2: The basis elements that are sensitive to one state variable are also sensitive to another state variable.

4.2 Experimental Setup and Data Analysis

Six healthy individuals (3 women and 3 men) participated in this study. Average age was 25 years (range: 23 to 26 years). The study protocol was approved by the Johns Hopkins University School of Medicine Institutional Review Board and all subjects signed a consent form.

4.2.1 Task

Subjects sat on a height adjustable chair in front of a 2D robotic manipulandum (InMotion2, Cambridge MA) and held its handle. A vertical monitor was placed about 75 cm in front of subjects and displayed a cursor (diameter 3 mm) representing hand position and circles (diameter 10 mm) representing start and target positions of reaching.

The task was to reach to a displayed target (displacement of 15 cm) within 550±50 ms. Feedback on performance was provided immediately after target acquisition as described in chapter 2. Target configuration is shown in the Figure 4.2a. The reaching movements were in an out-and-back pattern. In Figure 4.2a, the targets for the odd number trials are displayed as black arrows. In the even trials, the target always appeared at the center position. The direction of movement in the even numbered trials is displayed with gray arrows in Figure 4.2a.

In some trials, the robot produced forces f on the hand that depended on hand acceleration $\ddot{x}$:

$$f = I\ddot{x}$$

where $I = \begin{bmatrix} 0 & -2 \\ 2 & 0 \end{bmatrix} N \cdot s^2 / m$. Hand acceleration was measured using an accelerometer mounted on the handle (Crossbow Technology Inc). In this field, forces on the hand are always

perpendicular to the hand acceleration vector (as in Figure 4.1a). Figure 4.2b provides an example hand trajectory in this field. The movement is toward 0° (downward). The forces initially push the hand to the right. When the hand reaches peak velocity, forces reverse direction.

4.2.2 Force channel

An important technique was recently introduced by Scheidt et al. (2000) that allows one to directly measure the forces $\hat{f}$ produced by the internal model. Both in the null sets and in the field sets, a force channel is imposed on some trials so that it prevents movements from straying from the straight line that connects the start and end points of the movement. Depending on the strength of the channel walls, one can severely limit the kinematic errors in the trial (in our case, typically around 1mm). To measure $\hat{f}$, we compared the forces that subject produced in the channel trials of the null set $f_{baseline}$ with the forces that were produced in the channel trials of the field set f_{field}. The difference in hand forces was assumed to be the result of adaptation of the internal model:

$$\hat{f} = f_{field} - f_{baseline}$$

In the channel trials, the walls had a stiffness of 1000 N/m and a viscosity of 200 N.s/m. Figure 4.2c shows the hand paths of a typical subject in the channel trial. We measured the forces that the subjects produced during the channel trials using a six degree of freedom load cell mounted at the handle of the robot (Assurance Technology). The forces we present here were post processed with a zero delay ten-point moving average digital filter. Sampling rate was 200Hz.
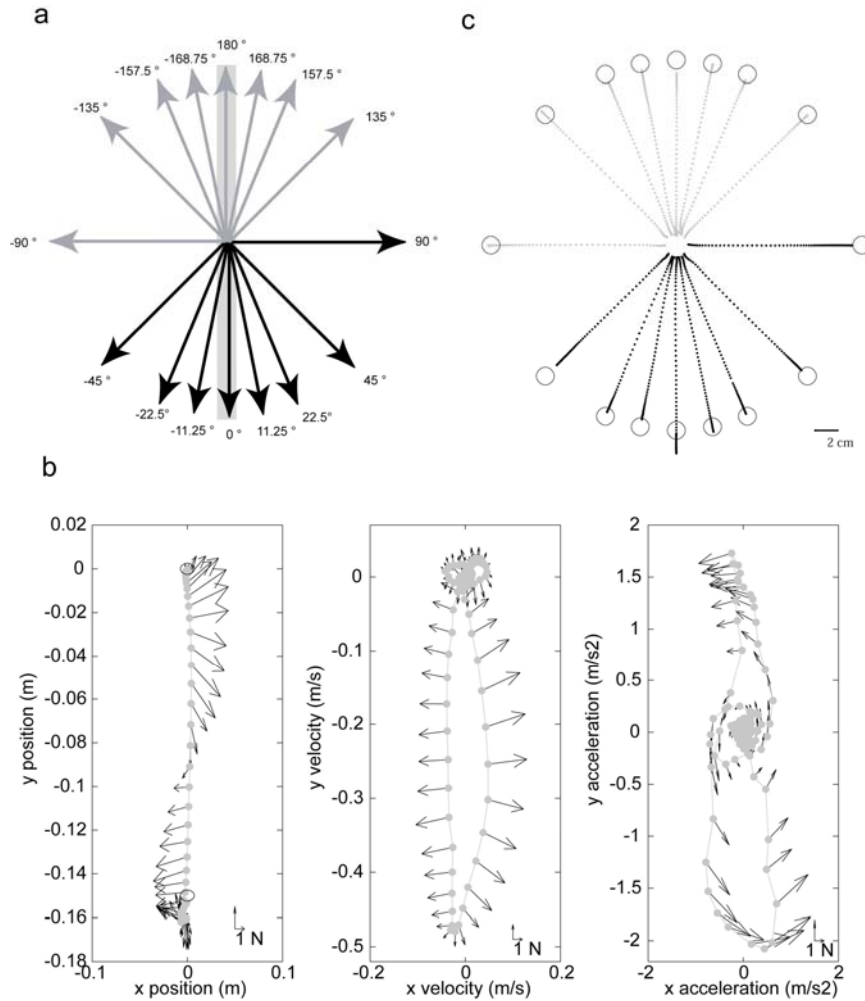
Figure 4.2. Experimental setup to test acceleration dependent force fields. **(a)** The experiment consisted of one baseline (null field) and five force field sets. During the baseline set, the first field set, and the fifth field set, subjects made movements in all 16 directions in a random order. However, center-out movements were always followed by out-center movements. The black lines indicate center-out movements and the grey lines indicate out-center movements. The out-center movements were drawn at the shifted positions for the purpose of illustration. During the second, third and forth field sets, the subjects make movements only in the 0° and 180° directions. **(b)** In field trials, an acceleration dependent curl field was imposed on the hand for movements toward 0°. Representative hand trajectory and the robot imposed forces are plotted here in position, velocity, and acceleration space. The example is from a trial in the last field set. Dots are sampled hand position every 20ms. **(c)** Movements in the force channel. Dots are sampled hand position (200 Hz) from single trials in the force channel from the fifth field set.

4.2.3 Experimental procedure

To familiarize the volunteers with the task, i.e., dynamics of the passive robot and other characteristics of the task, subjects began with four to seven sets of 96 movements in the null field. Once this pre-training was completed, the main experiment began with one set of 96 movements in the null field (baseline set) followed by five sets of 96 movements in a force field. During the baseline set, the first field set, and the last field set, subjects made movements in all sixteen directions. During the second, third and forth field sets, subjects made movements only in 0° and 180°. Movements in all directions except 0° were always performed in the channel. For movements at 0°, the channel was present occasionally (probability of 1/12~1/5). Therefore, the acceleration dependent field acted on the hand only during movements toward 0°. The channel allowed us to quantify generalization of the adaptation to other directions.

4.2.4 Performance measures

An acceleration dependent field makes movements somewhat unstable by forcing the hand to make a spiral path as it approaches the target, making it difficult to terminate a movement. Therefore, one fair measure of performance in an acceleration dependent field is the total path length.

With training, hand path length can improve either because the nervous system learns to predict the environmental forces or because the arm stiffens and better reacts to perturbations in general. To test between these scenarios, we quantified forces that the hand produced in the channel trials. Because the robot imposed forces were known, we calculated the forces subjects needed to produce to fully compensate for the external forces as: $-I\ddot{x}$. We also measured forces that the

subjects actually produced in the channel $\hat{f}$. To compare $\hat{f}$ with $-I\ddot{x}$, we computed three

related measures: a correlation coefficient, a regression coefficient, and a mean squared error.

The correlation coefficient is simply the covariance of the two signals divided by the square root

of the individual variances. However, note that a correlation coefficient will indicate perfect

correlation even when $\hat{f} = -aI\ddot{x}$ and $a \neq 1$. Therefore, in addition to the correlation coefficient

we computed the regression coefficient a:

$$a = \frac{\text{cov}(\hat{f}, -I\ddot{x})}{\text{var}(-I\ddot{x})} = \frac{\text{cov}(\hat{f}, -I\ddot{x})}{\sqrt{\text{var}(-I\ddot{x})} \cdot \sqrt{\text{var}(\hat{f})}} \cdot \frac{\sqrt{\text{var}(\hat{f})}}{\sqrt{\text{var}(-I\ddot{x})}} \qquad (4.1)$$

In addition to the regression coefficient, we computed the mean squared difference between $\hat{f}$

and $-I\ddot{x}$ along a sampled trajectory of the two variables during a movement.

4.3 Kinamatic analysis of adaptation

Figure 4.3a displays representative hand paths from the baseline set (grey dots) as well as a trial

in the first field set (black dots). When no external forces were applied to the hand, the

movement was nearly straight from the start to the end point. As the acceleration dependent curl

field was applied, the movement was initially curved to the right because the hand initially had

positive acceleration. As the movement progressed and the hand decelerated, hand acceleration

became negative and the direction of forces reversed, making the movement come back toward

the straight line and go beyond it. The result was a spiraling hand path. Spirals were consistent

characteristics of this field, as illustrated by the cross-subject averaged hand paths in Figure 4.3c.

Figure 4.3b displays a representative hand path from the last field set (black dots). The movement

became straighter and the spiral at the end clearly decreased. The last movement in the fifth field
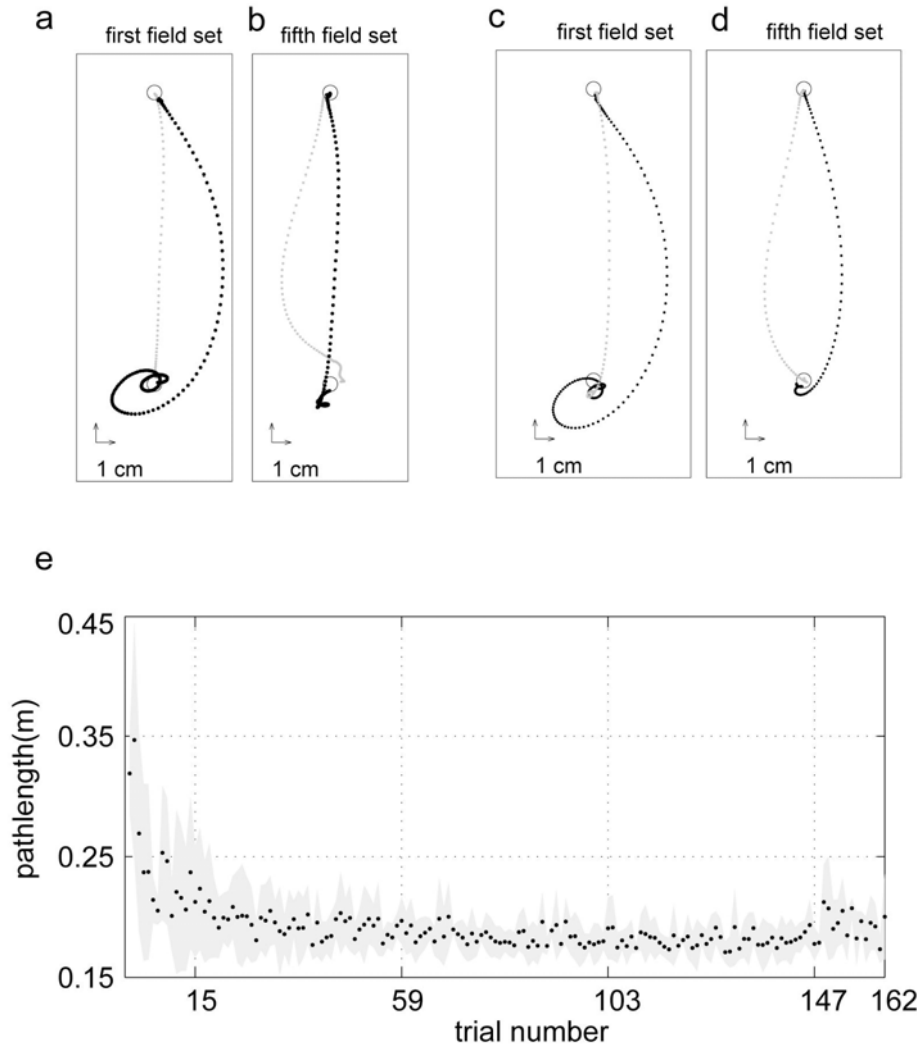
Figure 4.3. Hand trajectories during adaptation to an acceleration dependent force field. **(a)** Hand paths of a typical subject. The grey dots are sampled hand trajectory (200 Hz) in the baseline set (robot motors turned off). Black dots are from a trial in the first field set. **(b)** The block dots are from a field trial in the last set and the grey dots are from a catch trial (final trial of that set). Top circle is the start position. **(c)-(d)** Averaged hand paths across six subjects in the same format as (a)-(b). Movements were aligned to hand position at peak hand speed. **(e)** Across subject averaged hand path lengths as a function of trial number. The shaded area represents the standard deviation. Vertical dotted lines indicate each of the 5 field sets. In the first and last field sets, movements were performed in all 16 directions whereas in the middle 3 field sets, movements were only toward 0° and 180°.

set was a catch trial during which the external force was removed. During this catch trial, the movement was curved in the opposite direction to the movement in the field trial, indicating that subjects predicted some of the forces in the field. However, note that the large loops at the end of the movement in the field trials were not present in this catch trial.

Figure 4.3e displays the averaged path length across six subjects as a function of trial number. The path length gradually decreased with the training. At the end of training (the last force trial), path length was significantly smaller than that at the beginning of the training (the first force field trial) (t-test, t=5.06, d.f.=10, p=2.4×10-4).

4.4 Quantification of adaptation using a force channel technique

Improvement in performance is likely due to both feed-forward mechanisms that associate desired limb states to forces $\left(\theta, \dot{\theta}, \ddot{\theta}\right) \rightarrow \hat{f}$, and feedback mechanisms that learn to better respond to errors that are sensed online. We interspersed channel trials during the field sets to quantify the feed-forward forces. In the channel, the maximum deviation from a straight line was 1.4 ± 0.3 mm (mean+/-SD of maximum deviation across the 6 subjects). Because the channel minimized kinematic errors perpendicular to the movement direction, the forces at the hand could not be due to online compensation of kinematic errors.

Figure 4.4a shows the forces $\hat{f}$ that a subject produced in the first and last channel trials in the field sets. Two field trials preceded the first channel trial. In the first channel trial, $\hat{f}$ in this subject begins by pushing to the left, but at halfway into the movement (near peak velocity), the forces are near zero. By the end of training, $\hat{f}$ is now very similar to the forces in the acceleration dependent field.
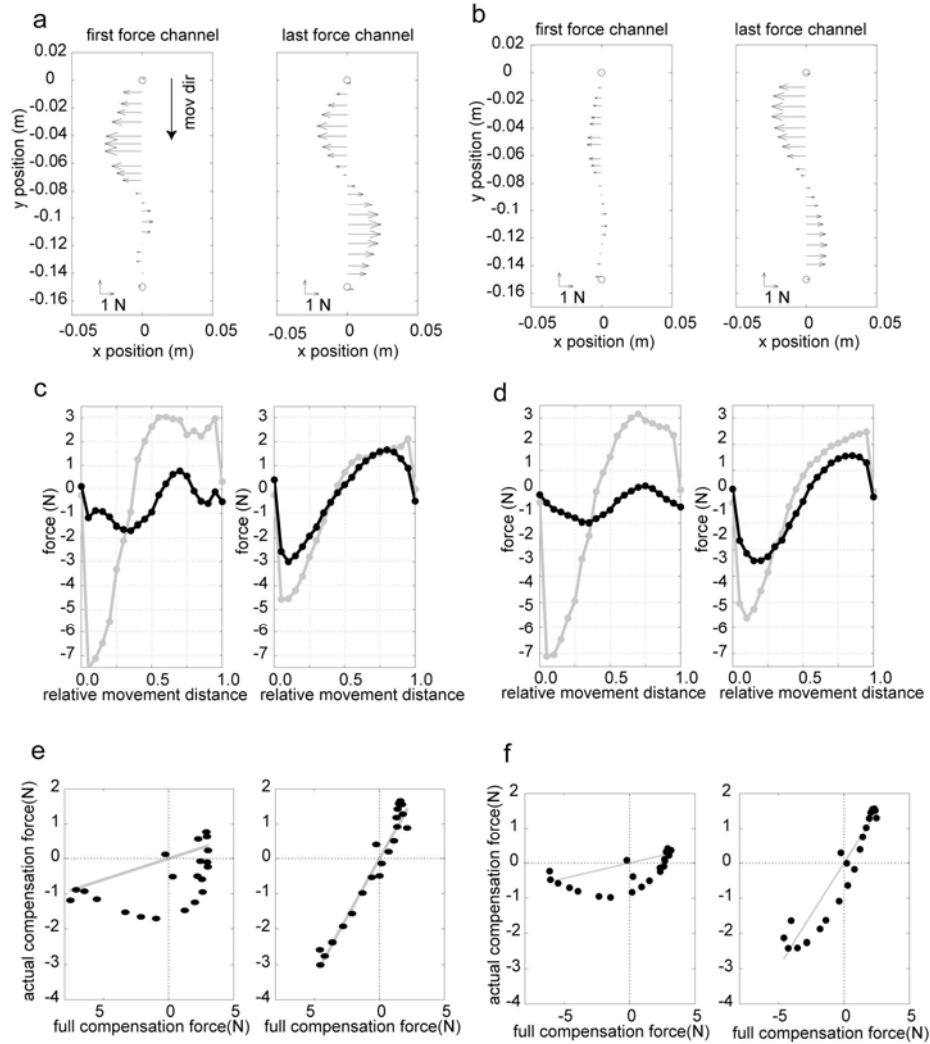
Figure 4.4. Forces that subjects produced in the channel trials for movements toward target at 0°.

(a) $\hat{f}$ produced by a typical subject in the first and last channel trials plotted as a function of hand position between start and end of the movement. **(b)** Across subject averaged $\hat{f}$ for the first and last channel trials. **(c)** Comparison of forces produced in the channel trials $\hat{f}$ and forces required for compensation of the field $-I\ddot{x}$. $\hat{f}$ (black trace) produced by a typical subject as a function of movement displacement in the first and last channel trials. The grey trace is $-I\ddot{x}$. **(d)** Averaged $\hat{f}$ and $-I\ddot{x}$ across six subjects. **(e)** The linear regression between $\hat{f}$ (y-axis) and $-I\ddot{x}$ (x-axis) in the first and last channel trials. The data are for the two trials in (c). **(f)** The linear regression for the averaged data shown in (d).

55

That is, this subject produced forces that pushed initially to the left and then at middle of the movement switched and pushed to the right. Figure 4.4b shows the average $\hat{f}$ across six subjects in the first and last channel trials. Little compensation is present in the first channel trial. However, in the last channel trial a clear acceleration-like force pattern is present. These data demonstrate that subjects learned to predict the acceleration dependent curl force pattern.

We examined how well $\hat{f}$ matched the theoretical force $-I\ddot{x}$ required to counter the robot imposed field of forces. For each channel trial, we considered 21 evenly spaced points along the movement direction. The black line in Figure 4.4c is $\hat{f}$ for a single subject in a typical trial. The grey line is the quantity $-I\ddot{x}$. (The data for the black line in Figures 4.4c and 4d are same as the data in Figures 4.4a and 4b.) In the first channel trial, $\hat{f}$ did not match the estimated external forces very well. However, in the last channel trial, $\hat{f}$ was more similar to the external force. Figure 4.4d shows the cross-subject averaged $\hat{f}$ and $-I\ddot{x}$ for the first and last trials. With training, the forces that subjects produced in channel trials approximated what was need to counter the field.

Figure 4.5a shows the correlation between $\hat{f}$ and $-I\ddot{x}$ for each channel trial, averaged across subjects. By the end of training the two variables were highly correlated (r=0.89±0.04) and the measure appeared to plateau by the second training set. Because correlation is insensitive to linear dependence between the variables, a large correlation is indicative of a high similarity between the shapes of the waveforms but not necessarily a match between the absolute values of the waveforms. We therefore computed a regression coefficient a (Equation4. 1), where $\hat{f} = -aI\ddot{x}$. In the beginning of training, a was close to zero but it gradually increases to about 0.6 by the end of training. The data in Figure 4.5b indicates that the rise time for a was somewhat
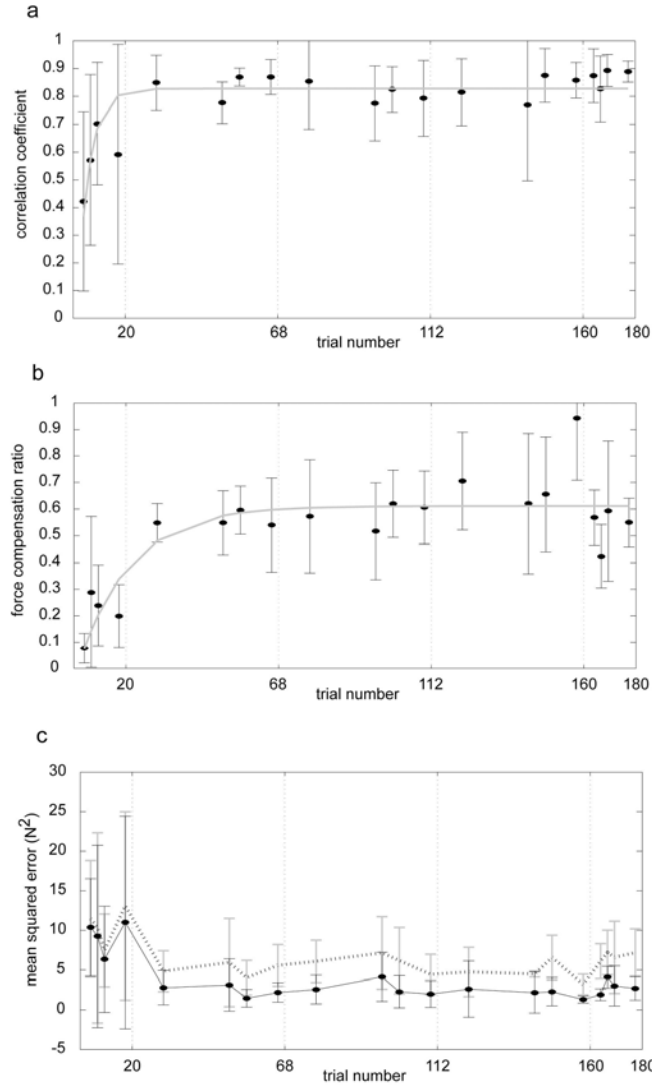
Figure 4.5. Evolution of compensation forces during adaptation to an acceleration dependent force field. **(a)** Correlation coefficient between of forces produced in the channel trials $\hat{f}$ and forces required for compensation of the field $-I\ddot{x}$, averaged across subjects, plotted as a function of trial number. Error bars are standard deviations. Each dot indicate the channel trial in that set. The solid line is an exponential fit to the data: $b(1-e^{-a(x-1)})$ where x is the trial number. a=0.29 and b=0.83. **(b)** Slope of the linear regression. The solid line is an exponential fit to the data: $b(1-e^{-a(x-1)})$. a=0.067 and b=0.61. **(c)** Mean squared errors. The solid line is $mean(\sum(-I\ddot{x}-\hat{f})^2)$ and the dotted line is $mean(\sum(-I\ddot{x})^2)$.

slower than the correlation coefficient. Figure 4.5c plots the mean squared difference between $\hat{f}$

and $-I\ddot{x}$ (solid line). The dotted line indicates the expected difference when there is no

compensation for the field, i.e., $\hat{f} = 0$. The ratio between the solid and dotted line is a decreasing

function (not shown) that starts at 1 and plateaus near the middle of the third set to around 0.4.

This implies that by the end of training, $\hat{f}$ compensated for around 60% of the external forces.

Thus, the various measures suggested that $\hat{f}$, the feed-forward component of adaptation, was

highly correlated with the time-dependent waveform of the external forces but ultimately

compensated for only about 60% of these forces. Because the various measures converged in the

second or third sets, it is unlikely that further training will have significantly changed this

incomplete compensation.

4.5 Generalization across movement direction

We next examined how learning an acceleration dependent field in one direction was generalized

to other directions. Figure 4.6a shows $\hat{f}$ for all sixteen directions during the last set of training.

During this last set, all movements were performed in the channel except for some trials in 0°

where the acceleration dependent field was present. Figure 4.6a shows that in directions near the

training direction, there are acceleration dependent force patterns but this generalization decayed

quickly with angular distance. To quantify generalization, we computed the regression

coefficient (Eq. 1) between $\hat{f}$ and $-I\ddot{x}$ for each movement direction. Figure 4.6b shows this

measure for all sixteen directions. Generalization decayed quickly with the angular distance. Only

in directions -22.5°, -11.25°, and 11.25°, significant amount of generalization was observed (t-test,

p<0.01). Beyond ±45°, there is no significant generalization.
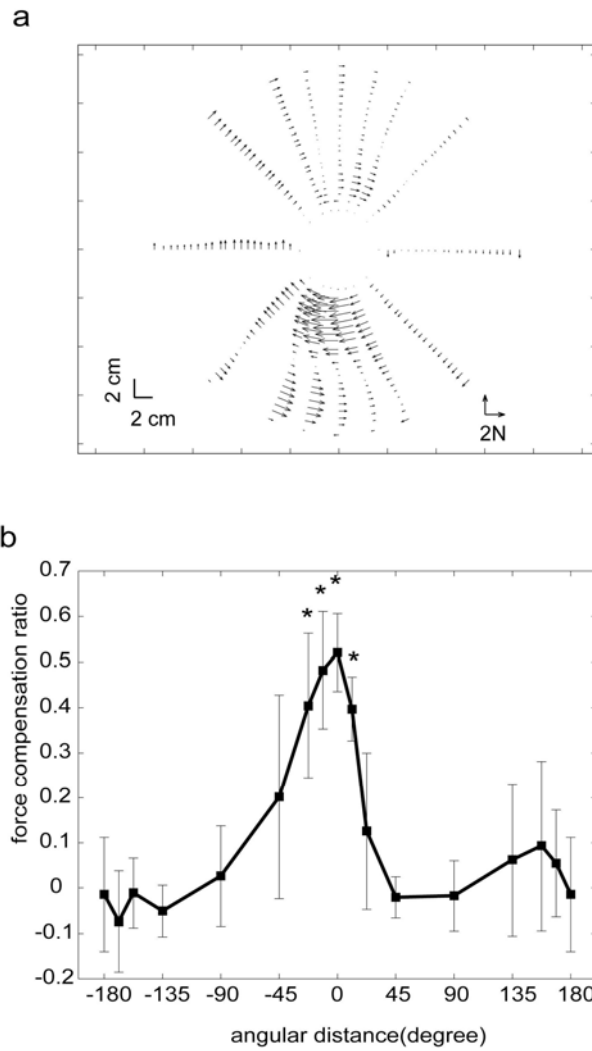
Figure 4.6. Generalization of the acceleration dependent field. **(a)** Across subject averaged $\hat{f}$ recorded in force channels plotted as a function of displacement. The trained direction is for the downward movement and all other movements are measures of generalization. The data comes from the last set of training. **(b)** Generalization as a function of angular distance of the movements in the last training set. The measure is regression coefficient (Eq. 1) between $-I\ddot{x}$ and $\hat{f}$ in the last training set. Error bars are standard deviation. * indicates that the measure is significantly different from zero (p<0.01).

Note that there is no generalization in the 180° direction although this movement experiences nearly the same acceleration and deceleration as the 0° direction. If learning were with two separate groups of basis elements, one that was sensitive to limb acceleration and one that was sensitive to limb velocity (hypothesis 1), then subjects should have learned a pure acceleration and force relationship and there should be near perfect force compensation for 180° direction. Instead, subjects seemed to have learned a more specific mapping, i.e., force as a function of all available arm states including arm acceleration, velocity and position, consistent with the hypothesis 2.

4.6 Discussion

We examined adaptation of reaching movements in a force field that depended exclusively on hand acceleration. Our first result was that in force channels that prevented the hand from moving outside of a straight line, the adapted system produced forces at the hand that closely approximated the acceleration dependent external forces along the entire hand trajectory. This is a crucial prediction of the hypothesis that the CNS learned a map that associated states of the limb to forces, i.e., an internal model that computed $\left(\theta, \dot{\theta}, \ddot{\theta}\right) \rightarrow \hat{f}$. Our second result was that when this map was learned for movements toward a given direction it generalized locally to ±45°. Importantly, adaptation did not generalize to 180°. Because movements to 180° visit nearly the same acceleration space as the trained movements but at very different velocities, the lack of generalization suggests that the basis elements that form the internal model cannot be separated in to groups that are exclusively sensitive to limb acceleration but not velocity. Instead, it agrees with our second hypothesis that the basis elements are sensitive to both acceleration and velocity. Indeed, the sensitivity to limb velocity is the dominant factor.

Traditionally, adapting to altered dynamics of reaching has been assessed by examining change in kinematic features of reaching. Uncompensated dynamics tend to displace the hand from a straight line trajectory to the target, and with adaptation this displacement declines in field trials while the displacement increases in catch trials. Here we found that in an acceleration dependent field, movements became straighter and clear after effects existed. It is possible that this improvement was due to formation of an internal model that mapped desired states of the limb to forces $\left(\theta, \dot{\theta}, \ddot{\theta}\right) \rightarrow \hat{f}$.

Alternatively, performance improvements might have occurred because of adaptive changes in arm compliance (Burdet et al., 2001) or because of adaptive changes in how the CNS responded to kinematic errors that occurred during a movement (Wang et al., 2001). For example, in an acceleration dependent field where forces change direction at maximum hand speed, it is possible that subjects learned to predict only the forces that were present during the initial part of the movement and then relied on feedback-error measures to correct for the forces that were present in the later part of the trial. This strategy is particularly relevant in acceleration dependent fields because the main effect is a spiraling of the hand near the target. Increased stiffness of the arm as it nears the target is a potential strategy for improving control. This strategy does not involve learning to predict an acceleration dependent force pattern and yet could account for both the improved straightness and the after effects of training. Indeed, the trajectories in catch trials did not show the consistent spiraling pattern near the target that we had observed in field trials. Therefore, kinematic analysis of field and catch trials could not provide strong evidence that the CNS learned to predict the acceleration dependent forces.

The internal model theory assumes that the CNS learns to associate desired states of the limb with forces. Therefore, if the limb follows the desired state trajectory, the force $\hat{f}$ produced by the

subject should predict the external dynamics. Scheidt et al. (2000) pioneered the use of a force

channel to directly measure $\hat{f}$. In a force channel, changes in limb stiffness or improved error

feedback control can not produce field-specific changes in hand forces because hand position

does not deviate significantly from a straight line (presumably the intended trajectory). Scheidt et

al. (2000) demonstrated that in a velocity dependent field $\hat{f} \approx f(\dot{\theta})$. Here we used their

approach and measured $\hat{f}$ when the field was somewhat more complex and depended on

acceleration. We found that with practice, $\hat{f}$ became highly correlated with $f(\ddot{\theta})$. Therefore,

the data appeared in agreement with a crucial prediction of the hypothesis that during adaptation,

the CNS learned to compute a map $(\theta, \dot{\theta}, \ddot{\theta}) \rightarrow \hat{f}$ that approximated $f(\ddot{\theta})$.

However, the regression coefficient between $\hat{f}$ and $f(\ddot{\theta})$ saturated around 0.6. This implies

that the "feed-forward" motor commands learned for only 60% of the external force. .

Subjects experienced the acceleration field only for movements to a single target. Movements to

all other target directions were in a channel. This allowed us to directly measure the

generalization pattern from the trained region of the limb state space to neighboring regions. We

found a generalization pattern that quickly decline with angular distance. This is similar to the

generalization patterns in a field that depended on both acceleration and velocity (Sainburg et al.,

1999). Therefore, the limited generalization pattern was independent of whether the field was

acceleration dependent or dependent on both acceleration and velocity. Importantly, we did not

observe any significant generalization to movements at 180° away from the direction of training.

This lack of generalization may be due to two reasons. First, movements at 180° include the

same accelerations as the trained movements but in reversed temporal order. Second, movements

at 180° involve very different limb velocities than movements in 0°. (In our experiment design,

movements at 180° visit precisely the same limb position and limb acceleration space of

movements at 0°). Therefore, lack of generalization may have been due to difference in the temporal order in which the states were visited in the trained and test movements or the difference in limb velocity.

The temporal order difference is unlikely because movements made in straight lines generalize to circular movements (Conditt et al., 1997;Conditt and Mussa-Ivaldi, 1999). This suggests that as long as the states of the two movements are similar, the temporal order in which those states are visited generally does not affect generalization. Furthermore, note that the accelerations experienced at the same velocity in straight and circular movements are very different. Despite that, the velocity dependent force field learned in straight line movements were generalized to the circular movements as if subjects learned a velocity dependent force field in the circular movements (Conditt et al., 1997). Thus, the receptive field of the basis elements must be relatively wider with respect to acceleration than with respect to velocity. This suggests that the lack of generalization to 180° was due to the difference between those two movements in velocity space.

Our results reject the hypothesis that the internal model has basis elements that specialize in one limb state (acceleration) but not the other (velocity). Instead, the basis elements probably encode all state variables in a combined way. For example, a previous study suggested that the basis elements encoded position and velocity multiplicatively (Hwang et al., 2003). Similarly, the basis elements in the internal model might encode acceleration with other variables in a multiplicative or some other nonlinear fashion.

Several neurophysiological studies have reported that no cell or only a small population of cells in both the peripheral and central nervous system have activities correlated with limb acceleration (Ashe and Georgopoulos, 1994;Hasan, 1983;Hasan and Houk, 1975;Matthews, 1981). This might

result if cells respond to all sensory information in a nonlinear way. For example, a common representation of position, velocity, and acceleration of the limb in muscle spindles is with firing rates that encode these variables multiplicatively (Hasan, 1983). In this scenario, the response during a point-to-point reach appears more correlated with velocity than acceleration.

Chapter 5

Bases whose properties resemble muscle spindle responses

The implementation of the internal model has been theorized to be via basis elements, each encoding some aspect of the limb's sensory state (Thoroughman and Shadmehr, 2000;Donchin et al., 2003). The tuning function of basis elements can be inferred by examining how learning a new sensorimotor transformation in one region of space is generalized to another region. Typically, the shape of the tuning function is assumed to be one of the special functions, e.g., Gaussian, cosine or linear function, and the generalization pattern predicted by each special function is compared to the actual human behavior. For example, in chapter 3, we showed that the tuning function of basis elements is Gaussian in the velocity space and its amplitude is linearly modulated by arm position (so called "gain-field"). Although the tuning function chosen from the special functions gives insight into the computational structure of the internal model, and appears to match behavioral results, its physiological basis remains to be shown.

Because the coordinates of the bases are in intrinsic coordinates of the limb, then a likely representation may be those of muscle spindles (Shadmehr and Moussavi, 2000;Malfait et al., 2002). In this chapter, we hypothesize that the bases that form the internal model code the desired state of the limb with functions that are similar to the tuning functions found in muscle spindles. The idea is that in the internal model, the neural representation of desired limb states would be similar to the neural response of the sensory system when the desired states are achieved. We

derive a set of basis functions using a mathematical model of spindles and using these bases, simulate learning of position, velocity, and acceleration dependent force fields, respectively.

5.1 Muscle spindle model

Several studies proposed mathematical models for muscle spindle response (Houk et al., 1981;Lin C.K. and Crago P.E., 2002;Schaafsma et al., 1991;Poppele and Boyd, 1970). Among those, a model that is based on the physical properties of muscle fibers, i.e., tension-length relationship, fits well not only the passive stretch responses but also the active motion evoked responses (Hasan, 1983;Prochazka and Gordon, 1998). In this model, a spindle responds to muscle length change in a way that its response is not separable as a linear combination of independent position- ,velocity- or, acceleration-encoding components (Hasan, 1983). The model divides the spindle into two physically different zones, non-sensory zone and sensory zone. The complex response of muscle spindles can be attributed to a nonlinear relationship of tension and length of the non-sensory part of muscle spindle ($y(t)$) and its first derivative ($\dot{y}(t)$) as shown in equation 5.1. On the other hand, tension at the sensory zone is a simple spring as indicated in equation 5.2.

$$f(t) = k_1 \cdot (y(t) - c) \cdot (1 + (\frac{\dot{y}(t)}{a})^{1/3}) \qquad (5.1)$$

$$f(t) = k_2 \cdot z(t) \qquad (5.2)$$

Combining these two equations and the relationship $x(t) = y(t) + z(t)$ reduces the problem into a single differential equation that describes the relationship between total muscle spindle length $x(t)$ and the sensory zone length $z(t)$ as shown in equation 5.3. Note that $b = (k_1 + k_2)/k_2$. The receptor potential of spindle is linearly proportional to the sensory zone length $z(t)$ while the firing rate $g(t)$ is a linear combination of the receptor potential and its first derivative (equation

5.4). This does not mean that the firing rate of muscle spindle is a linear combination of total

muscle spindle length and velocity since the sensory zone length is not the same as the total

spindle length. Instead, length of the sensory zone, the solution of the differential equation, is a

complex combination of the muscle spindle length and its derivatives as indicated by equation 5.3.

$$\dot{z}(t) + a\left(\frac{bz(t) - x(t) + c}{x(t) - z(t) - c}\right)^3 = \dot{x}(t) \qquad (5.3)$$

$$g(t) = h \cdot z(t) + p \cdot \dot{z}(t) \qquad (5.4)$$

A wide range of spindle responses can be reproduced by varying the three parameters, a, b, and c

in equation 5.3 (Hasan, 1983). For example, Hasan (1983) suggested a=100, b=100 and c=-25 for

the static-γ neuron activated primary ending response and a=0.1, b=250, c=-15 for the dynamic-γ

neuron activated primary ending response. Note that it is the history of the muscle length, not

simply muscle length or its derivatives at a certain time point, that determines the response of

spindle. Thus, the response could be different for the same state of muscle length and its

derivatives depending on how those states are achieved, i.e., the history of the trajectory.

5.2 Spindle-like basis set

The spindle response from the above model is for the 1D muscle length change. Thus, to compute

the spindle response for a whole arm movement, it is necessary to transform the multi-

dimensional movement trajectory to one dimensional spindle length history. For a given point-to-

point reaching movement, change of muscle length varies depending on which joint the muscle

crosses over. For example, the muscle spindle embedded in the anterior deltoid would be

responding mostly to the shoulder joint extension whereas the muscle spindle embedded in the

brachioradialis would be responding mostly to the elbow joint extension. Thus, assigning the joint

over which the spindle crosses is equivalent to assigning a preferred direction in the joint

displacement. Another point to consider is the moment arm of each muscle spindle. Equation 5.5 summarizes the process to transform from a 2D joint displacement to a muscle spindle length.

$$\Delta x(t) = k \cdot \theta_{pref}^T \cdot \Delta \underline{q}(t) = k \cdot \theta_{pref}^T \cdot (\underline{q}(t) - \theta_0) \qquad (5.5)$$

$\underline{q}$ is a 2×1 vector consisting of shoulder and elbow joint angles and θ_0 is resting joint position.

θ_{pref} is a 2×1 unit vector representing a preferred direction in joint angle space. For example,

$\theta_{pref} = [1 \quad 0]^T$ corresponds to 0° preferred direction which represents pure shoulder flexion

while $\theta_{pref} = [0 \quad 1]^T$ corresponds to 90° preferred direction which represents pure elbow flexion.

The inner product of θ_{pref} and $\Delta \underline{q}$ computes the change of joint angle in the preferred direction,

reducing the dimension from 2D to 1D. Finally, multiplying the inner product by *k*, moment arm,

transforms the joint angle into the change of muscle spindle length. In order to have a rich set of

basis elements, we varied seven parameters as shown in table 5.1. The total number of basis

elements that we used to cover the whole limb state is 80.

5.3 Tuning functions

Figure 5.1a shows the response of an example basis element with *a*=100, *b*=100, *c*=-25, *k*=80,

θ_{pref} =22.5°, *h*=1, and *p*=0.1 to a point-to-point reaching movement on a horizontal plane at

shoulder level. Each curve at 8 different locations represents the response for a 500 ms reaching

from a fixed center to a 10 cm periphery in that direction. The center is aligned with the body

midline and 43 cm away from the body of the model arm. The trajectory for these movements

was assumed to follow the minimum jerk rule. The preferred direction 22.5° of this basis element

corresponds to mostly shoulder flexion, thus, the most active direction is down and left in this

arm configuration. The octagon inside of the rectangle in figure 5.1b contains the same message

as the figure 5.1a. The size of circle represents the mean firing rate during the center-hold period
and the distance from the center to each vertex represents the mean firing rate while moving in
that direction. Similarly, we computed tuning functions of this element at eight other center
locations. The tuning curve shown here is similar to that of gain-field basis functions as it appears
to encode both position and velocity in a nonlinear way. Refer to the tuning function of the gain-
field cell in figure 3.1.

Table 5.1 List of parameters used in simulations

| a	b	c	k	θ_{pref}	h	p
100	100	-25	80	0°, 22.5°, 45°, 67.5°, 90°, 112.5°, 135°, 157.5°, 180°, 202.5°, 225°, 247.5°, 270°, 292.5°, 325°, 347.5°	1	0.1
100	100	-25	80	0°, 22.5°, 45°, 67.5°, 90°, 112.5°, 135°, 157.5°, 180°, 202.5°, 225°, 247.5°, 270°, 292.5°, 325°, 347.5°	0.1	1
0.1	1.1	-20	10	0°, 22.5°, 45°, 67.5°, 90°, 112.5°, 135°, 157.5°, 180°, 202.5°, 225°, 247.5°, 270°, 292.5°, 325°, 347.5°	1	0.1
0.1	1.1	-20	10	0°, 22.5°, 45°, 67.5°, 90°, 112.5°, 135°, 157.5°, 180°, 202.5°, 225°, 247.5°, 270°, 292.5°, 325°, 347.5°	0.1	1
3.2	250	-15	1	0°, 22.5°, 45°, 67.5°, 90°, 112.5°, 135°, 157.5°, 180°, 202.5°, 225°, 247.5°, 270°, 292.5°, 325°, 347.5°	0.2	0.1
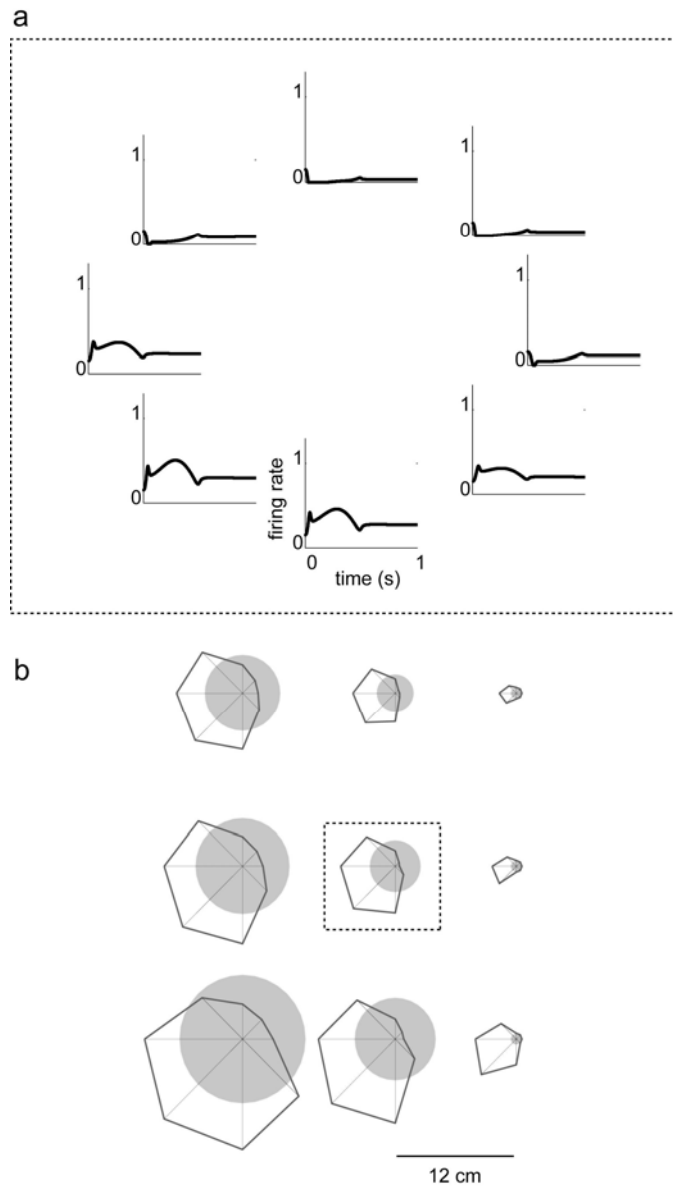
Figure 5.1 A tuning curve of an example muscle spindle-like basis element in center-out reaching task (a=100, b=100, c=-25, k=80, h=1 and p=0.1). **(a)** Firing rate as a function of time for 8 directional center-out reaching movements on a horizontal plane. A minimum jerk trajectory was calculated for 10 cm long during 500 ms in each direction. **(b)** Tuning curves at nine different locations on a horizontal plane at shoulder level. Size of circle at each location represents the firing rate during the center-hold period. Distance from center of circle to vertex of polygon represents the firing rate for 10 cm, 500 ms movement in that direction. The direction with the largest distance from the center is the preferred direction of this cell. The plot in the center bounded by a rectangle uses the same data in (a).
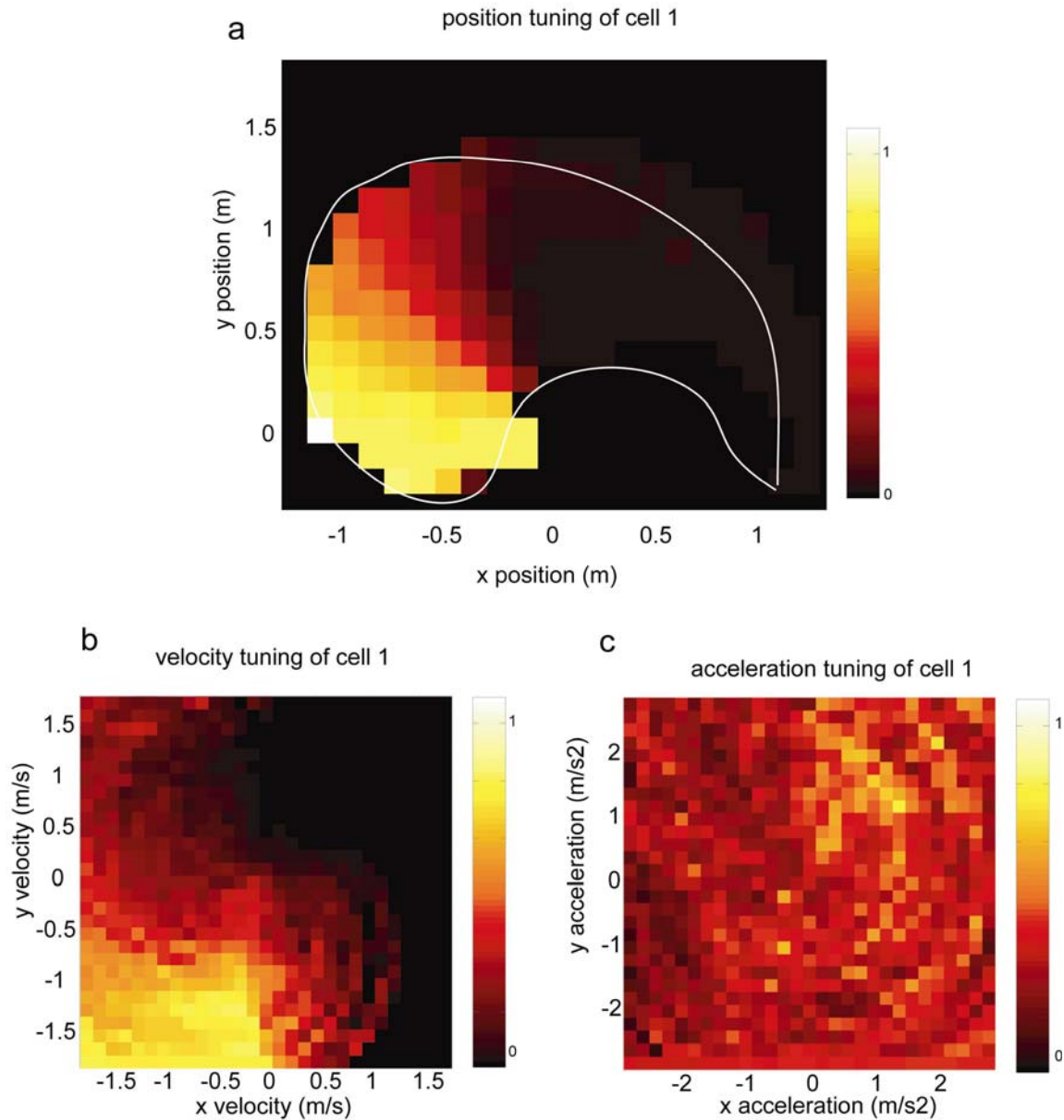
70

Figure 5.2 Firing rate as a function of limb states in hand coordinates for an example basis element. The same cell from figure 5.1. For 400-1000 random point-to-point reaching movements, average firing rate for each hand state was calculated. **(a)** Firing rate as a function of hand position. The white boundary indicates an approximate boundary of workspace that the model arm can reach. This cell is the most active for the position near the left side of the body. **(b)** Firing rate as a function of hand velocity. This cell is the most active for directions down and to the left, toward the left side of the body. **(c)** Firing rate as a function of hand acceleration. No specific pattern is shown.

71
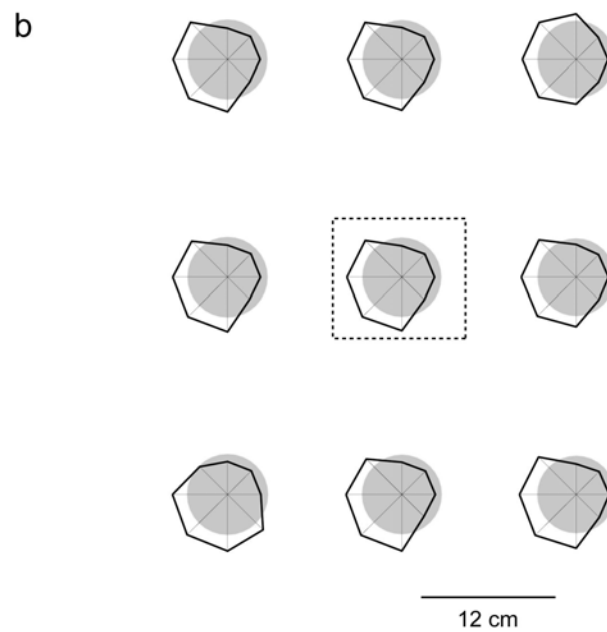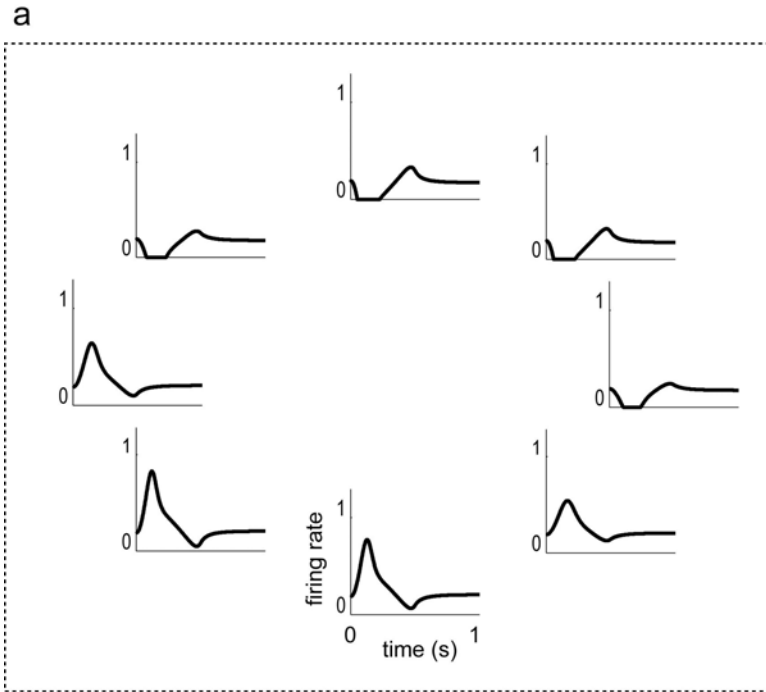
Figure 5.3 A tuning curve of another example muscle spindle-like basis element in center-out reaching task (*a*=3.2, *b*=250, *c*=-15, *k*=1, *h*=0.2 and *p*=0.1). Same formation as figure 5.1.

a

position tuning of cell 65

b

velocity tuning of cell 65

c

acceleration tuning of cell 65

Figure 5.4 Firing rate as a function of limb states in hand coordinates for another example basis element. The same cell from figure 5.3. The same format as figure 5.2.

The tuning function of the same cell was more closely examined in three different state spaces, hand position, velocity and acceleration separately. We generated temporal responses of the cell for 400-1000 random point-to-point reaching movements within a reachable workspace so that the cell explores the state space in many possible ways. For example, for a given hand position, the cell can visit this hand position as a s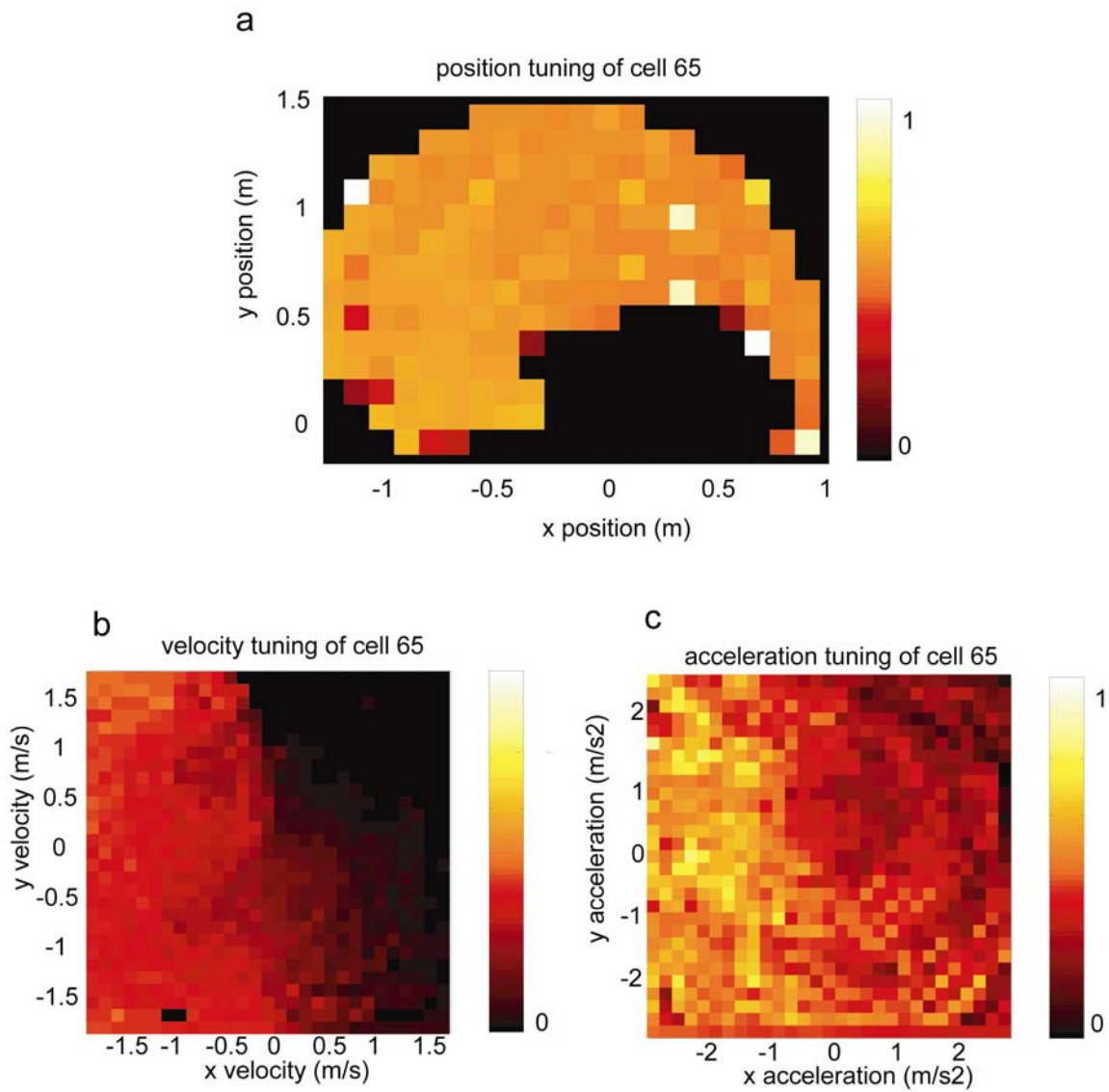tarting position, or any intermediate position or end position. As a mean response of the cell for this specific hand position, we took the average of firing rates generated by all possible trajectories. Figure 5.2a displays the average response at each hand position of the same cell as in figure 5.1. A monotonic increase of response is seen as the hand position moves in the down and left direction. In the same way, we computed average responses in hand velocity space and acceleration space (figure 5.2a and b). This cell responds the most actively for the velocity in the direction down and to the left. No specific pattern is seen in acceleration space.

Figure 5.3 and 5.4 display tuning functions for the cell with parameters, a=3.2, b=250, c=-15, k=1, θ_{pref} =22.5°, h=0.2 and p=0.1 in the same format as figure 5.1 and 5.2. Unlike the cell in figure 5.1, this cell does not show any specific position tuning. Velocity tuning and acceleration tuning is also very broad although the response as a function of time appears to be encoding acceleration information to some extent.

5.4 Adaptation to velocity dependent curl fields

With 80 basis functions (refer to table 5.1), we simulated learning of a velocity dependent curl field. The learning algorithm and the simulation of arm dynamics is the same as the one described in chapter 3. However, activation of each basis function followed the rules described in equation 5.3-5.5 instead of the gain-field model. First, the change of muscle spindle length as a function of

74

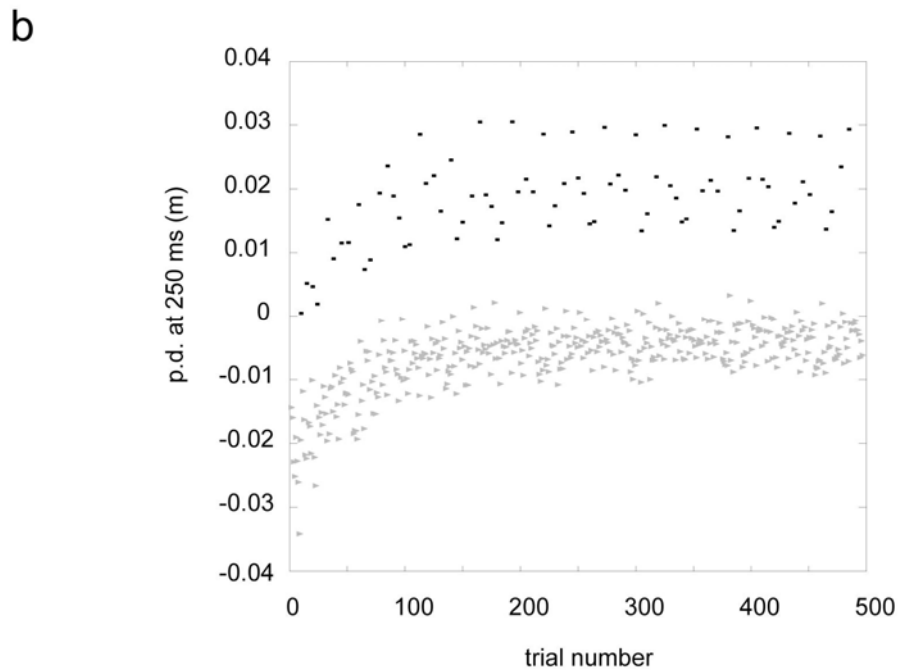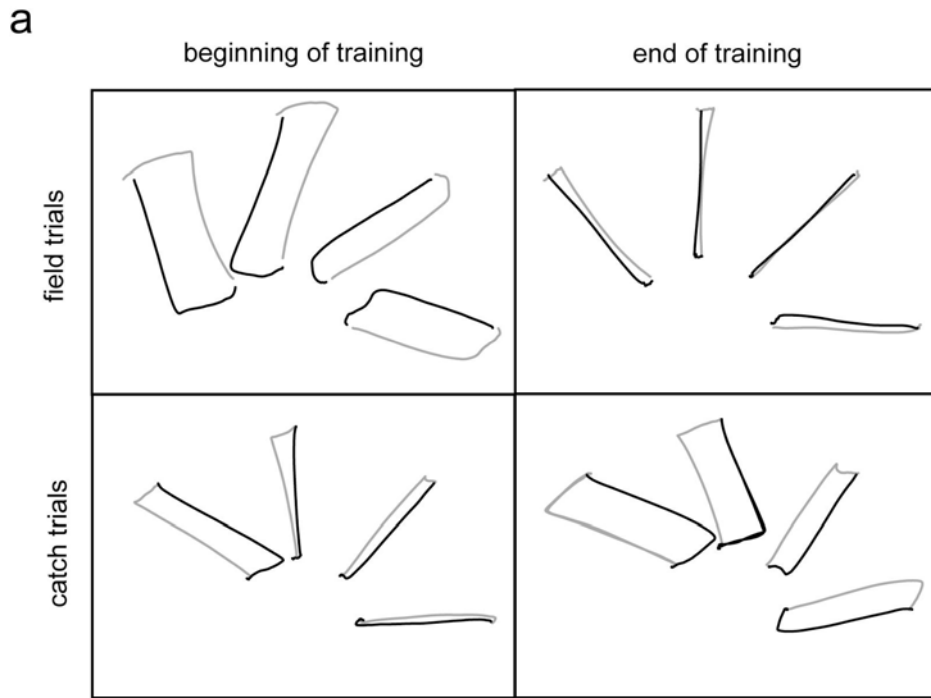**Figure 5.5** Simulation of adaptation to a velocity dependent curl field using a spindle-like basis set. **(a)** Hand paths from the early and late phases of training. The grey lines are center-out movements and the black lines are out-center movements. **(b)** Movement errors (perpendicular error at 250 ms into the movement) as a function of trial number. Grey dots are field trials and block dots are occasional catch trials.

time, $x(t)$ is computed using equation 5.5. Second, the change of the length in the sensory zone, $z(t)$ is computed by numerically solving the differential equation 5.3. Finally, the firing rate, $g(t)$ is computed using equation 5.4. Then, the expected torque at each time point is

$\hat{\tau}_{env}(t) = \sum_i w_i \cdot g_i(t)$. Using the gradient decent rule, weights are updated to approximate the

actual velocity dependent force field, $\tau(t) = J^T \cdot \begin{bmatrix} 0 & -13 \\ 13 & 0 \end{bmatrix} \cdot J^{-1} \cdot \dot{\underline{q}}(t)$.

Figure 5.5 displays the simulated hand paths and movement errors. In the beginning of the training, as the model expects zero forces, it produces large errors but the error decrease as the model gradually fits the actual force field. In parallel, growing of aftereffects with training is seen.

5.5 Adaptation to position-velocity dependent force fields

Similarly, we simulated adaptation to a position-velocity dependent force field described in chapter 2 and 3. The same 80 spindle-like basis functions used in section 5.3 produced the learning index and generalization modulated by the separation distance. Figure 5.6a displays the simulated perpendicular errors for the separation distances 0.5 and 12 cm. Only in the 12 cm separation group, decrease of errors in field movements and increase of aftereffects are seen. The learning index and generalization index closely match the experimental data reported in chapter 2.

In addition, we found that spindle-like basis representation could reproduce the results that a non-linear position-velocity dependent force field is more difficult to learn than a linear force field and hypergeneralization occurs when a linear position dependent force field is trained (Figures 5.7 and 5.8).
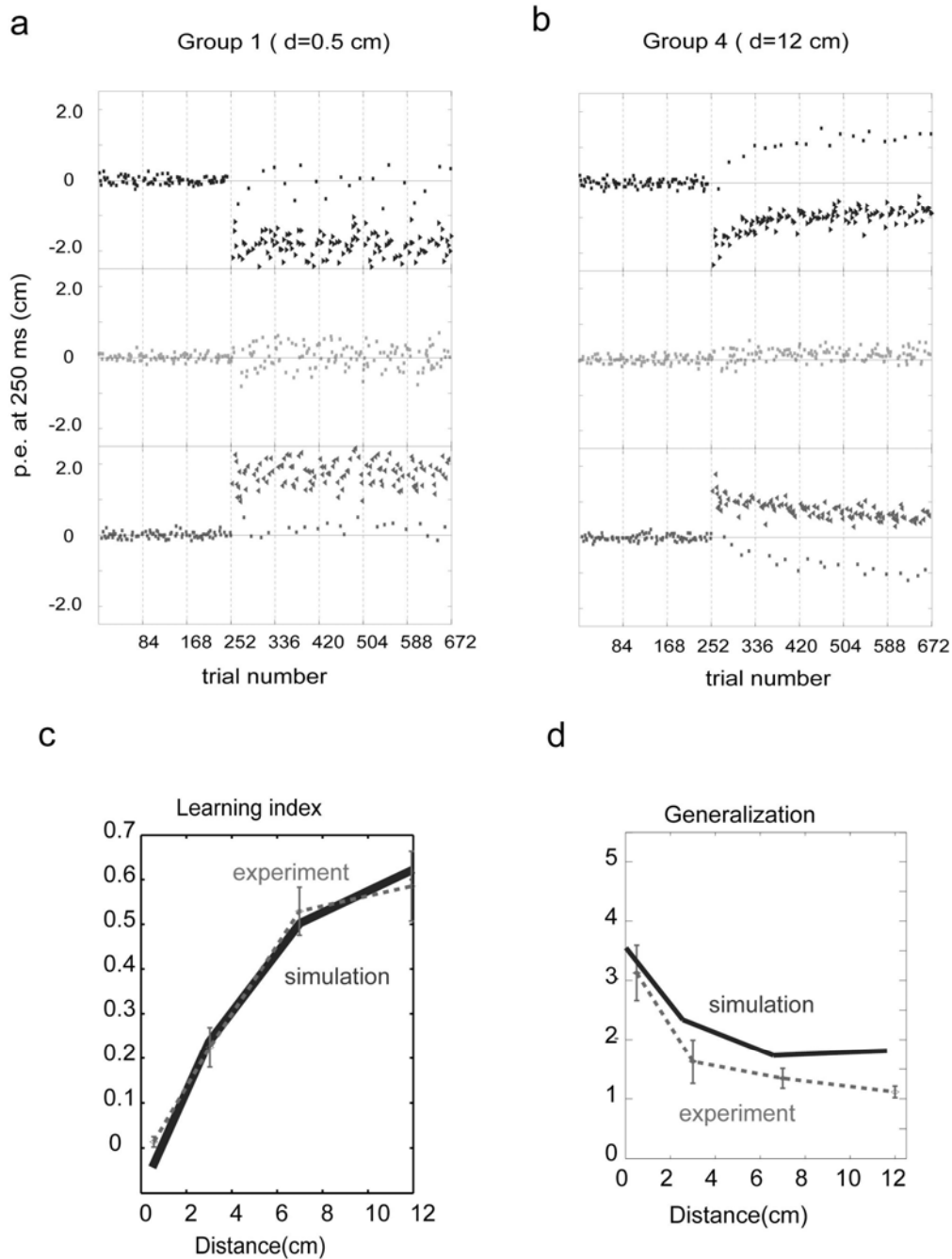
Figure 5.6 Simulation of adaptation to a position-velocity dependent force field using a spindle-like basis set. **(a)-(b)** Perpendicular errors as a function of trial number. The format is same as in figure 2.3. Movement errors from the left, center and right positions are plotted in the top, middle and bottom panels, respectively. Left plot is for the separation distance = 0.5 cm and right plot is for the separation distance=12 cm. **(c)-(d)** Learning index and generalization index as a function of separation distance.
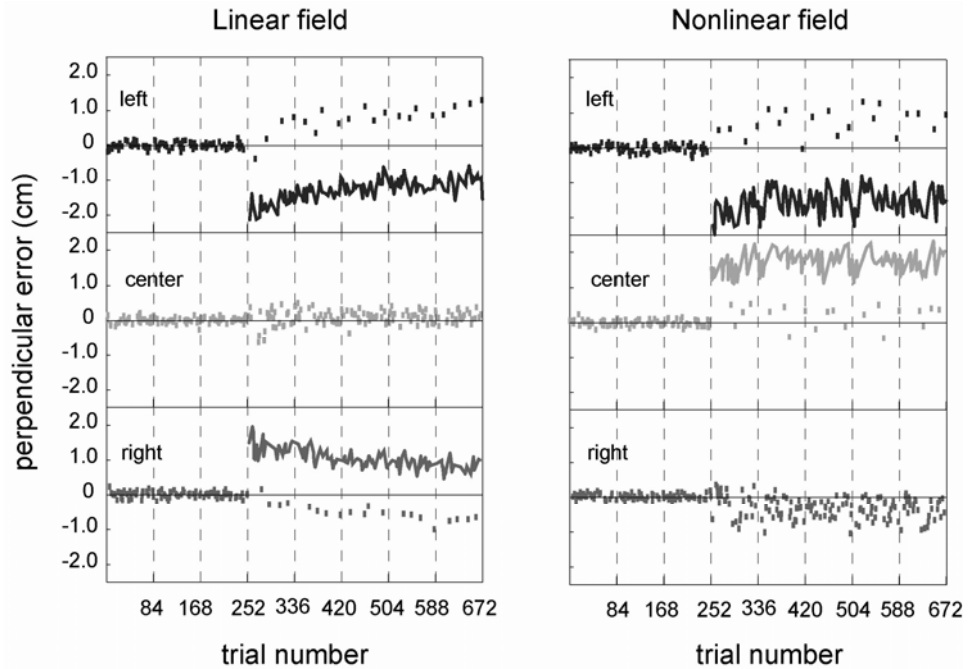
Figure 5.7 Simulation of the linear vs. nonlinear force fields. The two force fields are described in figure 3.7. Notice that reduction of errors and increase of after-effects with training are bigger in the linear force field than the nonlinear force field.
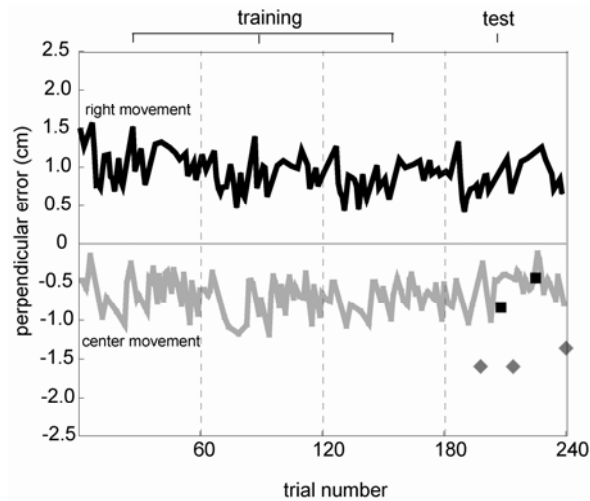
Figure 5.8 Simulation of hypergeneralization. The format is the same as in figure 3.9(c). Aftereffects in the untrained location (diamonds) are bigger than those in the trained location (squares).

5.6 Transfer of learning a viscous force field across workspace

We also simulated a transfer experiment. The model was trained in a velocity dependent force field at the left workspace and then tested in the same field at the right workspace that was 80 cm away from the training location. The performance in the right workspace in the transfer condition was compared to the performance in the right workspace in the naïve condition which started with zero initial weights. The mean size of errors in the first bin is bigger than the experimental data in both conditions. Yet, it still reproduced the experimental result that the performance in the transfer condition is better than that in the naïve condition.
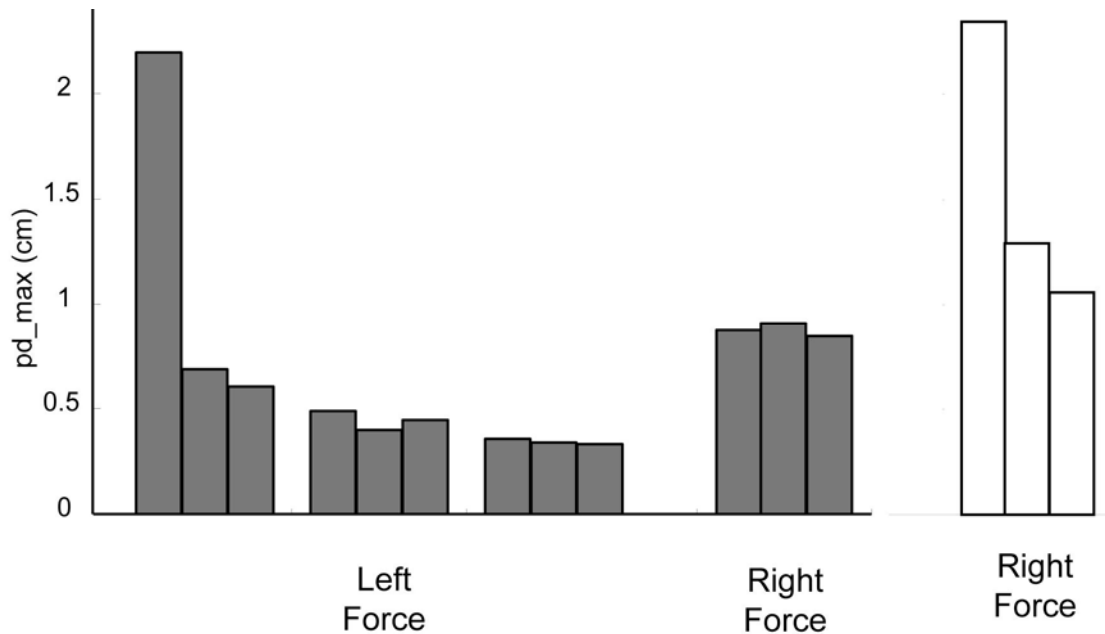
Figure 5.9 Simulated transfer of a viscous field learning across workspace. Black bars are errors for the transfer condition and white bars are for the naïve condition. In the transfer condition, the model was trained for the viscous field at the left workspace first and then exposed to the same field at the right workspace. In the naïve condition, the model was trained for the viscous field at the right workspace with zero initialization for the expected force.

5.7 Reaching with an attached mass

Sainburg et al.(1999) conducted a series of experiments in which subjects made reaching movements with a point mass attached to their arm (figure 5.8a). Attaching a mass changes the inertial property of the arm and imposes position-acceleration dependent and position-velocity dependent force fields. They found that people adapted to this new arm dynamics with practice. To simulate this paradigm, we computed the equations of motion when a mass was attached to the arm. Equations 5.5-5.7 show equations of motion for a simplified 2-D arm model without any mass attached. Notations are the same as in the arm simulation section of chapter 3 except that θ and ϕ were used for shoulder and elbow angles instead of $q_{shoulder}$ and q_{elbow}.

$$\tau = H(q) \cdot \ddot{q} + C(q, \dot{q}) \cdot \dot{q} \tag{5.5}$$

$$H(\underline{q}) = \begin{bmatrix} a_3 + a_1 \cdot l_1{}^2 + a_4 + 2 \cdot a_2 \cdot l_1 \cdot \cos(\phi) & a_2 \cdot l_1 \cdot \cos(\phi) + a_4 \\ a_2 \cdot l_1 \cdot \cos(\phi) + a_4 & a_4 \end{bmatrix} \tag{5.6}$$

$$C(\underline{q}, \dot{q}) = \begin{bmatrix} -a_2 \cdot l_1 \cdot \sin(\phi) \cdot \dot{\phi} & -a_2 \cdot l_1 \cdot \sin(\phi) \cdot (\dot{\theta} + \dot{\phi}) \\ a_2 \cdot l_1 \cdot \sin(\phi) \cdot \dot{\theta} & 0 \end{bmatrix} \tag{5.7}$$

where l_1= 0.33 m, l_2= 0.34 m, a_1 = 1.5187 kg, a_2 = 0.3442 kg·m, a_3 = 0.0667 kg·m^2, and a_4 = 0.0968 kg·m^2.

Equations 5.8-5.10 show equations of motion when a mass is attached medially to the distal part of the forearm.

$$\tau = H(q) \cdot \ddot{q} + C(q, \dot{q}) \cdot \dot{q} + H'(q) \cdot \ddot{q} + C'(q, \dot{q}) \cdot \dot{q} \tag{5.8}$$

$$H'(\underline{q}) = \begin{bmatrix} a_5 + a_6 + 2 \cdot a_7 \cdot \cos(\phi + \delta) & a_7 \cdot \cos(\phi + \delta) + a_6 \\ a_7 \cdot \cos(\phi + \delta) + a_6 & a_6 \end{bmatrix} \tag{5.9}$$

$$C'(\underline{q}, \dot{q}) = \begin{bmatrix} -a_7 \cdot \sin(\phi + \delta) \cdot \dot{\phi} & -a_7 \cdot \sin(\phi + \delta) \cdot (\dot{\theta} + \dot{\phi}) \\ a_7 \cdot \cdot \sin(\phi + \delta) \cdot \dot{\theta} & 0 \end{bmatrix} \tag{5.10}$$

where $a_5 = m_m \cdot l_1{}^2$, $a_6 = m_m \cdot r_m{}^2$, and $a_7 = m_m \cdot l_1 \cdot r_m$.
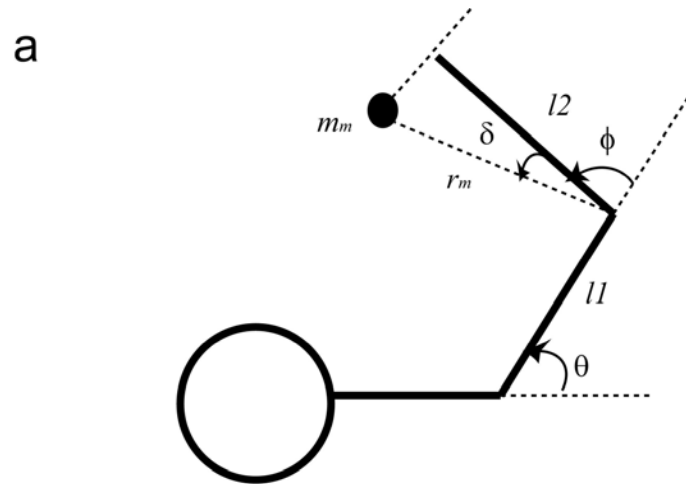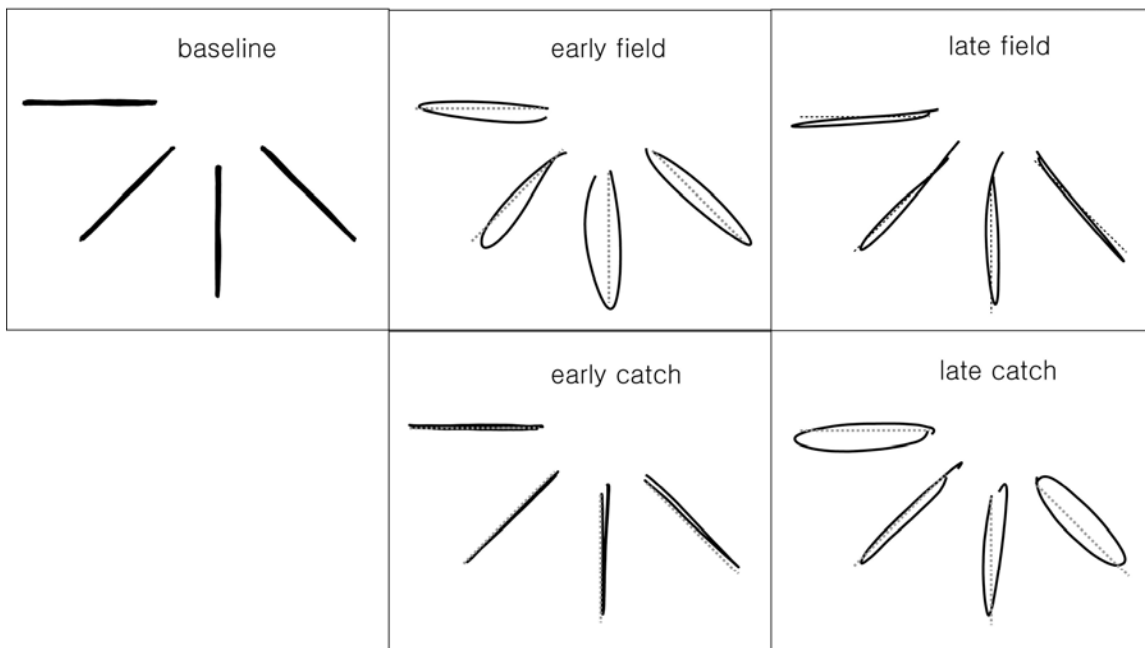
Figure 5.10 Simulation of adaptation to a medially attached mass ($m_m = 1.2\ kg$ and $\delta = 15°$).

(a) Diagram of a simplified arm model. A point mass is attached medially to the distal part of the forearm (m_m). **(b)** Simulated hand paths during the baseline, early training and late training set. Movements are all out-and-back as a single movement.

Thus, adding a mass at the distal part of the forearm is equivalent to applying position-acceleration dependent force and position-velocity dependent force simultaneously. With these equations of motion, we simulated out-and-back movements as in the original experiment with $m_m = 1.2\,kg$ and $\delta = 15^o$. To simulate out-and-back movements, we derived the following minimum-jerk trajectory for out-and-back movements.

$$\left\{ \begin{array}{ll} x = x_0 + (x_f - x_0) \cdot \dfrac{1}{3} \cdot \left\{ 8\left(\dfrac{t-t_0}{T/2}\right)^5 - 25\left(\dfrac{t-t_0}{T/2}\right)^4 - 20\left(\dfrac{t-t_0}{T/2}\right)^3 \right\} & t_0 < t \le T/2 \\[4mm] x = x_0 + (x_f - x_0) \cdot \dfrac{1}{3} \cdot \left\{ -8\left(\dfrac{t-t_0}{T/2}-2\right)^5 - 25\left(\dfrac{t-t_0}{T/2}-2\right)^4 - 20\left(\dfrac{t-t_0}{T/2}-2\right)^3 \right\} & T/2 < t \le T \end{array} \right.$$

Here, x_0 is the initial position, x_f is the target position, T is the desired movement time, t_0 is the initial time. Figure 5.8b displays the simulated hand paths for the baseline, early training and late training sets. In the beginning of training, movements are perturbed by the new dynamics but with practice, movements begin to resemble those of the baseline set. Similarly, aftereffects, that are almost equal and opposite to the initial perturbation, are seen.

5.8 Discussion

In this chapter, we attempted to suggest a basis set that was derived from mathematical properties of the actual proprioceptive sensors in our body. The key idea is that the desired sensory state is represented in a similar the way to the sensory system response when the desired sensory state is actually achieved. To implement this idea, we formed a basis set in which response of each basis function resembles response of muscle spindle to a whole arm movement. Surprisingly, some of basis functions showed gain-field like tuning properties, i.e. nonlinear combinations of velocity and position coding. With only 80 basis elements, we could reproduce many previous

experimental results including adaptation to a velocity-position dependent force field and transfer of velocity dependent force field learning across a large workspace. Note that we used 968 basis elements in the gain-field basis set to reproduce these results. With these 80 basis elements, we could also demonstrate that the model adapts to a modified dynamics imposed by an attached mass to the arm. These results strongly encourage the further investigation of spindle-like basis representation.

However, there are some specific issues to be solved by further study. First, it has to be systemically determined how to distribute the parameters in the model. Each parameter has an associated physical meaning. Parameter a is the sensitivity of tension to the velocity and parameter b is the ratio of length sensitivities of the non-sensory zone and the sensory zone of spindle. Parameter c determines the zero length tension and parameter k is the moment arm of each spindle. Parametera h and p determine the relative contributions to firing rate of receptor potential and its derivative. Parameter θ_{pref} is a preferred joint displacement. Thus, realistic distribution of these values can be inferred from the physical properties of spindle structure. For example, we distributed the preferred joint displacement uniformly across all directions. However, it is unclear if there are spindles that are mostly activated by the combination of shoulder flexion and elbow extension or for the combination of shoulder extension and elbow flexion, although such cells were found in M1. Second, we used a simple linear conversion from a whole arm movement to a muscle length using a constant moment arm. However, anatomical studies show that the moment arm is not constant and rather varies as a function of arm position (Murray et al., 1995). The consideration of nonlinear moment arm effect might be able to make a better prediction for the behavior across a wider workspace. Finally, the spindle model we used was derived from a passive stretching experiment using isolated muscle spindles. This model was shown to fit some spindle responses during an active motion relatively well (Prochazka and

Gordon, 1998). However, when the muscle in which a spindle is embedded is actively recruited during the active motion, the model deviates from the actual response, indicating that the model needs to take into account the components of fusimotor action linked to extrafusal muscle activity (Prochazka and Gorassini, 1998). Thus, the consideration of fusimotor action might change the tuning property and pattern of generalization in some cases.

Chapter 6

Effects of vision and proprioception on acquisition of implicit and explicit internal models of limb dynamics

So far, we demonstrated that the internal model depends on the states of the limb, e.g., position, velocity, acceleration. These states can be sensed by both vision and proprioception (Rossetti et al., 1995;Lateiner and Sainburg, 2003;Ernst M.O and Banks M.S., 2002). However, it is unclear which modality plays a dominant role in the sensory representation used in the internal model. Sober and Sabes (2003) demonstrated that the relative contribution of vision and proprioception to planning and execution of a movement varies depending on the specific computation that requires arm position estimate. In the planning stage of a movement, estimates of hand position are closely tied to visual information (Henriques et al., 1998). In contrast, in the execution stage of a movement, the state of the limb is likely to be estimated predominately from proprioception (Scott and Kalaska, 1997). Considering that the internal models of arm dynamics depend on computations that are in the later category, one would expect that representation of limb state in the internal model of dynamics relies primarily on proprioception.

In procedural learning tasks, like acquisition of internal models of limb dynamics, explicit knowledge of the task has been considered unnecessary (Goschke, 1998;Gabrieli et al., 1993;Milner, 1962;Corkin, 1968;Tranel et al., 1994). For instance, subjects with severe impairment in their declarative memory system, e.g., amnesic patients, show normal learning and retention in force field adaptation despite the fact that they may not be able to recall the training episodes (Shadmehr et al., 1998). However, this does not imply that procedural learning does not benefit from explicit knowledge (Boyd and Winstein, 2001;Eliassen et al., 2001;Russeler and

Rosler, 2000). For example, unilateral stroke patients do not improve their reaction time in a serial-reaction task even with extended practice. However, when the sequence of a serial-reaction task (SRT) is explicitly learned prior to the practice, reaction times improve with practice (Boyd and Winstein, 2001). Similarly, improvement of reaction time is demonstrated when normal subjects were provided with explicit knowledge of the sequence (Eliassen et al., 2001) or when they discover the sequence by themselves (Russeler and Rosler, 2000). Therefore, in at least some types of procedural learning, explicit knowledge can affect rates of acquisition of the motor skill. However, the role of explicit knowledge in acquisition of internal models has been ignored.

Therefore, in this chapter, we made an attempt to elucidate three points: 1) the relative contribution of vision and proprioception to implicit force field learning, 2) the relative contribution of vision and proprioception to awareness of the force field pattern, and 3) the role of awareness in force field learning.

6.1 Experimental setup

Fifty healthy individuals (16 women and 34 men) participated in this study. Average age was 25 years (range: 19 to 35 years). The study protocol was approved by the Johns Hopkins University School of Medicine Institutional Review Board and all subjects signed a consent form.
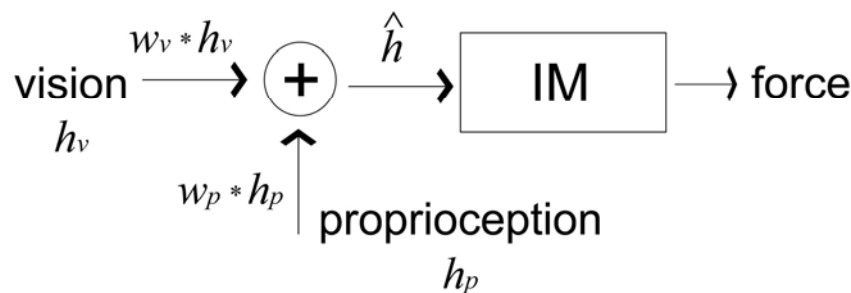
Figure 6.1 Internal model depends on the limb position information that is sensed by both vision and proprioception. The relative contribution of these two modalities are unknown.
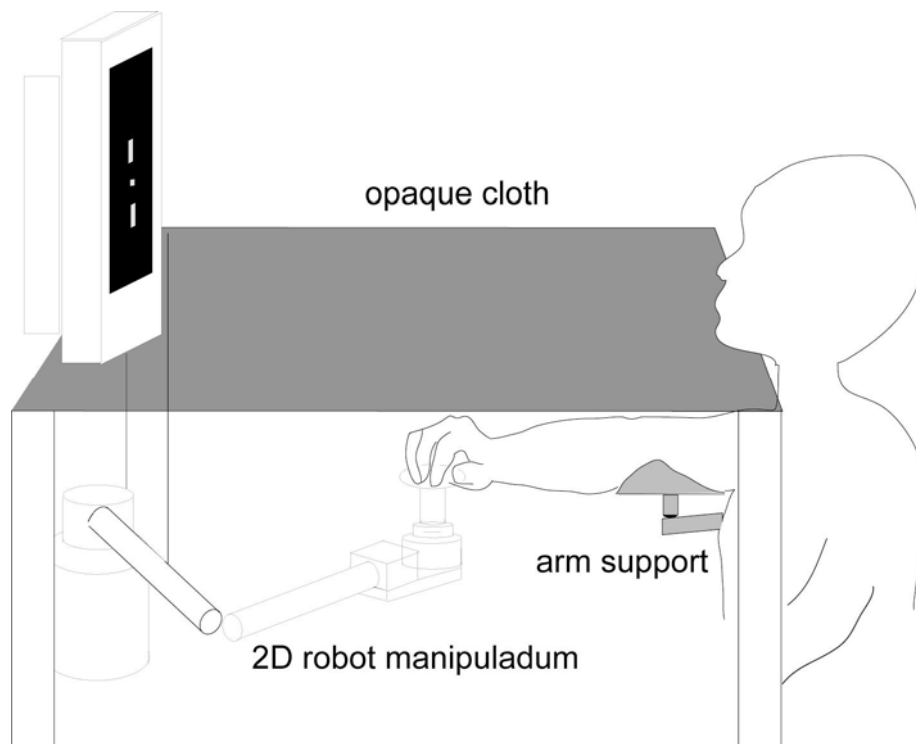
Figure 6.2 Experimental setup to test relative contribution of vision and proprioception. A subjects makes a point-to-point reaching while holding a robot handle. The direct vision of their arm is occluded by a black cloth spread at their shoulder level. The visual feedback of start position, target position and current position is shown on the monitor.

6.1.1 Task

Subjects sat on a chair in front of a 2D robotic manipulandum and held its handle (figure 6.2). Their upper arm rested on an arm support attached to the chair and they reached in the horizontal plane at the shoulder height. We spread a sheet of black heavy cloth horizontally above the movement plane. This sheet occluded view of the entire body below the neck.   A vertical monitor was placed about 75 cm in front of subjects and displayed a cursor (2×2 mm^2) representing hand position and squares (6×6 mm^2) representing start and target positions of

reaching. The relationship between this visual display and hand position varied in the five experimental groups.

The task was very similar to one described in chapter 2 except that here we used a vertical monitor to display visual feedback instead of a horizontal projector. After a completion of one reach, the robot moved the subject's hand to a new start position. During this transition period, the cursor feedback indicating hand position was blanked until the hand was within 2 cm of the start position for the next trial. After the hand became stationary within 5 mm of the new start position for 300 ms, the video monitor displayed the next target.

6.1.2 Modifying the relationship between visual feedback and hand position

In the matched group (figure 6.3a), at the start of each reach the robot positioned the hand at one of three pseudo-randomly chosen locations - left, center and right - evenly spaced (d=7 cm apart from each other) on a line about 48 cm in front of the subject and centered about the subject's midline. The cursor representing the hand position was veridical in the sense that the location of the cursor precisely varied with the actual hand displacement.

In the proprioception-only group (figure 6.3b), at the start of each reach the robot similarly positioned the hand at one of three pseudo-randomly chosen start locations. However, the cursor was always displayed in the midline of the monitor regardless of the actual hand position.

In the vision-only groups (figure 6.3c), at the start of each reach the robot always positioned the hand at the middle of the workspace. However, the cursor was displayed at a pseudo-randomly chosen place from three possible locations - left, center, and right of the monitor space. For one vision-only group, the distance between left and right movements was 7 cm. For the other vision-only group, this distance was 14 cm.
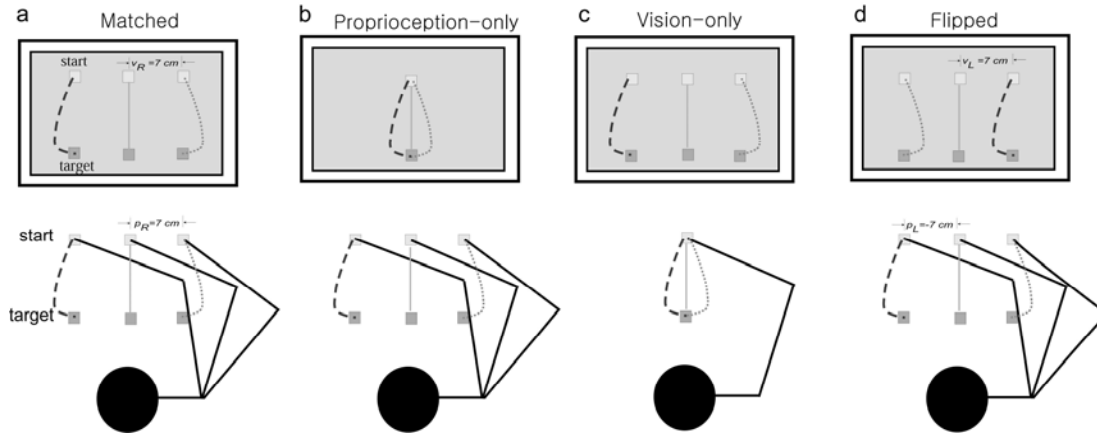
Figure 6.3 Experimental design. Top row displays the cursor trajectory. The bottom row displays the corresponding hand trajectory. The curved paths represent perturbed movements by the force field, either clockwise or counter-clockwise. **(a)** Matched group. The cursor position was aligned with subject's hand position. **(b)** Proprioception-only group. Hand position varied but not cursor position. **(c)** Vision-only group. The cursor position varies but not hand position. **(d)** Flipped group. The cursor was displayed on the opposite side of the hand position**.**

In the <u>flipped group</u> (figure 6.3d), at the start of each reach the robot positioned the hand at one of three pseudo-randomly chosen start locations as in the matched group. However, the cursor was displayed opposite to the location of the hand. For example, when the hand was at the right location, the cursor was displayed at the left of the monitor midline and vice versa.

6.1.3 Force fields

To perturb reaching movements, the robot applied a velocity-dependent force field (a viscous field). The force on the hand $\vec{F}$ depended on hand velocity $\vec{x}$ according to $\vec{F} = B \cdot \vec{x}$. We modified B during movements from different starting position in order to make the field dependent on hand position as well as velocity as shown in Figure 1a. In the matched, proprioception-only, and flipped groups, for movements from the left starting position of the hand

89

the robot perturbed the hand with a clockwise curl field (B = [0 13; -13 0] N·sec/m, pushing the hand leftward during the reach). During movement from the right starting position the field was counterclockwise (B = [0 -13; 13 0] N·sec/m, pushing the hand rightward during the reach). For movements starting at the center position, no field was applied (i.e., always a null field). In the vision-only groups, start position of the hand did not vary. However, in this group the perturbing force depended on the start position of the cursor, i.e., leftward force was applied when the cursor indicated that the movement was at left, rightward force at right and no force in the middle.

6.1.4 Experimental procedure

To familiarize the volunteers with the task and produce baseline performance, subjects began with three sets of 84 movements in the null field. Following this, subjects did five force field sets of 84 movements in which fields were applied as described above. All subjects in a given group performed the same sequence. During training in the field, occasional pseudo-randomly designated trials were performed without forces (i.e., catch trials). Approximately one in seven trials was a catch trial.

After the experiment, subjects completed a written questionnaire (figure 6.6). The form contained questions about self-evaluation of performance, notice of any force field patterns, use of any strategy to succeed in the task, and level of attention during the experiment. The purpose of the questions was to help us categorize subjects into "aware" or "unaware" groups. All subjects who answered "yes" to the first question and correctly described the force pattern (as in the box in figure 6.6) were assigned to the "aware" group. Only one subject marked "no" to the first question and then answered "yes" to the second question. This subject was also categorized "aware".

Some subjects became consciously aware of the pattern of forces. These subjects were able to describe or confirm the correct relationship between upcoming force direction and the start position of a movement whereas unaware subjects either incorrectly described the relationship or were unable to confirm the correct relationship (Figure 6.6). When the subjects were asked to describe the relationship between the force direction and the start position, most subjects drew a diagram. The typical diagram included boxes at the three start locations and subsequent hand paths. The hand paths were curved toward the force direction often with arrows indicating the force direction (Figure 6.6b). Some subjects reported verbally, e.g., "when presenting targets on the right, the robot pushed right, when presenting targets on the left, the robot pushed left and there was no resistance in the middle."

6.1.5 Performance Measures

As a measure of error, we report the displacement perpendicular to target direction at 250 ms into the movement (perpendicular error, p.e.). Using p.e. at 250 ms, we computed a learning index (Hwang et al., 2003), the same measure described in chapter 2.

For each subject, we calculated learning index for each adaptation set then averaged these indices across the five adaptation sets to use as a single subject's overall learning index.

6.2 Relative effects of proprioceptive and visual cues

In chapter 2, we showed that when visual feedback regarding state of the end-effector matched proprioceptive feedback (Figure 6.3a, matched group), performance in the position-velocity dependent force field increased monotonically with the distance between the left and right start positions (Hwang et al., 2003) and generalization was in intrinsic coordinates (Shadmehr and Moussavi, 2000;Malfait et al., 2002) We hypothesized that if the internal model of limb dynamics relied solely on proprioception to encode state of the limb, there should be no significant learning in the vision-only group. On the other hand, if encoding of limb state depended solely on visual cues, then learning in the vision-only group should be significantly better than proprioception-only group. In theory, comparison of learning among the various groups should reveal the relative influence of each modality on representing state of the end-effector.

Figures 6.4a-c display hand paths of a typical subject from each the matched, vision-only, and proprioception-only groups. In the first set of field trials, hand paths were strongly disturbed by forces in the left and right locations in all three groups. Catch trials were either straight or slightly curved in the same direction of the fields, indicating that subjects did not have correct internal models for the applied force fields. After training, in the matched and proprioception-only group the last field trials were straighter and the last catch trials were curved in the opposite direction of the fields, indicating that subjects formed correct internal models.
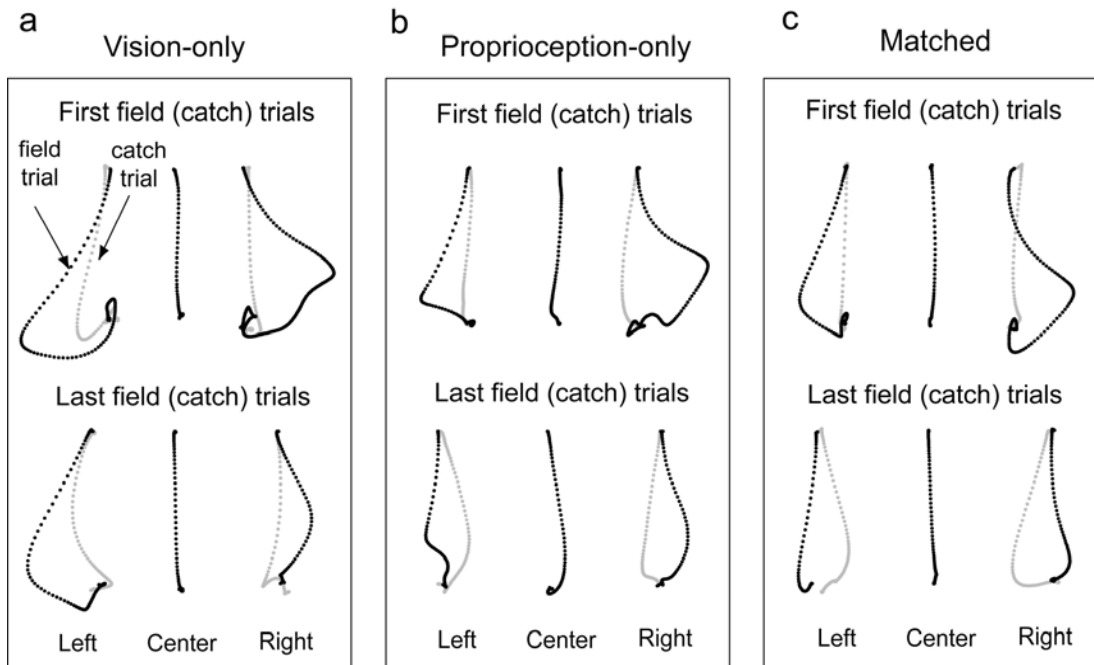
92

Figure 6.4 Implicit learning depends primarily on proprioceptive information. **(a)** Hand paths of a typical subject in the vision-only group. Top panel shows the first field (black) or catch (gray) trials and bottom panel shows the last field or catch trials for each location. **(b)** Hand paths of a typical subject in the proprioception-only group. **(c)** Hand paths of a typical subject in the matched group.

However, in the vision only-group, training resulted in smaller changes in both field and catch trials than the other two groups. We quantified performance for each subject using a learning index. Figure 6.5 shows averaged learning across subjects in the three experimental conditions. In all three groups, the learning index increases with practice. However, we found that learning indices of the three groups were significantly different from one another ($F(2,21)=13.2$, $p<0.0003$). Furthermore, post hoc testing revealed that the proprioception-only group learned significantly faster than the vision-only group ($t=2.30$, $df=12$, $p=0.02$). This result rejected the possibility that encoding of state depended solely on visual cues. Instead, this finding indicated that the encoding depended primarily on proprioceptive cues from the limb.
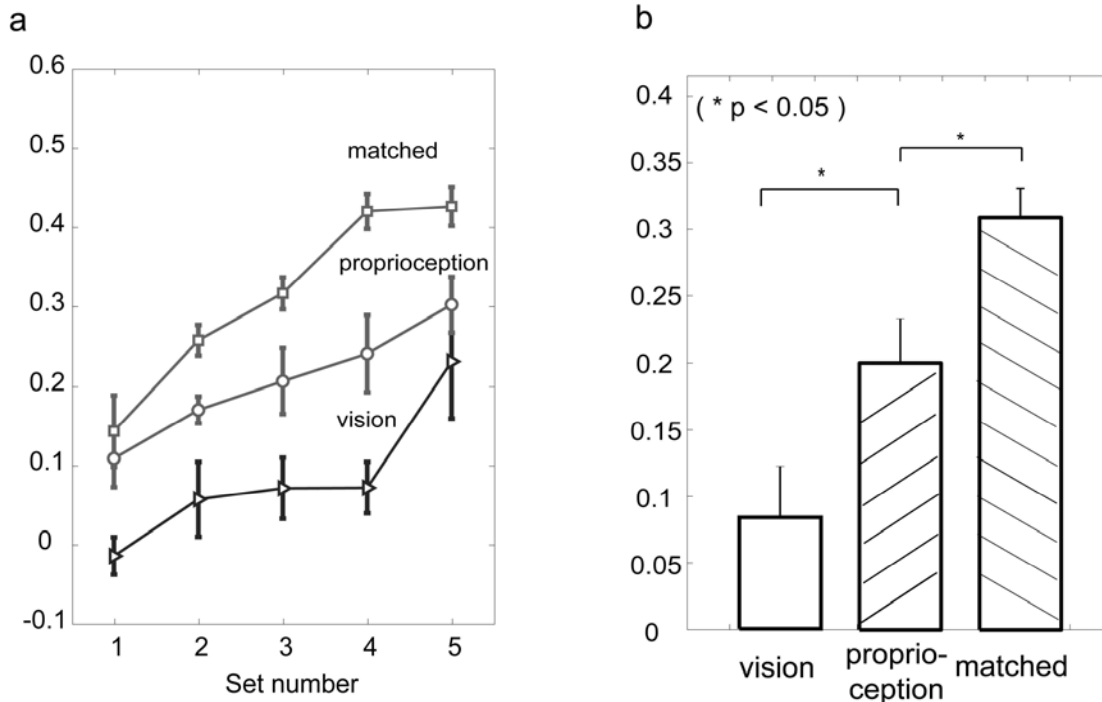
Figure 6.5 Comparison of learning index from the vision-only, proprioception-only and matched groups. **(a)** Learning index as a function of set number for the three groups, averaged across subjects. Each error bar indicates SEM across subjects. **(b)** Overall learning index, averaged across subjects.

However, visual cues were not irrelevant. The learning index of the matched group was significantly larger than the proprioception-only group (t=2.80, df=13, p=0.008) despite the fact that proprioceptive cues were identical in the two groups. Additionally, the learning index of the vision-only group was significantly greater than zero (t=-2.16, df=6, p=0.037) despite the fact that in this group no proprioceptive cues were available that could aid learning. The difference between the matched and proprioception-only group was an estimate of the influence of visual cues. This difference was roughly half of the proprioception-only group and roughly equal to the size of the vision-only group. These results suggest that, visual cues were only about half as effective in promoting the learning of force patterns as the corresponding proprioceptive cues. Furthermore, the contribution that visual cues made to learning was largely independent of the contribution of proprioceptive cues.

94

Based on these results, we hypothesized that the state of the end-effector was estimated through a weighted sum of visual and proprioceptive cues. In a given trial i, the distance of the visual cue from the midline is represented by $v^{(i)}$, and distance of the proprioceptive cue from the midline by variable $p^{(i)}$. If the confidence in the visual cue is noted with c_v and the confidence in the proprioceptive cue is noted with c_p, then the perceived state $q^{(i)}$ is (Ernst M.O and Banks M.S., 2002):

$$q^{(i)} = \frac{c_v v^{(i)} + c_p p^{(i)}}{c_v + c_p} \quad (6.1)$$

If the learning index s depends linearly on the perceived distance between the left and right movements (Hwang et al., 2003), then we have:

$$s = k\left(q^{(r)} - q^{(l)}\right) \quad (6.2)$$

Here, k is the sensitivity to changes in position. It represents the amount of position dependent learning. Full learning in the matched condition would occur if k matches the slope of the applied position-dependent force field. Learning in the matched group was better than the proprioception-only group because in the matched group the visual cues confirmed the proprioceptive cues, thereby producing a larger perceived distance between the movements, $q^{(r)} - q^{(l)}$. Overall, the results of the matched, proprioception-only, and vision-only groups indicate that $c_p \approx 2c_v$.

Eqs. (6.1) and (6.2) made two predictions: when the arm is to the left but the visual cue indicates that the end-effector is to the right (flipped condition, Figure 6.3d, $v^{(i)} = +7$, $p^{(i)} = -7$), then learning should be worse than both the conditions where the visual cue is at center (Figure 6.3b,

$v^{(i)} = 0, p^{(i)} = -7$) and the condition where visual cues match proprioception (Figure 6.3a,

$v^{(i)} = -7, p^{(i)} = -7$). We therefore recruited a new group of subjects (n=16) and tested them in

the flipped condition. Despite the large number of subjects, we found that only one of the

predictions was confirmed. Learning of the flipped group was significantly worse than the

matched group (t=-2.24, d.f.=22, p=0.018). However, contrary to the prediction, learning of the

flipped group was not worse than the proprioception group (Figure 6.5). Whereas previous work

(Hwang et al., 2003) had found that when vision and proprioception matched, learning improved

as the distance between neighboring movements increased, current results suggested that in case

of a mismatch, performance was not due to a simple weighing of the two sensory modalities.

6.3 Dissociable effects of explicit and implicit learning

The learning index s is a gross measure of how well the motor system predicted and

compensated for an externally imposed force field. In principle, this compensation may be due to

both an implicit and an explicit knowledge of that force by the brain, i.e., $s = E + I$. In motor

control studies, we routinely ignore potential contributions from explicit information, as in Eq.

(6.2), but here we thought that this omission might have played a central role in the inability of

the model to fit the data.

Explicit knowledge implies awareness of the force patterns. We represented awareness as a

binary variable a and assumed that the probability of becoming aware, $\Pr(a)$. $\Pr(a)$ depended

on the presence of visual and proprioceptive cues, $\Pr(a) = g(v, p)$. We hypothesized that if a

subject was aware, then the resulting explicit knowledge would contribute an amount e to the

learning index. In a group of subjects, the expected value of the contribution due to awareness is
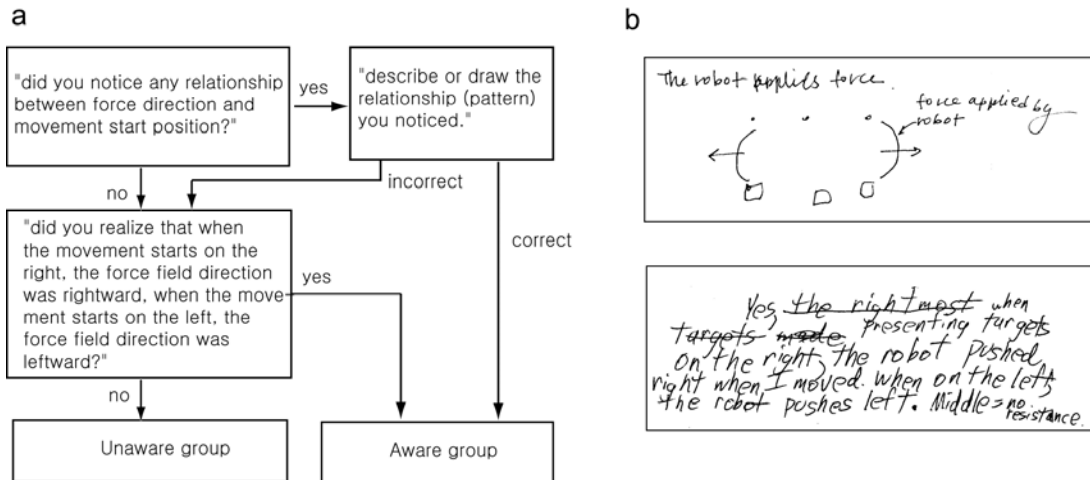
Figure 6.6 Assessment of force field awareness. **(a)** After the completion of the experiment, each subject was asked these questions in order to determine whether they were consciously aware of the force field pattern. **(b)** Examples from two subjects. Some subjects were able to accurately describe the force field pattern with diagrams or in writing.

$E = e \Pr(a)$. We assumed that the contribution due to an implicit internal model was similar to Eqs. (6.1) and (6.2), i.e., $I = k\left(q^{(r)} - q^{(l)}\right)$. The result was the following model of performance:

$$s = e \Pr(a) + k\left(q^{(r)} - q^{(l)}\right) \qquad (6.3)$$

Eq. (6.3) made the simple predictions that in every group of subjects, aware subjects should perform better than unaware subjects, and the performance improvement due to awareness should be similar in all groups. To assess awareness, we examined the written interview that each subject had provided immediately after completion of the task. Aware subjects were able to describe or confirm the correct relationship between starting positions and force directions whereas unaware subjects were unable to confirm the correct relationship. Figure 6.7 displays average learning index of unaware and aware subjects separately within each group. Note that in every group, the sub-group of aware subjects performed better than the sub-group of unaware subjects. An example of the time course of performance in the aware and unaware subgroups (for
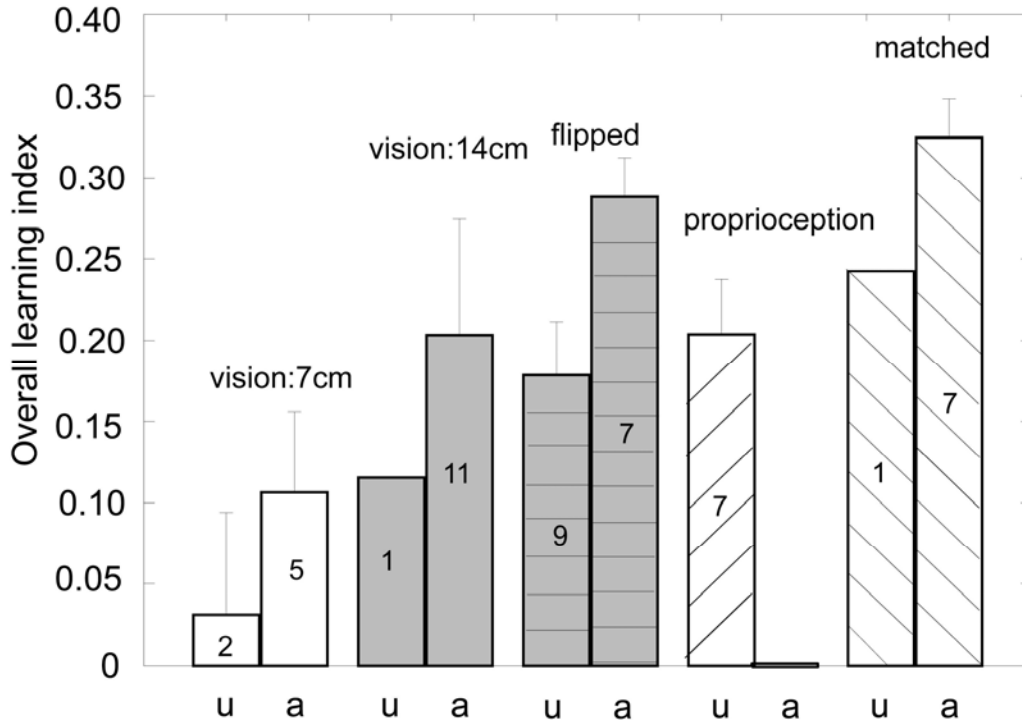
Figure 6.7 Aware subjects perform better than unaware subjects. Averaged learning indices across unaware subjects (u) and aware subjects (a) separately for each group. Numbers inside bars are the number of subjects in each group. Each error bar indicates SEM across subjects.

the flipped group) is shown in Figure 6.8. In both groups, errors in field trials gradually decreased and errors in catch trials gradually increased. However, learning rate of the aware group was faster than the unaware group. We found that awareness, and by definition explicit knowledge, significantly improved performance (t=2.5, d.f.=14, p=0.013) in the flipped group. This was consistent in every group.

However, it was possible that awareness did not lead to improved performance, but rather that strong performance led to awareness. In such a scenario, awareness would be triggered when a subject's performance reached a certain threshold. Our data rejected this alternate hypothesis: In the proprioception-only group, where performance was high, $\Pr(a) = 0$, whereas in the vision:7cm group, where performance was poor, $\Pr(a) = 0.71$.

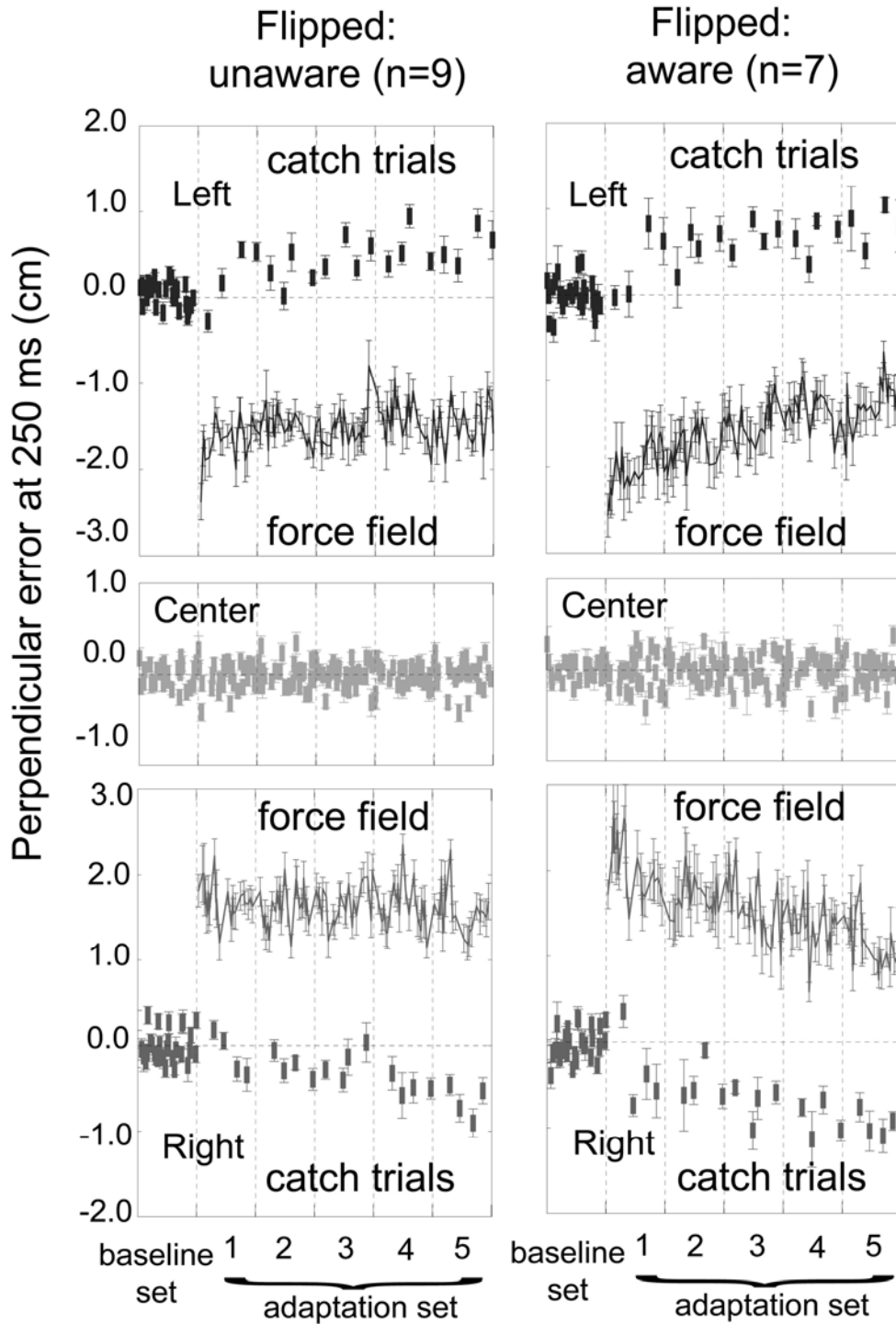**Figure 6.8** Comparison of movement errors between aware and unaware subjects. Perpendicular errors averaged across subjects of the flipped unaware and flipped aware groups. Top panel shows errors in the left location, middle panel shows errors in the center location and bottom panel shows error in the right location. Squares indicate catch trials. Error bars show SEM.

We fitted Eqs. (6.1) and (6.3) to the aware and unaware subgroups of the vision:7cm, flipped, proprioception, and matched groups and found the following values: e=0.09, k=0.015, c_v=0.1, and c_p=0.9. These values suggested that implicit leaning was almost entirely due to proprioceptive information, but that performance was affected by both this implicit motor learning and probability of awareness.

We then tested two predictions of the model: 1) as the perceived distance between visual and proprioceptive cues increased (Eq. 6.1), performance should improve, and 2) the contribution that awareness made to learning should be the same in all groups. We recruited a new group of subjects (n=12) and trained them with visual cues at 14cm, i.e., $v^{(i)} = 14, p^{(i)} = 0$. The results for that group are shown in Figure 6.7. In agreement with the first prediction, performance of this group was better than the group that trained with visual cues at 7cm, i.e., $v^{(i)} = 7, p^{(i)} = 0$, (t=1.22, d.f.=17, p=0.12). In agreement with the second prediction, the difference in performance of aware and unaware subjects in this group was similar to the other groups. The difference in the vision 14 cm group was 0.082 while the differences in the other groups were 0.091±0.017. The fit between all the data and the model of Eqs. (6.1) and (6.3) is shown in Figure 6.9a. The x-axis of this figure is the perceived distance between the two movements for each condition, computed with Eq. (6.1). The bottom solid line represents the performance component due to implicit motor learning, while the top dotted line is total performance if explicit knowledge is present. The difference between these two lines is the constant term e that estimates the contribution of explicit knowledge to motor learning performance.

Secondly, we considered how the probability of becoming aware $\Pr(a)$ depended on visual and proprioceptive cues. Figure 6.9b plots $\Pr(a)$ for all groups. In the vision:7cm and vision:14cm groups proprioceptive cues were identical but $\Pr(a)$ increased from 0.72 to 0.92. This suggested
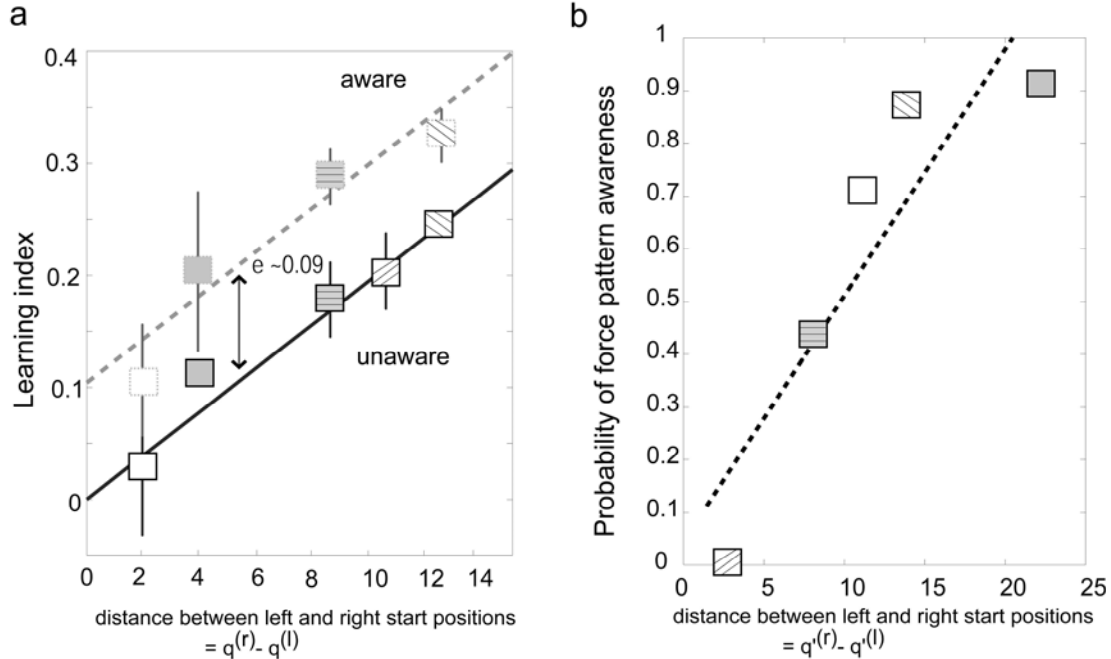
Figure 6.9 Model fit of learning performance and probability of awareness. **(a)** The data in Fig. 4a were fit to Eqs. (1) and (3). For unaware subjects, a=0 and for aware subjects, a=1. Thus, e indicates improvement of learning by awareness. The model fit was r^2=0.27, p<0.001 when k= 0.015, e=0.09 and c_v= 0.1, c_p=0.9. □: vision 7 cm, ■: vision 14 cm, ▤: flipped, ▨: proprioception, ▧: matched. **(b)** The model fit to probability of awareness

$$\Pr(a) = k'\left(q'^{(l)} - q'^{(r)}\right),$$ where q' is perceived state as in Eq. (4). Parameter values: k'=0.047, c_v'=0.8, and c_p'=0.2.

that $\Pr(a)$ depended on the visually perceived distance of the movements. However, proprioception was also a factor because while visual distances of the cues were identical in the flipped and matched groups, $\Pr(a)$ increased from 0.44 to 0.875. Therefore, both visual and proprioceptive cues affected awareness. To estimate the relative importance of each cue, we assumed that q' was the perceived state as in Eq. (6.1), except with new confidence coefficients c_1' and c_2'. Probability of awareness depended on q':

101

$$q'^{(i)} = \frac{c_v' v^{(i)} + c_p' p^{(i)}}{c_v' + c_p'}$$

$$\Pr(a) = k'\left(q'^{(r)} - q'^{(l)}\right) \qquad (6.4)$$

The fit of this model to the data in Figure 5b produced values: $k'=0.047$, $c_v'=0.8$, and $c_p'=0.2$ ($r^2=0.88$, $p<0.05$). That is, probability of becoming aware was four times more dependent on visual cues than proprioceptive cues.

Finally, we examined the kinematic features of movements in aware and unaware groups. To eliminate the kinematic differences due to different performance level, we compared two groups with similar learning performance, vision 14 cm aware and proprioception unaware groups. Figure 6.10a displays the average hand paths in the last training set from these two groups. The velocity perpendicular to the movement direction from each group is also displayed in Figure 6.10b. For the left movement, both the field and catch trials in these two groups show very similar hand paths and velocity profiles. For the right movement, the aware vision 14 cm group shows less perturbation in both the field and catch trials, indicating larger stiffness of arm in the vision 14 cm group. But the relative ratio of perturbation in the field and catch trials remains similar in the two groups. We found no specific differences in kinematics between aware and unaware groups when the performance level was similar.
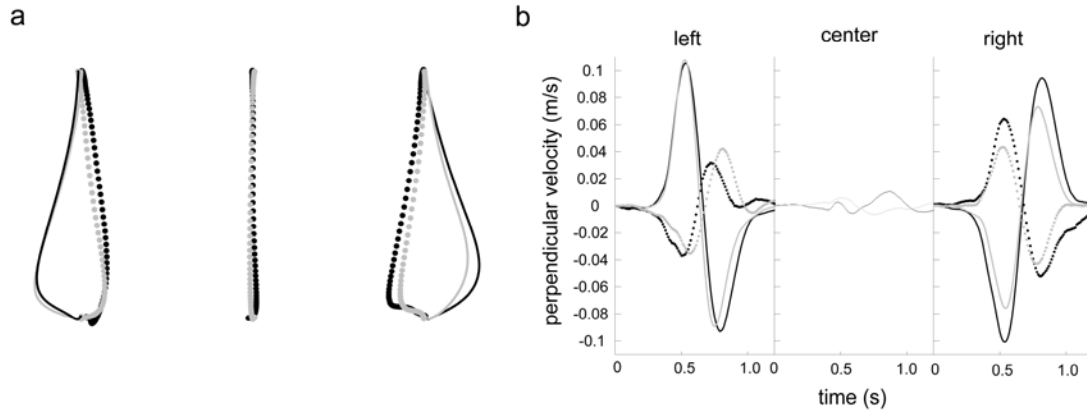
Figure 6.10 No kinematic differences between aware and unaware groups when at similar performance level. **(a)** Average hand paths in the last training set from the aware vision 14 cm group (grey) and unaware proprioception group (black). Solid lines are field trials and dotted lines are catch trials. **(b)** Average profiles of velocity perpendicular to the movement direction. The format is same as in **(a)**.

6.4 Discussion

We found that in learning dynamics of reaching, the brain relied on both implicit and explicit learning systems. Performance was dominated by the implicit learning system and that system relied primarily on proprioception to form internal models of dynamics. However, performance was significantly affected by an explicit learning system that became aware of the force patterns and that awareness was a probabilistic function that depended primarily on visual cues in the task.

In many motor skill tasks that have been studied in the laboratory setting, e.g. prism adaptation, visual rotation, and serial reaction time (SRT) sequence learning, there are distinct components of performance that may be due to awareness. For example, in the SRT task awareness of the underlying sequence can develop as a consequence of prolonged training (Stadler, 1994) or

103

simply through a cue that signals the introduction of the sequence (Willingham et al., 2002).

Patients with unilateral parietal cortex damage show no ability to learn the SRT task (Boyd and

Winstein, 2001). However, their performance improves significantly if they first learn the

sequence explicitly. These results not only support the anatomical distinction between regions

that support explicit and implicit learning, but that explicit knowledge can help improve

acquisition of implicit information.

The force field adaptation paradigm has been widely used as a tool to study mechanisms of

implicit learning, yet the explicit component of this task, if any, has never been quantified.

Profoundly amnesic individuals (Shadmehr et al., 1998) as well as Huntington's disease patients

(Smith et al., 2000) retain the ability to adapt in this task while cerebellar patients are severely

impaired (Smith et al., 2000;Maschke et al., 2004). After adaptation, normal individuals

sometimes think that their improvement in performance was due to the experimenter turning off

the forces (Shadmehr and Mussa-Ivaldi, 1994a). While these results indicate that acquisition of

explicit information may not be necessary for improved performance, they do not imply that if

explicit information were available, it would play no role in adaptation. For example, in a recent

study, Osu et al. (Osu et al., 2004) provided explicit verbal information (in addition to visual cues

that reinforced that information) to subjects as they learned force fields. However, when such

instructions were not provided, extensive training on a similar task did not produce any

improvement in performance (Rao and Shadmehr, 2001). Therefore, it is possible that even in the

force field task, explicit knowledge can play a role in improving performance. Our results

quantify these effects.

However, there are some limitations on the ability our study to answer some of the more

profound questions with regard to explicit learning. First, since we did not control awareness of

explicit knowledge and rather relied on each subject's report in the post-experiment survey, it is

unclear at which point during the experiment each subject became aware and the causality

between awareness and performance improvement is unclear. Second, we made a binary categorization for each subject, aware or unaware but awareness might not be an all or none phenomena. Thus, even among aware subjects, degree of awareness may vary. Despite these limitations, our results suggest that awareness had a positive impact on force field learning and the acquisition of awareness was primarily dependent on visual cues.

How did aware subjects perform better? One might expect that aware subjects developed some strategies to succeed in the task, e.g. aiming the target differently depending on the expected force field direction. However, in our post-experiment survey all of our subjects denied that they aimed differently depending on the expected force field direction. Instead, most of subjects reported that they were mentally getting prepared to resist against the expected force field direction. Moreover, our comparison of kinematics features like hand paths, speed profile, and perpendicular velocity profile did not reveal any noticeable strategic difference between aware and unaware groups.

One possible mechanism of the effect of awareness on performance is that in the basis function model of force field learning (Hwang et al., 2003), visually-driven awareness modulates sensitivity of the bases to changes in arm position. For a given spatial distance between two movements, increasing the sensitivity of the bases to changes in arm position is equivalent to increasing the separation distance between two movements, thus resulting in improved learning. Attention or other cues can indeed modulate tuning of neurons (Reynolds et al., 2000;Moran and Desimone, 1985;Musallam et al., 2004). For example, visual stimuli with low luminance contrast elicit higher activation of V4 neurons when attention is directed to the stimulus location than when attention is directed away from the stimulus location, demonstrating that attention increases the sensitivity to luminance contrast (Reynolds et al., 2000). Thus, if effect of awareness is similar to effect of attention, sensitivity of the bases to changes in perceived arm position might be enhanced, resulting in improved learning.

An alternate approach is to assume that the system that acquires explicit information relies on fundamentally different bases and forms a fundamentally different model of the force field. In this scenario, the result of training is formation of potentially two different internal models: the implicit and explicit internal models would reside in parallel and together contribute to performance. Willingham(2001) has argued that the system that acquires explicit information can guide motor behavior so that performance improves, but that this guidance requires attention. Therefore, one way to test the explicit component of a force field adaptation task might be to provide a distracting task and determine its effect on both awareness and performance.

Chapter 7

Discussion

The goal of this thesis was to investigate how the brain represents proprioceptive information about limb state, i.e., position, velocity and acceleration to generate reaching movements. To achieve this goal, human behaviors during point-to-point reaching in multiple new dynamic environments were examined and neural coding schemes in the brain were inferred from the observed behaviors, e.g. the pattern of generalization. The patterns of generalization across limb position in multiple dynamic conditions suggested that the internal model encodes limb position and velocity in intrinsic coordinates via a gain-field scheme. That is, the neural elements in the brain have directionally dependent tuning that is modulated monotonically with limb position. The monotonic position encoding makes a counter-intuitive prediction that effect of learning can be larger outside the trained space when the training dynamics are linearly position dependent. This prediction of hypergeneralization was confirmed with corroborating experimental results. Neurophysiology reports that some cells in M1 and S1 show multiplicative interaction between limb position and directional tuning further support the gain-field like neural representation (Sergio and Kalaska, 1997;Prud'homme and Kalaska, 1994).

The gain-field scheme might not be a surprising way to represent these state variables considering that the brain always needs to deal with forces that result from multiplicative interaction of limb position and velocity in multi-joint movements (Slotine, 1991). By the same logic, it might not be necessary to encode limb velocity and acceleration multiplicatively since these two variable related forces are always linearly separable in the naturally occurring dynamic environments.

Interestingly, however, the pattern of generalization across acceleration space suggested that neural elements do not encode acceleration and velocity in a linearly separable way. Instead, all sensory information on limb state seems to be encoded in a combined way that is not linearly separable.

This combined sensory representation might be related with the properties of the proprioceptive sensors in our body. Muscle spindles are known to be the most important proprioceptive sensors encoding muscle length, and its rate of change. Several neurophysiological recordings and mathematical models show that spindles are not a pure position, or pure velocity or pure acceleration sensor (Lennerstrand, 1968b;Lennerstrand, 1968a). Rather it, encodes all three variables at the same time in a nonlinear way (Hasan, 1983). Surprisingly, some tuning functions that were independently derived from a mathematical model of muscle spindle closely resembled the tuning functions that were derived from a gain-field scheme. Indeed, Houk et al. (1981). proposed that the spindle response to stretching can be simplified as a multiplicative interaction of muscle length and the third power of its derivative. As cells that show spindle-like responses to ramp displacements of hindlimb joint are found in area 3a, M1, and S1 (Wise and Tanji, 1981), it seems plausible to have neural representations of proprioceptive information that is similar to spindle response.

The pattern of generalization produced by muscle spindle-like neural elements matched well the observed pattern in various experimental conditions including a position-velocity dependent force field learning and transfer of a velocity dependent force field learning across large workspace. However, the pattern of generalization in an acceleration dependent force field shows a discrepancy from the observed pattern. The spindle-like representation predicts a wider generalization across movement direction. One reason for this discrepancy might be the assumption that the same model can be used for both shortening and lengthening of the muscle.

Then, the responses for shortening and lengthening are almost anti-symmetric to each other, which causes a significant amount of generalization to 180° direction. Thus, a critical study seems to be finding a tuning curve of muscle spindles for a whole arm reaching not just for passive stretching.

In a force field paradigm, motor learning has been considered to be an implicit process and the effect of awareness or explicit knowledge has not been studied. However, in other kinds of motor learning, e.g. serial reaction time task, the explicit knowledge of sequence was known to have an impact on performance (Boyd and Winstein, 2001;Eliassen et al., 2001;Russeler and Rosler, 2000). In this thesis, a proper assessment of explicit knowledge relevant to task reveals that explicit knowledge has a small but significant impact on learning performance. More interestingly, the formation of explicit knowledge depends primarily on visual information while the formation of implicit internal model depends primarily on proprioceptive information. However, the mechanism through which explicit knowledge would affect motor learning is unclear. In one scenario, explicit knowledge helps forming a separate internal model that is different from implicit internal model that depends on proprioceptive information and this separate internal model produces an additive motor output on top of the motor output from the implicit internal model. In another scenario, explicit knowledge enhances the sensitivity of neural elements in the implicit internal model to propriopceptive information and speeds up adaptation. A useful experiment to distinguish these two possibilities might be an fMRI imaging study. In the first scenario, the formation of separate internal model is likely to activate additional brain areas for aware subjects. In the second scenario, the enhancement of sensitivity is likely to enhance the activity in the same area that was activated by unaware subjects.

In sum, the brain seems to control movements using an internal model that translate the desired sensory states into motor commands. The internal model can adapt to a novel dynamic

109

environment implicitly using proprioceptive information on limb states while explicit knowledge can accelerate the adaptation process. Neural representation of desired proprioceptive states might be similar to neural response of our sensory systems to proprioceptive input. That is, each neural element in the internal model responds to all sensory states, limb position, velocity and acceleration in a combined way that is not linearly separable. Specifically, limb position and velocity coding appears to be combined multiplicatively via a gain-field scheme.

References

Andersen RA, Essick GK, Siegel RM (1985) Encoding of spatial location by posterior parietal neurons. Science 230:456-458.

Ashe J, Georgopoulos AP (1994) Movement parameters and neural activity in motor cortex and area 5. Cereb Cortex 4:590-600.

Atkeson CG (1989) Learning arm kinematics and dynamics. Ann Rev Neurosci 12:157-183.

Bastian AJ, Martin TA, Keating JG, Thach WT (1996) Cerebellar ataxia: Abnormal control of interaction torques across multiple joints. J Neurophysiol 76:492-509.

Bhushan N, Shadmehr R (1999) Evidence for learning of a forward dynamic model in human motor control. Cambridge, MA. In: Advances in Neural Information Processing Systems 11 (Kearns MS, Kearns MS, eds), MIT Press.

Bosco G, Rankin A, Poppele RE (1996) Representation of passive hindlimb postures in cat spinocerebellar activity. J Neurophysiol 76:715-726.

Boyd LA, Winstein CJ (2001) Implicit motor-sequence learning in humans following unilateral stroke: the impact of practice and explicit knowledge. Neurosci Letters 298:65-69.

Burdet E, Osu R, Franklin DW, Milner TE, Kawato M (2001) The central nervous system stabilizes unstable dynamics by learning optimal impedance. Nature 414:446-449.

Caminiti R, Johnson PB, Urbano A (1990) Making arm movements within different parts of space: dynamic aspects in the primate motor cortex. J Neurosci 10:2039-2058.

Coltz JD, Johnson MTV, Ebner TJ (1999) Cerebellar Purkinje cell simple spike discharge encodes movement velocity in primates during visuomotor arm tracking. J Neurosci 19:1782-1803.

Conditt MA, Gandolfo F, Mussa-Ivaldi FA (1997) The motor system does not learn the dynamics of the arm by rote memorization of past experience. J Neurophysiol 78:554-560.

Conditt MA, Mussa-Ivaldi FA (1999) Central representation of time during motor learning. Proc Natl Acad Sci USA 96:11625-11630.

Cordo P, Flores-Vieira C., Verschueren M.P.S., Inglis J.T., Gurfinkel V. (2002) Position sensitivity of human muscle spindles: single afferent and population representation. J Neurophsyiol 87:1186-1195.

Corkin S (1968) Acquisition of motor skill after bilateral medial temporal-lobe excision. Neuropsychologia 6:255-265.

Criscimagna-Hemminger SE, Donchin O, Gazzaniga MS, Shadmehr R (2003) Learned dynamics of reaching movements generalize from dominant to non-dominant arm. J Neurophsyiol 89:168-176.

Donchin O, Francis JT, Shadmehr R (2003) Quantifying generalization from trial-by-trial behavior of adaptive systems that learn with basis functions: theory and experiments in human motor control. J Neurosci 23:9032-9045.

Donchin O, Shadmehr R (2002) Linking motor learning to function approximation: Learning in an unlearnable force field. Cambridge, MA. In: Adv Neural Inform Proc Systems (Dietterich T. G., Becker S., Ghahramani Z., eds), MIT Press.

Edin B.B., Vallbo A.B.. (1990) Dynamic response of human muscle spindle afferents to stretch. J Neurophsyiol 63:1297-1306.

Eliassen JC, Souza T, Sanes JN (2001) Human brain activation accompanying explicitly directed movement sequence learning. Exp Brain Res 141:269-280.

Ernst M.O, Banks M.S. (2002) Humans integrate visual and haptic information in a statistically optimal fashion. Nature 415:429-433.

Flament D, Hore J (1988) Relations of motor cortex neural discharge to kinematics of passive and active elbow movements in the monkey. J Neurophysiol 60:1268-1284.

Flash T, Gurevich I (1997) Models of motor adaptation and impedance control in human arm movements. In: Self-organization, computational maps, and motor control (Morasso P, Sanguineti V, eds), pp 423-481. Amsterdam: Elsevier Science BV.

Flash T, Hogan N (1985) The coordination of arm movements: an experimentally confirmed mathematical model. J Neurosci 5:1688-1703.

Fu QG, Flament D, Coltz JD, Ebner TJ (1997a) Relationship of cerebellar Purkinje cell simple spike discharge to movement kinematics in the monkey. J Neurophysiol 78:478-491.

Fu QG, Mason CR, Flament D, Coltz JD, Ebner TJ (1997b) Movement kinematics encoded in complex spike discharge of primate cerebellar Purkinje cells. Neuroreport 8:523-529.

Gabrieli JDE, Corkin S, Mickel SF, Growdon JH (1993) Intact acquisition and long-term retention of mirror-tracing skill in Alzheimer's disease and in global amnesia. Behav Neurosci 107:899-910.

Gandolfo F, Mussa-Ivaldi FA, Bizzi E (1996) Motor learning by field approximation. Proc Natl Acad Sci USA 93:3843-3846.

Georgopoulos AP, Caminiti R, Kalaska JF (1984) Static spatial effects in motor cortex and area 5: quantitative relations in a two-dimensional space. Exp Brain Res 54:446-454.

Ghahramani Z, Wolpert DM (1997) Modular decomposition in visuomotor learning. Nature 386:392-395.

Ghez C, Krakauer JW, Sainburg RL, Ghilardi MF (2000) Spatial representation and internal models of limb dynamics in motor learning. Cambridge, MA. In: The New Cognitive Neurosciences (Gazzaniga MS, Gazzaniga MS, eds), pp 501-514. MIT Press.

Goodbody SJ, Wolpert DM (1998) Temporal and amplitude generalization in motor learning. J Neurophysiol 79:1825-1838.

Goschke T (1998) Implicit learning of perceptual and motor sequences: evidence for independent learning systems. In: Handbook of implicit learning (Stadler MA, Frensch P, eds), Thousand Oaks, CA: Sage.

Gribble PL, Scott SH (2002) Overlap of internal models in motor cortex for mechanical loads during reaching. Nature 417:938-941.

Hasan Z (1983) A model of spindle afferent response to muscle stretch. J Neurophsyiol 48:989-1006.

Hasan Z, Houk JC (1975) Analysis of response properties of deefferented mammalian spindle receptors based on frequency response. J of Neurophysiology 38:663-672.

Henriques DY, Klier EM, Smith MA, Crawford JD (1998) Gaze-centered remapping of remembered visual space in an open-loop pointing task. J Neurosci 18:1583-1594.

Houk JC, Rymer WZ, Crago P.E. (1981) Dependence of dynamic response of spindle receptors on muscle length and velocity. J Neurophsyiol 46:143-166.

Hwang EJ, Donchin O, Smith MA, Shadmehr R (2003) A gain-field encoding of limb position and velocity in the internal model of arm dynamics. PLoS Biology 1:209-220.

Krakauer JW, Ghilardi MF, Ghez C (1999) Independent learning of internal models for kinematic and dynamic control of reaching. Nature Neurosci 2:1026-1031.

Lackner JR, Dizio P (1994) Rapid adaptation to coriolis force perturbations of arm trajectory. J Neurophysiol 72:299-313.

Lateiner JE, Sainburg R (2003) Differential contributions of vision and proprioception to movement accuracy. Exp Brain Res 151:446-454.

Lennerstrand G (1968a) Dynamic analysis of muscle spindle endings in the cat using length chagnes of different length-time relations. Acta Physiol Scand 73:234-250.

Lennerstrand G (1968b) Position and velocity sensitivity of muscle spindles in the cat. I. Primary and secondary endings deprived of fusimotor activation. Acta Physiol Scand 73:281-299.

Li CSR, Padoa-Schioppa C, Bizzi E (2001) Neuronal correlates of motor performance and motor learning in the primary motor cortex of monkeys adapting to an external force field. Neuron 30:593-607.

Lin C.K., Crago P.E. (2002) Structural model of the muscle spindle. Ann Biomed Eng 30:68-83.

Malfait N, Shiller D.M., Ostry DJ (2002) Transfer of motor learning across arm configurations. J Neuroscience 22:9656-9660.

Maschke M, Gomez CM, Ebner TJ, Konczak J (2004) Hereditary cerebellar ataxia progressively impairs force adaptation during goal-directed arm movements. J Neurophsyiol 91:230-238.

Matthews PB (1981) Evolving views on the internal operation and functional role of the muscle spindle. J Physiol London 320:1-30.

Milner B (1962) Les troubles de la memoire accompagnant des lesions hippocampiques bilaterales. Paris. In: Physiologie de l Hippocampe pp 257-272. Centre National de la Recherche Scientifique.

Moran J, Desimone R (1985) Selective attention gates visual processing in the extrastriate cortex. Science 229:782-784.

Murray WM, Delp SL, Buchanan TS (1995) Variation of muscle moment arms with elbow and forearm position. J Biomechanics 28:513-525.

Musallam S, Corneil BD, Greger B, Scherberger H, Andersen RA (2004) Cognitive control signals for neural prosthetics. Science 305:258-262.

Osu R, Hirai S, Yoshioka T, Kawato M (2004) Random presentation enables subjects to adapt to two opposing forces on the hand. Nat Neurosci 7:111-112.

Poggio T, Girosi F (1990) Regularization algorithms for learning that are equivalent to multilayer networks. Science 247:978-982.

Poppele RE, Boyd LA (1970) Quantitative description of linear behavior of mammalian muscle spindles. J Neurophsyiol 33:59-72.

Pouget A, Sejnowski TJ (1997) Spatial transformations in the parietal cortex using basis functions. J Cog Neurosci 9:222-237.

Prochazka A, Gorassini M (1998) Ensemble firing of muscle afferents recorded during normal locomotion in cats. J Physiol 507:293-304.

Prochazka A, Gordon AM (1998) Models of ensemble firing of muscle spindle afferents recorded during normal locomotion in cats. J Physiol 507:277-291.

Prud'homme MJ, Kalaska JF (1994) Proprioceptive activity in primate primary somatosensory cortex during active arm reaching movements. J Neurophysiol 72:2280-2301.

Rao AK, Shadmehr R (2001) Contextual cues facilitate learning of multiple models of arm dynamics.

Reynolds JH, Pasternak T, Desimone R (2000) Attention increases sensitivity of V4 neurons. Neuron 26:703-714.

Rossetti Y, Desmurget M, Prablanc C (1995) Vectorial coding of movement: Vision, proprioception, or both? J of Neurophysiology 74:457-463.

Russeler J, Rosler F (2000) Implicit and explicit learning of event sequences: evidence for distinct coding of perceptual and motor representations. Acta Psychol 104:45-67.

Sainburg RL, Ghez C, Kalakanis D (1999) Intersegmental dynamics are controlled by sequential anticipatory, error correction, and postural mechanisms. J Neurophysiol 81:1045-1056.

Schaafsma A, Otten E, Van Willigen JD (1991) A muscle spindle model for primary afferent firing based on a simulation of intrafusal mechanical events. J Neurophsyiol 65:1297-1312.

Scheidt RA, Reinkensmeyer DJ, Conditt MA, Rymer WZ, Mussa-Ivaldi FA (2000) Persistence of motor adaptation during constrained, multi-joint, arm movements. J Neurophysiol 84:853-862.

Scott SH, Kalaska JF (1997) Reaching movements with similar hand paths but different arm orientation: I. Activity of individual cells in motor cortex. J Neurophysiol 77:826-852.

Scott SH, Sergio LE, Kalaska JF (1997) Reaching movements with similar hand paths but different arm orientations. II. Activity of individual cells in dorsal premotor cortex and parietal area 5. J Neurophysiol 78:2413-2426.

Sergio LE, Kalaska JF (1997) Systematic changes in directional tuning of motor cortex cell activity with hand location in the workspace during generation of static isometric forces in constant spatial directions. J Neurophysiol 78:1170-1174.

Shadmehr R, Brandt J, Corkin S (1998) Time dependent motor memory processes in H.M. and other amnesic subjects. J Neurophysiol 80:1590-1597.

Shadmehr R, Moussavi ZMK (2000) Spatial generalization from learning dynamics of reaching movements. J Neurosci 20:7807-7815.

Shadmehr R, Mussa-Ivaldi FA (1994a) Adaptive representation of dynamics during learning of a motor task. J Neurosci 14:3208-3224.

Shadmehr R, Mussa-Ivaldi FA (1994b) Computational elements of the adaptive controller of the human arm. San Francisco. In: Advances in Neural Information Processing Systems (Cowan JD, Cowan JD, eds), pp 1077-1084. Morgan Kaufmann.

Slotine J-JE, Li W (1991) Applied nonlinear control. Englewood Cliffs, NJ. Prentice Hall.

Smith MA, Brandt J, Shadmehr R (2000) The motor dysfunction in Huntington's Disease begins as a disorder in error feedback control. Nature 403:544-549.

Sober SJ, Sabes PN (2003) Multisensory integration during motor planning. J Neurosci 23:6982-6992.

Stadler MA (1994) Explicit and implicit learning and maps of cortical motor output. Science 265:1601.

Taylor DM, Tillery SI, Schwartz AB (2002) Direct cortical control of 3D neuroprosthetic devices. Science 296:1829-1832.

Thoroughman KA, Shadmehr R (2000) Learning of action through adaptive combination of motor primitives. Nature 407:742-747.

Tillery SI, Soechting JF, Ebner TJ (1996) Somatosensory cortical activity in relation to arm posture: nonuniform spatial tuning. J Neurophysiol 7x:2423-2438.

Todorov E (2000) Direct cortical control of muscle activation in voluntary arm movements: a model. Nature 3:391-398.

Tong C, Wolpert DM, Flanagan JR (2002) Kinematics and dynamics are not represented independently in motor working memory: evidence from an interference study. J Neurosci 22:1108-1113.

Tranel D, Damasio AR, Damasio H, Brandt JP (1994) Sensorimotor skill learning in amnesia: additional evidence for the neural basis of nondeclarative memory. Learning and Memory 1:165-179.

Wang T, Dordevic GS, Shadmehr R (2001) Learning the dynamics of reaching movements results in the modification of arm impedance and long-latency perturbation responses. Biol Cybern 86:437-448.

Willingham DB (2001) Becoming aware of motor skill. Trends Cog Sci 5:181-182.

Willingham DB, Salidis J, Gabrieli JD (2002) Direct comparison of neural systems mediating conscious and unconscious skill learning. J Neurophysiol 88(3):1451-1460.

Wise SP, Tanji J (1981) Neuronal responses in sensorimotor cortex to ramp displacements and maintained positions imposed on hindlimb of the unanesthetized monkey. J Neurophsyiol 45:482-500.

Wolpert DM (1997) Computational approaches to motor control. Trends in Cog Sci 2:209-216.

CURRICULUM VITAE

Eun Jung Hwang : Born December 22nd, 1974 in Seoul, Republic of Korea

EDUCATION

1993-1997   Seoul National University, Seoul, Korea
               BS in Electrical Engineering
1997-1999   Seoul National University, Seoul, Korea
               MS in Electrical Engineering
1999-2004   Johns Hopkins University, Baltimore, MD
               Ph.D in Biomedical Engineering

PUBLICATIONS

Hwang EJ. Representation of proprioceptive information for generation of arm dynamics. Ph.D Thesis, 2004

Hwang EJ, Donchin O, Smith MA, Shadmehr R. A Gain-field encoding of limb position and velocity in the internal model of arm dynamics. *Public Library of Science Biology*, Vol. 1 Issue:2, 209-220, 2003.

Shadmehr R, Donchin O, Hwang EJ, Hemminger SE, Rao A. (in press) Learning to compensate for dynamics of reaching movements. *Motor Cortex and Voluntary Movements* (E. Vaadia, editor), CRC Press, 2003.

Yoon TH, Hwang EJ, Shin DY, Park SI, Oh SJ, Jung SC, Shin HC, Kim SJ. A micromachined silicon depth probe for multi-channel neural recording. *Biomedical Engineering, IEEE Transactions on* , Vol. 47 Issue: 8, 1082 -1087, 2000

Hwang EJ. Feasibility study of the semiconductor microelectrode arrays in central and peripheral nerve system. M.S. Thesis, 1999.

ABSTRACTS

Hwang EJ, Smith MA, Shadmehr R. Generalization properties of internal models of arm dynamics may be explained with bases that encode state of the limb similarly to muscle spindles. *Soc. Neurosci. Abs*. [533.6], 2004.

Smith MA, Hwang EJ, Shadmehr R. Learning to learn-optimal adjustment of the rate at which the motor system adapts. *Soc. Neurosci. Abs*. [533.7], 2004.

Hwang EJ, Shadmehr R. Bases that encode internal models of arm dynamics resemble functional properties of muscle spindles. *Neural Control of Movemen*, Sitges, Spain, 2004.

Hwang EJ, Smith MA, Shadmehr R. Understanding the roles of proprioception and vision in adapting to arm dynamics. *Soc. Neurosci. Abs*. [822.16], 2003.

Hwang E, Donchin O, Shadmehr R. Shape of the motor primitives in arm position space. *Neural Control of Movement*, Naples, FL, 2002.

Hwang E, Donchin O, Shadmehr R. Shape of the motor primitives in arm position space. *Soc. Neurosci*. *Abs.* [302.6], 2001.

Hwang E, Donchin O, Shadmehr R. Learning of position dependent dynamics in reaching movements. *Neural Control of Movement*, Seville, Spain, 2001.

Hwang E, Kim SJ, Yoon T, Shin D, Oh S, Jung S, Shin H. A simultaneous multichannel recording obtained from rat cortex using a plasma etched silicon depth probe. *BMES -IEEE EMBS Joint Conference*, Atlanta, GA, 1999.

AWARDS

Society for the Neural Control of Movement - Student Travel Fellowship (2002).

Society for the Neural Control of Movement - Student Travel Fellowship (2001).

PATENTS

Hwang E, Kim S, "Microelectrode arrays for culturing neuronal cell network" Korean Patent Register Number 1003382450000, May 2002.

Kim S, Hwang E, Yoon T, "Semiconductor microelectrode for neurophysiological application" Korean Patent Register Number 1003346090000, April 2002.

TEACHING EXPERIENCE

Teaching assistant for Models of The Neuron Fall 2002.

Teaching assistant for Biomedical Signal and Sytems Spring 2002.